



| | |
|--------------|-----------------------------------------------------------------------------------|
| Title | 非酸化物セラミックスの燃焼合成と高圧焼結に関する研究 |
| Author(s) | 山田, 修 |
| Citation | 大阪大学, 1987, 博士論文 |
| Version Type | VoR |
| URL | https://hdl.handle.net/11094/1599 |
| rights | |
| Note | |

The University of Osaka Institutional Knowledge Archive : OUKA

<https://ir.library.osaka-u.ac.jp/>

The University of Osaka

**Studies on Combustion Synthesis
and High Pressure Sintering for
Non-oxide Ceramics**

非酸化物セラミックスの燃焼合成と
高圧焼結に関する研究

Osamu YAMADA

Studies on Combustion Synthesis and High Pressure Sintering for Non-oxide Ceramics

(非酸化物セラミックスの燃焼合成と高圧焼結に関する研究)

CONTENTS

| | | |
|-----------|--------------------------------------------------------------------------------------|----|
| Chapter 1 | GENERAL INTRODUCTION | 3 |
| Chapter 2 | DEVELOPMENT OF NEW SYNTHESIS PROCESS OF REFRACTORY MATERIALS | 7 |
| 2-1 | Introduction | 7 |
| 2-2 | Experimental Procedure | 11 |
| 2-2-1 | Starting Materials | |
| 2-2-2 | Various Methods for Ignition of SHS | |
| 2-2-3 | Characterization of the Products | |
| 2-3 | Results of SHS Processing and Characteristics of the Products | 14 |
| 2-3-1 | Preparation and Properties of TiB_2 | |
| 2-3-2 | Preparation and Properties of TiC | |
| 2-3-3 | Preparation and Properties of SiC | |
| 2-4 | Discussion | 26 |
| 2-4-1 | Selection of Suitable Ignition Method by Adiabatic Temperatures | |
| 2-4-2 | Effect of SHS Reaction on Self-Purification | |
| 2-4-3 | Effect of Isostatic Pressure on SHS Reaction | |
| Chapter 3 | APPLICATION OF HIGH PRESSURE TECHNIQUE TO SINTERING OF REFRACTORY MATERIALS | 31 |
| 3-1 | Introduction | 31 |
| 3-2 | Experimental Procedure | 32 |
| 3-2-1 | Starting Materials | |
| 3-2-2 | High Pressure Sintering | |
| 3-2-3 | Characterization of the Products | |
| 3-3 | Results and Discussion | 35 |
| 3-3-1 | Preparation and Properties of Dense SiC Ceramics | |
| 3-3-2 | Preparation and Properties of Dense TiC Ceramics | |
| 3-3-3 | Preparation and Properties of Dense AlN Ceramics | |
| 3-3-4 | Preparation and Properties of $ZrN_{1-X}C_X$ Ceramics | |

| | | |
|-----------|--------------------------------------------------------------------------|----|
| Chapter 4 | DEVELOPMENT OF NEW SYNTHESIS AND SIMULTANEOUS SINTERING PROCESS | 56 |
| 4-1 | Introduction | 56 |
| 4-2 | Experimental Procedure | 56 |
| 4-2-1 | Starting Materials | |
| 4-2-2 | Cell Assemblage and Ignition Procedure | |
| 4-2-3 | Characterization of the Products | |
| 4-3 | Results of HPCS Processing and Characteristics of the Products | 60 |
| 4-3-1 | Preparation and Properties of TiB_2 Dense Ceramics | |
| 4-3-2 | Preparation and Properties of TiC Dense Ceramics | |
| 4-3-3 | Preparation and Properties of SiC Dense Ceramics | |
| 4-4 | Discussion | 75 |
| 4-4-1 | Intrinsic Volume Change of Product before and after Combustion | |
| 4-4-2 | Mechanism of Combustion Sintering under High Pressure | |
| Chapter 5 | APPLICATION OF HPCS PROCESS | 85 |
| 5-1 | Introduction | 85 |
| 5-2 | Experimental Procedure | 85 |
| 5-2-1 | Starting Materials | |
| 5-2-2 | Cell Assemblage for Welding by HPCS | |
| 5-2-3 | Characterization of the Products | |
| 5-3 | Results and Discussion | 88 |
| Chapter 6 | SUMMARY AND CONCLUSION | 92 |
| | Acknowledgement | 94 |
| | Appendix I, II, III | 95 |
| | References | 98 |

Chapter 1 GENERAL INTRODUCTION

Over the last 10 to 20 years, the demands have been rapidly increasing for new structural components with high performances such as higher strength, high hardness and toughness, low porosity, high purity, good chemical stability and strictly controlled composition. Most of these requirements have arisen from the leading technologies related to nuclear applications, aerospace and propulsion of energy-efficiency.

In these requirements, a particular attention has been paid to the refractory ceramic materials such as carbides and borides because they have either unique or outstanding properties of high temperature resistance, superior mechanical properties and greater chemical stability comparing to the metal components.

Most of borides and carbides have extremely high melting points (2000 ~ 4000°C), and therefore these compounds are frequently referred to as refractory materials. The physical and mechanical properties of selected borides and carbides are given in Tables I and II, respectively. High melting or decomposition temperatures and high elastic moduli reflected that the bond strength between atoms is strong because of high covalency in chemical bond.

Table I Some physical and mechanical properties of diborides. [1] [2]

| Property | TiB ₂ | ZrB ₂ | HfB ₂ | NbB ₂ | TaB ₂ |
|--------------------------------------------------------------|------------------|------------------|------------------|------------------|------------------|
| Crystal structure | Hexa. | Hexa. | Hexa. | Hexa. | Hexa. |
| Melting point (K) | 3190 | 3310 | 3520 | 3170 | 3470 |
| Density (g/cm ³) | 4.38 | 6.17 | 10.5 | 6.97 | 12.38 |
| Elastic modulus (x10 ⁴ kg/mm ²) | 3.4 | 3.5 | - | 6.5 | 2.62 |
| Heat of formation (kJ/mol) | 293 | 319 | 336 | 176 | 211 |
| Thermal expansion coefficient (x10 ⁻⁶ /deg) | 4.6 | 5.9 | 6.3 | 8.0 | 8.2 |
| Thermal conductivity (W/m·deg) | 65 | 58 | 51 | 24 | 16 |
| Specific heat (J/mol·deg) | 44.4 | 50.4 | 49.9 | 48.0 | 58.7 |
| Electrical resistivity (x10 ⁻⁶ Ωcm) | 6 - 9 | 9 - 16 | 10.6 | 25.7 | 32.5 |

Table II Some physical and mechanical properties of carbides. [2] [3] [4]

| Property | SiC | TiC | ZrC | B ₄ C | TaC |
|--------------------------------------------------------------|-----------------------|------|------|------------------|-------|
| Crystal structure | (β) Cub. (α) Hexa. | Cub. | Cub. | Rhom. | Cub. |
| Melting point (K) | 3120* | 3210 | 3690 | 2720 | 4150 |
| Density (g/cm ³) | 3.216 | 4.90 | 6.56 | 2.52 | 14.47 |
| Elastic modulus (x10 ⁹ N/m ²) | 400 | 450 | 348 | 289 | 285 |
| Heat of formation (kJ/mol) | 69 | 185 | 200 | 71 | 145 |
| Thermal expansion coefficient (x10 ⁻⁶ /deg) | 4.3 | 7.95 | 7.01 | 4.5 | 7.09 |
| Thermal conductivity (W/m·deg) | 80-170 | 30 | 20 | 27 | 22 |
| Specific heat (J/mol·deg) | 27.2 | 33.8 | 38.1 | 49.7 | 36.9 |
| Electrical resistivity (x10 ⁻⁶ Ωcm) | 10 ⁴ | 61 | 49 | - | 22 |

* decomposition temperature

The borides constitute a highly refractory group of ceramic materials characterized by extreme hardness, high electrical conductivity and stable up to very high temperatures. There are more than 30 binary borides with melting points higher than 2000°C. The most interested ones as structural materials are the diborides of titanium and zirconium.

The highest melting temperatures known today are found among the metal carbides. Interest in the carbides of silicon and transition metals originates from their good chemical stability, high temperature strength, good thermal shock resistance and relatively low specific gravity. Examples of the applications of these borides and carbides are listed in Table III.

However, there still exists many problems in processings and properties of refractory materials. Almost all the refractory materials are difficult to be sintered because of their high covalency and small diffusion coefficients of constituent elements. The use of sintering additives is effective to densify them, but it causes the degradation of high temperature strength. The difficulty in sintering complicates the manufacturing process and spends high energy cost inevitably.

Table III Examples of the applications of borides and carbides. [1] [5]

| Material | Application | Component |
|--------------------|---------------------|----------------------------|
| SiC | Automobile | Piston head |
| | | Piston rings |
| | | Valves |
| | | Cylinder liner |
| | Turbo-charger | Rotor |
| | Gas turbine | Combustor unit |
| | | Turbine rotors |
| Industrial machine | Turbine vanes | |
| Fusion reactor | Bearings | |
| | Roller | |
| | First wall | |
| | | Heat exchanger |
| TiC | Cutting device | |
| | Fusion reactor | First wall |
| TiB ₂ | MHD power generator | Electrode |
| | Cutting device | |
| AlN | Heat sink | Electric circuit substrate |
| | Crucible | Heat radiation fin |

Even if the dense ceramics can be fabricated, a serious problem that they are usually brittle remains. The research and development of composite ceramics and of joining to metals has been intensively performed in order to overcome this fault in recent years. Development of simple and economical processing of refractory materials and improvement of their qualities are the major and urgent subjects for their wide applications to structural components at the present.

The Wide objectives of the present research involves the development of high technologies which is related to fabricate advanced refractory materials under high pressure and/or high temperature. These are classified into the following three categories,

- 1) Examination of new synthesis method of refractory ceramics including some remarkable advantages such as purification of products, low energy require-

ments and losses, the simplicity and high productivity of the process.

(Chapter 2)

- 2) Application of high pressure technique to sintering of refractory materials.

(Chapter 3)

- 3) Development of new synthesis and simultaneous sintering process, investigation of the mechanisms of combustion reaction under high pressure, and applications of the process. (Chapter 4 and 5)

Chapter 2 DEVELOPMENT OF NEW SYNTHESIS PROCESS OF REFRACTORY MATERIALS

2-1 Introduction

Refractory materials have been produced by many synthesis methods, which are listed in Table IV. The solid state reaction synthesis is a usually available process, but requires long reaction time in high temperature furnace.

While, a unique process of self-propagating high temperature synthesis (SHS), also called as combustion synthesis, is a simple and efficient way to fabricate numerous high quality refractory materials and other compounds. This process was first developed by Merzhanov et al. in 1976 [6]. Similar process is known as thermite reaction between powdered aluminum and iron oxide, which has been used for welding.

The reactions of SHS can be divided into three categories depending on the situation of starting elements: (1) solid-solid system ($Ti+2B \rightarrow TiB_2$, $Si + C \rightarrow SiC$ etc.), (2) solid-liquid ($2Ti+N_2 \text{ liquid} \rightarrow 2TiN$ etc.), (3) solid-gas ($3Si+2N_2 \text{ gas} \rightarrow Si_3N_4$ etc.). The first category is often called gassless combustion and is the main subject investigated in the present work.

Table IV Introductory outline of the various methods to prepare TiB_2 , TiC and SiC powders.

TiB_2 [1]

| Method | Reaction |
|------------------------------------------------------------------------------------------------|-------------------------------------------------------------------------------------------------------------------------------|
| Direct combination of the elements | $Ti + 2B \rightarrow TiB_2$ |
| Reduction of a metal compound and boron halide with hydrogen | $TiCl_4(g) + 2BCl_3(g) + 5H_2(g)$ $\rightarrow TiB_2(s) + 10HCl(g)$ |
| Reduction of a metal oxide or some other metal compounds using carbon, boron and boron carbide | $TiO_2(s) + 4B(s)$ $\rightarrow TiB_2(s) + B_2O_3(g)$ $2TiO_2(s) + B_4C(s) + 3C(s)$ $\rightarrow 2TiB_2(s) + 4CO(g)$ |
| Reduction by using other metals | $TiO_2(s) + B_2O_3(s) + 5Mg(s)$ $\rightarrow TiB_2 + 5MgO$ |

TiC [11]

| Method | Reaction |
|----------------------------------------------------------------------|-----------------------------------------------------------------------------------------------------|
| Direct reaction of the elements or metal hydrides | $\text{Ti} + \text{C} \rightarrow \text{TiC}$ |
| Reduction of a metal oxide with excess carbon in reducing atmosphere | $\text{TiO}_2 + 3\text{C} \rightarrow \text{TiC} + \text{CO}$ |
| Reaction of a metal fluoride with a carbide and hydrogen gas | $2\text{TiCl}_4 + \text{CaC}_2 + 3\text{H}_2 \rightarrow 2\text{TiC} + \text{CaCl}_2 + 6\text{HCl}$ |

SiC [12] [13] [14]

| Method | Reaction |
|---------------------------------------------------------------------------------------|-----------------------------------------------------------------------------------------------|
| Direct reaction of the elements | $\text{Si} + \text{C} \rightarrow \text{SiC}$ |
| Reduction of a metal oxide with excess carbon in reducing atmosphere (Acheson method) | $\text{SiO}_2 + \text{C} \rightarrow \text{SiC}$ |
| Precipitation from the gas phase by reacting the metal halide in hydrogen | $4\text{SiCl}_4 + 2\text{C}_2\text{H}_5 + 3\text{H}_2 \rightarrow 4\text{SiC} + 16\text{HCl}$ |
| Thermal decomposition | $\text{CH}_3\text{SiCl}_3 \rightarrow \text{SiC} + 3\text{HCl}$ |

The SHS process is based on the fact that the strong exothermic reaction, which occurs during the formation of a compound, can propagate spontaneously through a cold pressed reactant in a few seconds. Figure 1 shows a schematic representation of the combustion reaction. The novel feature of SHS is that sufficient heat is released to support a self-propagating reaction after igniting at one end of the reactant. Figure 2 shows a photograph of combustion reaction of Ti-C system as an example. Titanium and carbon powders are first mixed and lightly pressed into a pellet. The pellet is ignited at one end by a suitable external high temperature heat source (above 2000°C), which provides the heat impulse to initiate the chemical reaction between Ti and C. The combustion zone propagates along the

axis of the cylindrical sample accompanying with formation of final product (TiC).

Typical characteristics of SHS process are

- 1) Reaction temperature : $1500^{\circ}\text{C} \sim 4000^{\circ}\text{C}$
- 2) Propagation velocity of combustion zone : $0.1 \sim 15 \text{ cm/sec}$
- 3) Heating rate : $10^3 \sim 10^6 \text{ }^{\circ}\text{C/sec}$

This SHS process can be distinguished by the following features.

- 1) Almost all the refractory ceramic powders can be synthesized easily and economically.
- 2) SHS is able to simplify the powder processing and thus need not high temperature furnace and sophisticated processing equipment.
- 3) Compounds can be synthesized within a few seconds.
- 4) Impurities can be excluded by evaporation accompanied with the released high heat at the combustion reaction. This feature is often called as "self-purification effect".

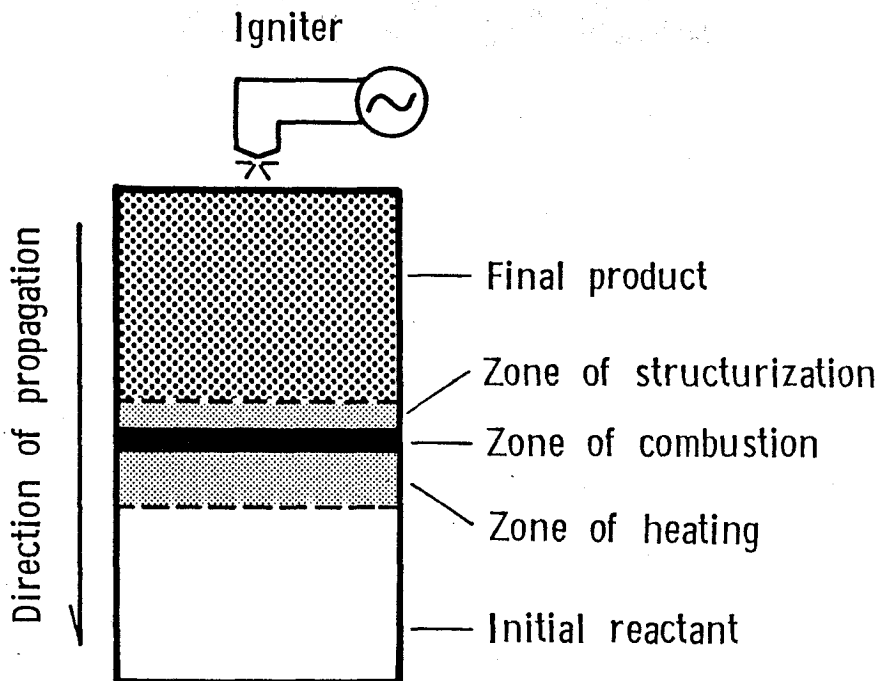


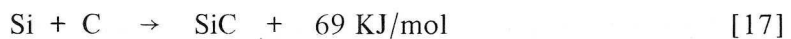
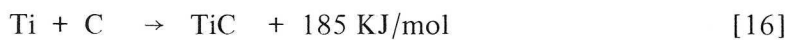
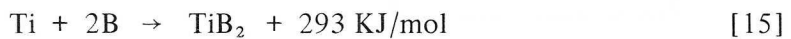
Fig. 1 Schematic representation of a combustion front moving down a cylindrical compact.



Fig. 2 Photograph of an ignited compact of a mixture of Ti and C powders.

The basic studies of the solid-solid reaction system in SHS process and its application have begun in recent years [8] - [10].

The possibility of self-sustaining combustion is basically dependent on the magnitude of heat of formation (ΔH). In the present study, three refractory materials, TiB_2 , TiC and SiC , were chosen to investigate the effect of their differences of ΔH on SHS reaction. Chemical reactions of the compounds are the followings.



2-2 Experimental procedure

2-2-1 Starting Materials

Ti and B element powders for TiB_2 , Ti and C for TiC and Si and C for SiC with a variety of particle sizes were used to examine their influences on the conversion efficiency into compound and on the particle size of products. The characteristics of each element powder are summarized in Table V.

They were well mixed with a desired molar ratio in n-hexane and dried in vacuum. Each mixed reactant was uniaxially compressed into a rod with 7 mm in diameter and 25 mm in length, and then supplied to SHS experiment.

Table V Characteristics of Ti, Si, B and C powders used as starting elements.

| No. | Materials | Manufacturer | Particle size (μm) | Purity (%) | Remarks |
|----------------|-----------|---------------------------------------------|---------------------------------|------------|---------|
| T ₁ | Titanium | Osaka Titanium, Co., Ltd. | < 40 | 99.5 | |
| T ₂ | Titanium | Osaka Titanium, Co., Ltd. | < 10 | 97.9 | |
| S ₁ | Silicon | Hgh Purity Chemical Laboratories, Co., Ltd. | < 5 | 99.9 | 1 |
| S ₂ | Silicon | Vacuum Metallurgical, Co., Ltd. | 0.1* | - | 1 |
| S ₃ | Silicon | Komatsu Electric Metal, Co., Ltd. | 0.001* | - | 2 |
| B ₁ | Boron | Wako Pure Chemical Industries, Ltd. | 2 | 95 | 3 |
| C ₁ | Graphite | Tokai Carbon, Co., Ltd. | 10** | 99.9 | |
| C ₂ | Carbon | Daicel Chemical Industries, Ltd. | 0.031** | 95.4 | 4 |
| C ₃ | Carbon | Mitsubishi Chemical Industries, Ltd. | 0.021** | - | 3 |

* : Mean particle size of the elements

** : Primary particle size of the elements

1 : Crystalline state

2 : Synthesized by the thermal decomposition of SiH_4 , amorphous state

3 : Almost X-ray amorphous

4 : Purified in Cl_2 gas at 2400K for 2h, partially crystalline state

2-2-2 Various Methods for Ignition of SHS

When compounds had a relatively high heat of formation, a cold pressed reactant was placed on a carbon ribbon heater and ignited at the one end as shown in Fig. 3 (a). Another several sources for ignition, such as electrically heated wire, electric spark and laser, etc., are also available [8] [16] [18].

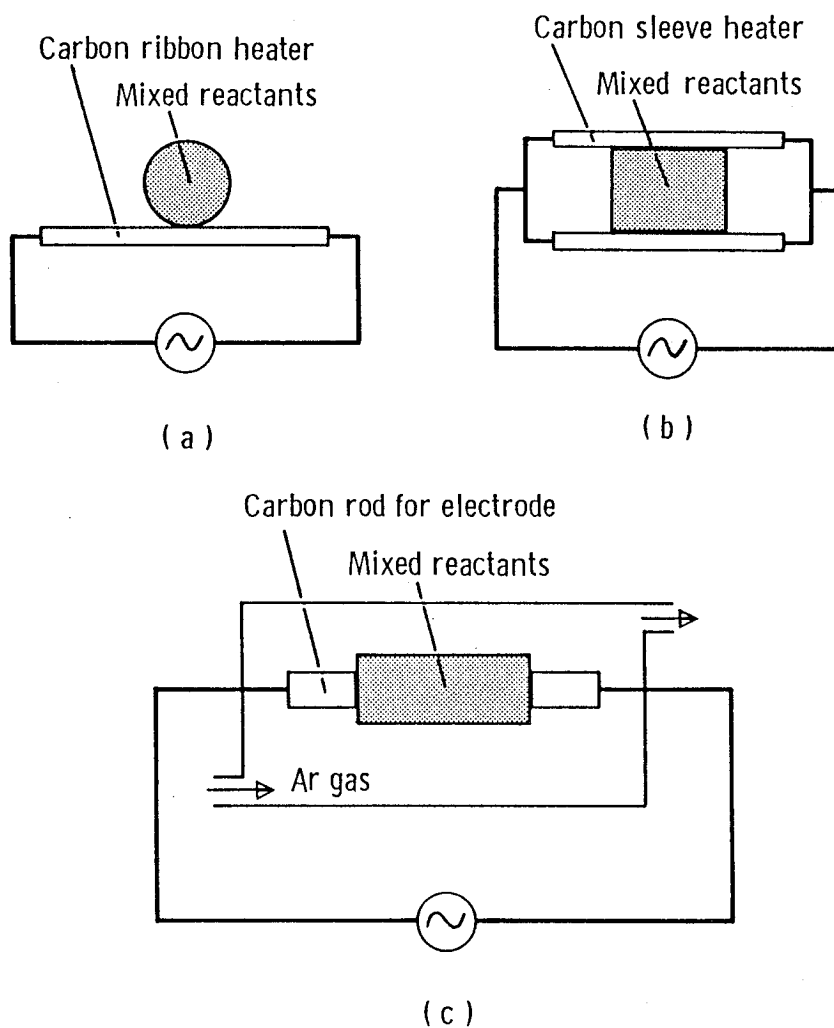


Fig. 3 Various excitation methods of SHS.

- (a) ignition by carbon ribbon heater
- (b) ignition by carbon sleeve heater
- (c) ignition by direct passing of electric current through the reactant

On the other hand, when the quantity of heat released on formation of compound is relatively low, the SHS reaction is liable to be incomplete because of the loss of reaction heat in the non-adiabatic system of the experiment. A carbon sleeve heater is useful in this case so as to prevent the heat loss and serves as a ignitor having large ignition area. The reactant is inserted into central part of the carbon sleeve. Schematic representation of the apparatus is shown in Fig. 3 (b).

Further, it was considered from the concept of these ignition processes that the heat generated when electric current passed directly through the reactant itself, instead of heating by external carbon heater, would supply the most effective thermal source for ignition, if the reactant is electrically conductive. The experimental arrangement for this ignition method is shown in Fig. 3 (c). The cold-pressed reactant was sandwiched carefully between the carbon rods for electrode.

The typical ignition program by direct passing of electric current through the reactant is shown in Fig. 4. The constant voltage (5V in this experiment) was

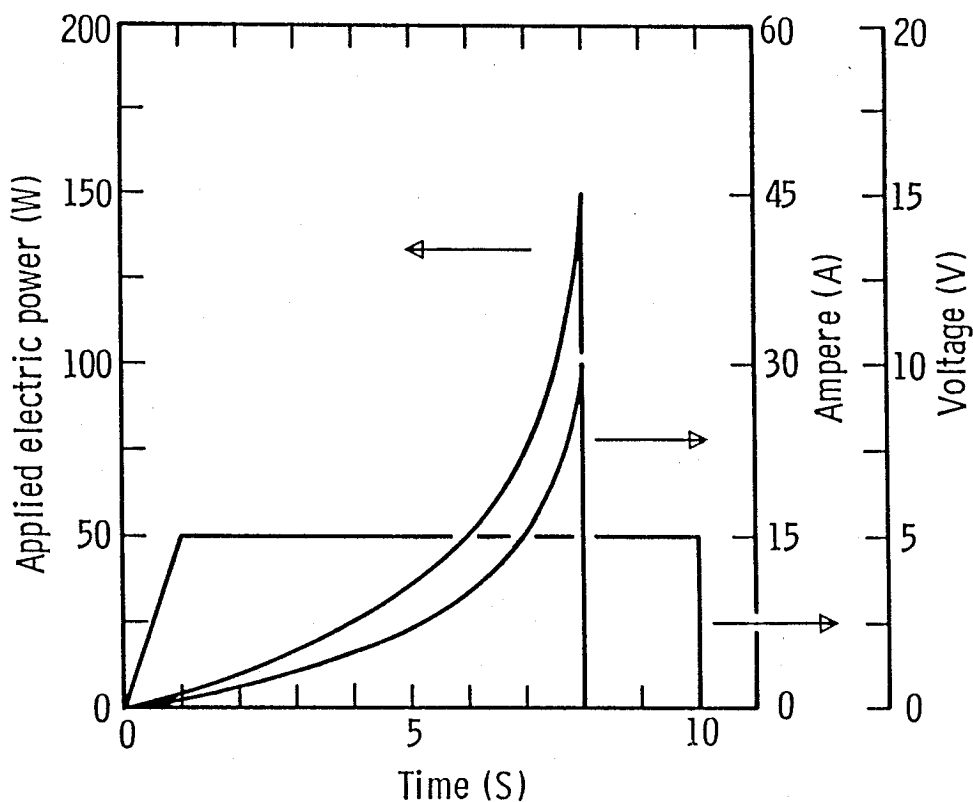


Fig. 4 Typical ignition program by direct passing of electric current through the reactant.

applied to the reactant placed in a vessel which was filled with Ar gas.

2-2-3 Characterization of the Products

The products were examined by using scanning electron microscopy and X-ray powder diffractometry with $\text{CuK}\alpha$ radiation. The conversion efficiency from initial reactant into compound was determined as the ratio in amount of C/(C + R) calculated from the areas of main peaks of C and R in X-ray powder diffraction pattern of the product. (The sign C and R denote the compound and the residual elements, respectively.) The lattice constants were calculated from X-ray diffraction pattern using Si powder as an internal standard.

Oxygen contents were analyzed by thermal decomposition method using "LECO" apparatus. The samples were decomposed in a graphite crucible with the aid of a flux of molten Ni metal. Oxygen within the sample is changed to CO_2 and determined by infrared absorption. The limit of detection is about 10-20 ppm.

2-3 Results of SHS Processing and Characteristics of the Products

2-3-1 Preparation and Properties of TiB_2

SHS processing of TiB_2

All of the reactions were carried out in Ar gas using the ignition apparatus of carbon ribbon heater as shown in Fig. 3(a). The cylindrical pellet, consisting of stoichiometric mixtures of Ti and B, burns almost explosively after igniting at one end surface of the pellet. The reaction temperatures were raised almost instantaneously up to over 2300K. The rate of reaction and the appearance of the products were dependent on the particle size distribution of the starting powder, in particular for Ti. Table VI lists the results for SHS reaction of TiB_2 . Increase of combustion velocity with decreasing the particle size of Ti, is considered due to the activation of reaction accompanied with the increase of the contact area between Ti and B particles.

Characteristics of TiB_2 powder

The product was identified as hexagonal TiB_2 , containing a small amount of TiB phase by X-ray analysis in case when mixing molar ratio of B/Ti was 2.0. The result is summarized in Table VII. Initial reactants converted entirely into stoichiometric compounds and residual elements were not detected. Boron element should be

Table VI Relation between particle size of the elements and combustion phenomena.

| Components (No.) | Combustion velocity | Appearance of the products |
|----------------------------------------------|---------------------|---------------------------------------------------------|
| Ti(T ₁ *) + 2B(B ₁) | Remarkably fast | Sponge-like product as large as twice of initial volume |
| Ti(T ₂ ***) + 2B(B ₁) | Explosively | Fragmentation into many small peaces |

* Particle size below 40 μm

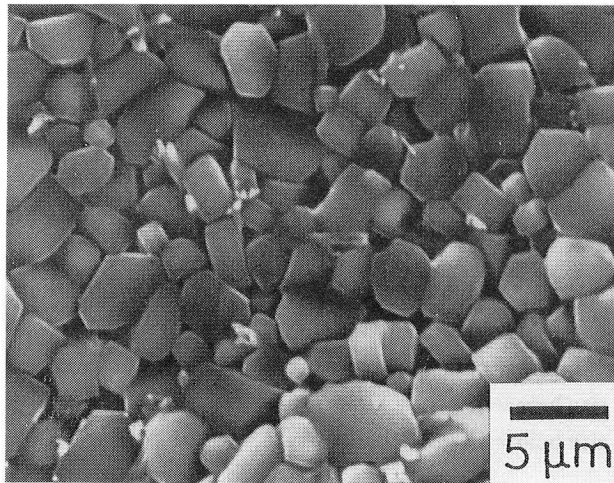
** Particle size below 10 μm

Table VII Characteristics of the product fabricated by SHS.

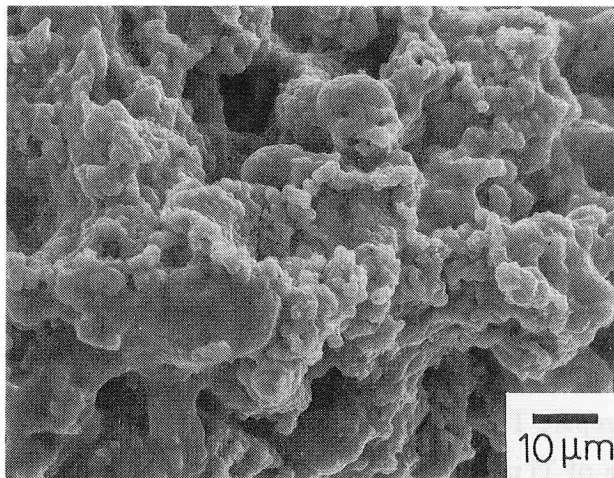
| Mixing molar ratio (B/Ti) | Crystalline phase | Intensity ratio of the main peak (%) | Lattice constant of the product | |
|---------------------------|-------------------|--------------------------------------|---------------------------------|--------|
| | | | a(nm) | c(nm) |
| 2.0 | TiB ₂ | 99 | 0.3029 | 0.3230 |
| | TiB | 1 | - | - |

spent not only to prepare TiB₂ phase, but also to reduce oxide film which probably exists on the surface of Ti particles. Therefore, the lack of boron might act to form TiB phase.

Figure 5 shows photographs of the fracture surfaces of the porous products. Fine particles of TiB₂ distributed uniformly with average grain sizes of 5 μm and 2 μm when the Ti powders with below 40 μm and around 10 μm in size were used for the starting metal element, respectively. In all cases, grain size of the products was much smaller than the particle size of starting Ti powder. And relatively dense parts were observed in some parts of the porous products. They seem to be produced by self-sintering of almost molten particles of TiB₂ which were formed due to the high reaction heat.



(a)



(b)

Fig. 5 Scanning electron micrographs of the fracture surface of the porous products which were fabricated by SHS using Ti powders with different particle sizes.

(a) $\text{Ti}(T_1) + \text{B}(B_1)$

(b) $\text{Ti}(T_2) + \text{B}(B_1)$

2-3-2 Preparation and Properties of TiC

SHS processing of TiC

The SHS experiments were conducted using various reactants with different mixing molar ratios of titanium and carbon. The reactant was ignited at one end of the cylindrical pellet on a carbon ribbon heater in a vessel which was filled with Ar gas as shown in Fig. 3(a). SHS reaction proceeded rapidly in the range of $C/Ti > 0.65$. The original shape of the compact was kept in this case. Figure 6 shows a typical appearance of the obtained porous product of TiC. On the other hand, it was impossible to ignite the reactants mixed in the region of excess metal ($C/Ti < 0.65$).

Characteristics of TiC powder

Conversion efficiency was related to the mixing molar ratio of each element but independent on the particle size of Ti powder. These results are shown in Fig. 7.

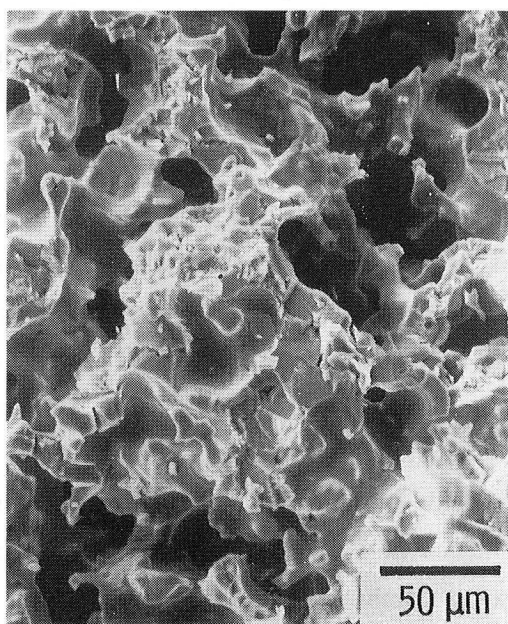


Fig. 6 Scanning electron micrograph of the fracture surface of the TiC compact which was fabricated using Ti and C powder mixtures with stoichiometric ratios as a reactant.

X-ray powder diffraction revealed that the mixture of Ti and C converted entirely to a single phase compound of titanium carbide in the range of C/Ti < 0.95. Whereas the starting elements remained when the mixing ratio was over 0.95. This value corresponded with the maximum solubility of carbon to titanium reported in the phase diagram of Ti-C system [19].

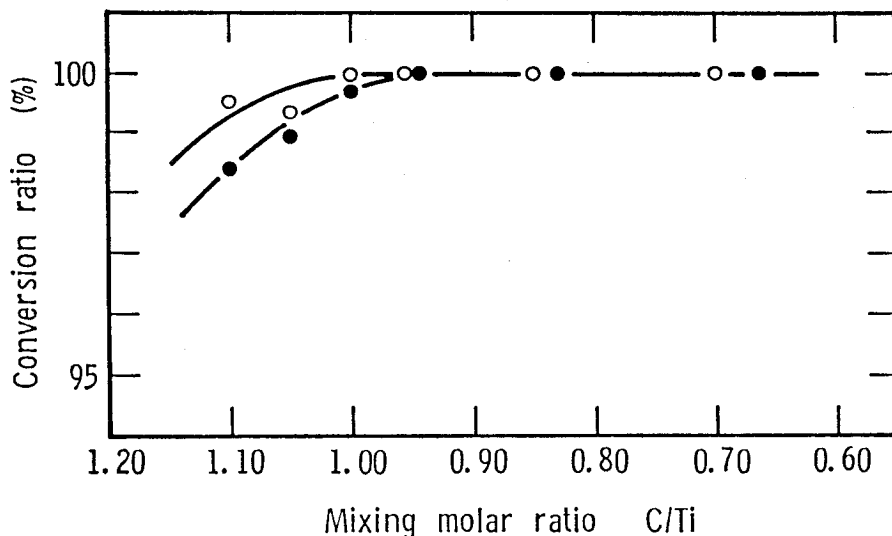


Fig. 7 Conversion efficiency into single phase compound of TiC_x as a function of mixing molar ratio of each Ti and C powder mixtures.

● $T_1 + C_2$ ○ $T_2 + C_2$

Figure 8 shows the lattice constant as a function of mixing molar ratio of each element. Variations of the lattice constant showed the similar tendency to the previous report concerning with that variations in Ti-C system [20], but the absolute values were lower especially when the fine $Ti(T_2)$ was used as a starting element. It was well known that oxygen substitution forms a series $Ti(C, O)$ and reduces the lattice constant with increasing oxygen content. Table VIII shows the oxygen contents of the two kinds of reactants and the products after combustion, which were measured by means of "LECO" apparatus. The oxygen contents did not change before and after combustion and was higher in the product obtained from reactant of $T_2 + C_2$ powders than in that from $T_1 + C_2$ powders. The self-purification effect was not recognized in this system. This is probably ascribed to the fact that oxygen can be easily introduced into TiC lattice before getting away as Co gas.

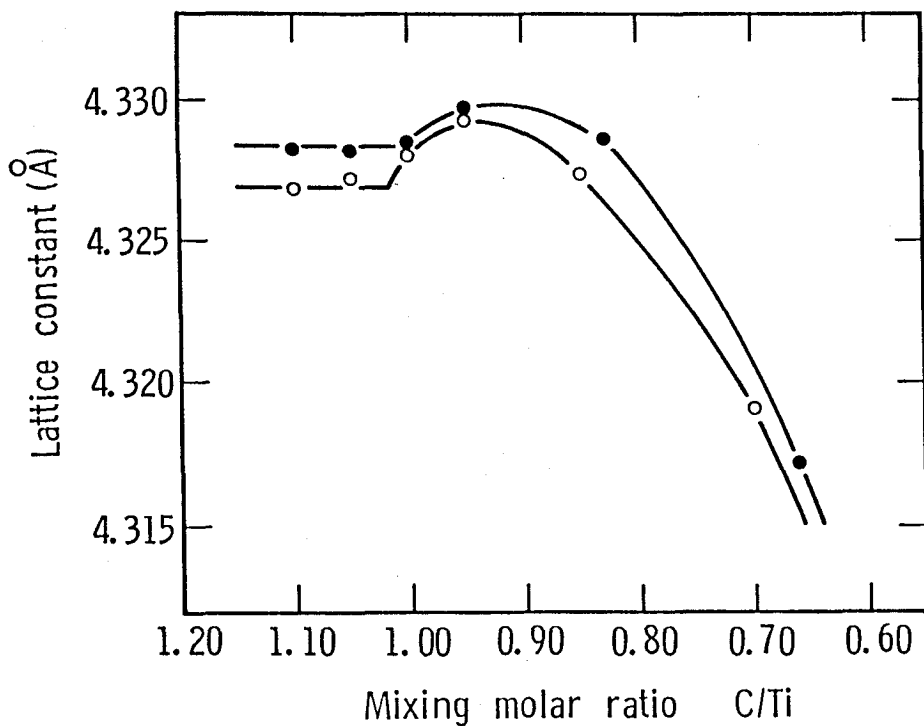


Fig. 8 Lattice constant as a function of mixing molar ratio of each powder mixture of Ti and C.

● T₁ + C₂

○ T₂ + C₂

Table VIII Oxygen contents of the reactant and the product obtained after combustion treatment.

| | Oxygen contents (wt%) | |
|-------------------|---------------------------------|---------------------------------|
| | T ₁ + C ₂ | T ₂ + C ₂ |
| Reactant | 0.34 | 0.93 |
| Product after SHS | 0.34 | 0.90 |

2-3-3 Preparation and Properties of SiC

The quantity of heat released on formation of SiC is reported as 69 kJ/mol at room temperature. Since this value is relatively low in comparison with the heat

released on TiB_2 formation (293 kJ/mol), SHS of SiC is liable to be incomplete. When the cold-pressed reactant was placed on a carbon ribbon heater and ignited by the way as shown in Fig. 3(a), the conversion efficiency into SiC was about only 64%.

So, in order to improve the ignitability and conversion efficiency of SiC, it is suggested to preheat the mixed reactant in a furnace prior to ignition in order to supplement the loss of heat in the actual non-adiabatic system [18]. However, the time of preheating becomes longer, the compound would be formed even in a small amount by solid-state reaction, which will inhibit the ignition. Therefore, the reactants must be preheated rapidly and uniformly prior to ignition.

A carbon sleeve heater was adopted from these considerations to improve the conversion efficiency. The reactant was ignited by the way as illustrated in Fig. 3(b), so that the conversion efficiency reached over 99%.

It was considered, however, that a large temperature gradient would appear in reactant when its volume increases to the industrial production size and the preheating would not reach to the interior of the reactant. A direct passing method of electric current for SHS of SiC was developed as a useful way to overcome this disadvantage.

SHS processing of SiC with direct passing of electric current

Time dependences of applied electric power directly to the reactant and the sample temperature measured by using optical pyrometer are shown in Fig. 9. It is considered that SHS process of SiC is classified into three stages, of which periods are denoted with numbers at the upper part of this figure.

The 1st stage – This is preheating stage prior to excitation of SHS reaction. Heat, generated by the resistivity of reactant, preheats the sample and raises the temperature of the middle part up to 1100K. When the applied electric power was cut off before excitation of reaction, SiC was not detected. It is proved that the reactants is subjected to very rapid preheating.

The 2nd stage – SHS reaction originated in the middle part of the sample, where the temperature was relatively higher than the other parts. As SiC was produced in the middle part of the sample, the electric resistivity increased rapidly and the current dropped suddenly as seen in Fig. 4.

The 3rd stage – The spontaneous reaction proceeded toward both ends of the

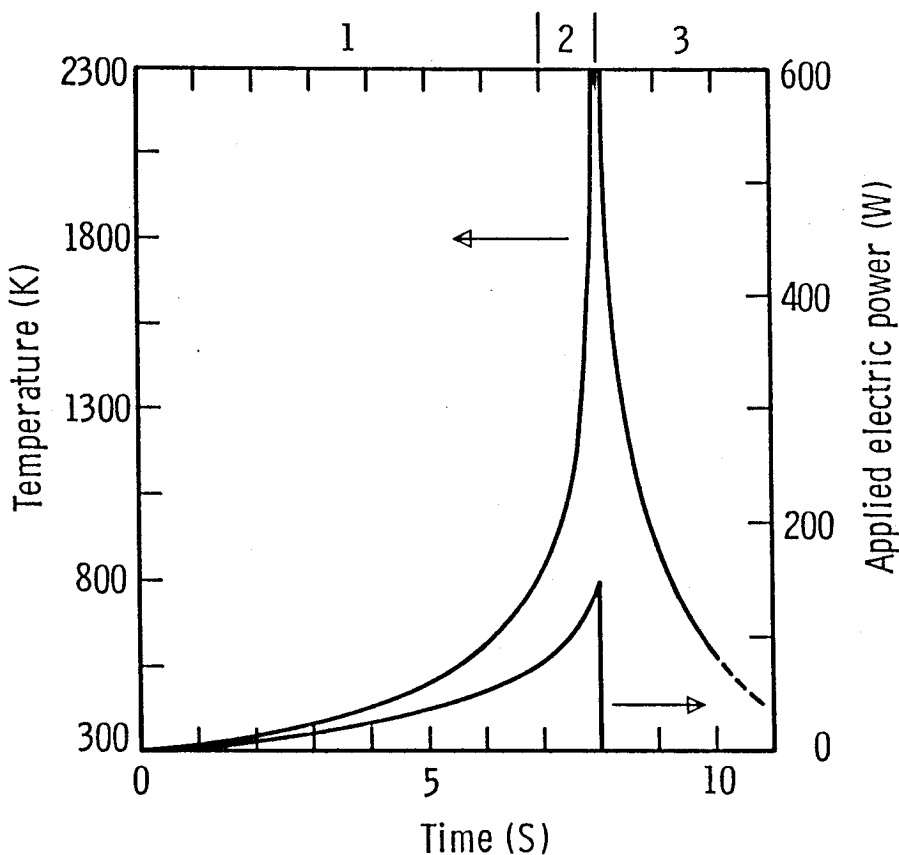


Fig. 9 Time dependence of sample temperature and applied electric power.

sample with emitting white heat after the applied electric power dropped and SiC was synthesized instantaneously.

The duration of the reaction measured by video tape recording was within 0.1s. The porous products with greenish or pale yellowish color were obtained, which could be easily pulverized into fine powders.

Since silicon can be easily oxidized in air, an oxide layer formed on the surface of Si particles is unfavourable to the excitation of SHS. This oxide layer is probably broken by an electric spark between particles during passing of electric current at the initial stage. The break-down of oxide layer should be effective for an activation of SHS reaction.

Characteristics of SiC powder

It was revealed from the typical X-ray diffraction pattern as shown in Fig. 10 that the product consisted of stoichiometric β -SiC containing a small amount of α -SiC. In addition, sharp β -SiC peaks indicated that the grains were well crystallized. Table IX lists the conversion efficiencies into SiC in reactions of the mixed powders with different mean particle sizes at the fixed molar ratio of $C/Si = 1.05$. The mixed reactant composed of relatively large particles, S_1 and C_1 , could not be ignited by the direct passing method of electric current. The conversion efficiency into SiC increased with decreasing particle size of Si and C, and reached up to 100% when mixed powders of S_3 and C_3 were used as a reactant. Conversion efficiency was related to the mixing molar ratio of starting elements, too. Figure 11(a), (b) and (c) show the conversion efficiencies and contents of residual elements as

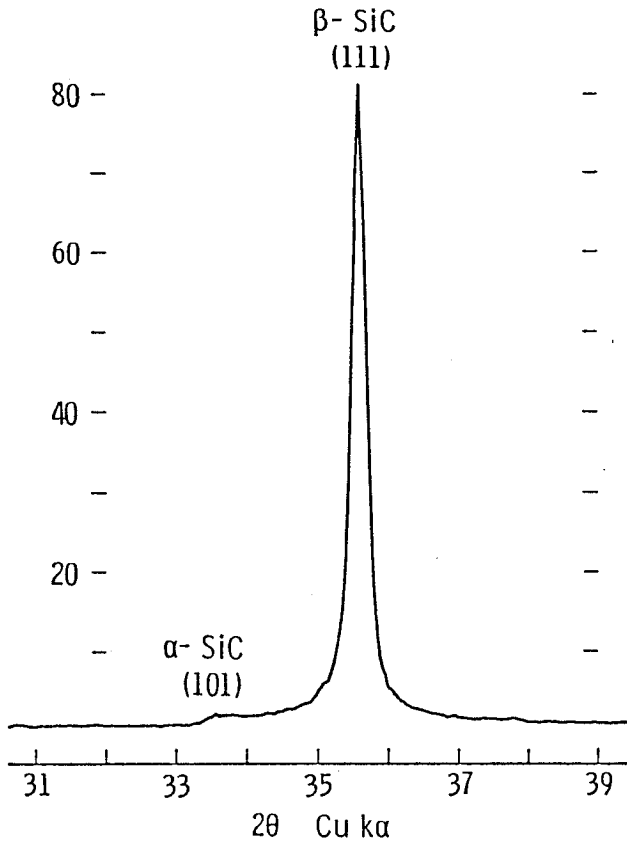


Fig. 10 Representative X-ray diffraction pattern of SiC powders fabricated by direct passing method of electric current.

Table IX Effect of particle size of starting elements on conversion efficiency into SiC powders at the molar ratio of C/Si = 1.05.

| Si \ C | C ₁ (10 μm) | C ₂ (0.031 μm) | C ₃ (0.021 μm) |
|-----------------------------|---------------------------|------------------------------|------------------------------|
| S ₁ (5 μm) | NI* | 99.1% | - |
| S ₂ (0.01 μm) | - | 99.8% | 100.0% |

* Not igniting

a function of molar ratio of reactants, S₁ + C₂, S₃ + C₂ and S₃ + C₃, respectively. The conversion efficiency was much improved at the molar ratio of C/Si = 1.05 in every reactant.

The presence of excess carbon in the starting mixture may act to reduce SiO₂ film which probably exists on the surface of Si particles. Figure 12 shows SEM photos of each SiC powder. It was observed that the particle size of SiC powder decreased with the decrease of that of starting elements. Submicron SiC powder which has narrow particle size distribution could be synthesized when S₃ + C₃ powder was used as reactant.

As another feature of the SHS reaction, a "self-purification" effect can be expected by evaporating volatile impurities contained in the reactants and by reducing oxide films on metal particles due to high temperature during the reaction [21]. It is well known that oxygen impurities in commercial ceramic powders cause a significant reduction of mechanical properties of refractory materials fabricated with them. In Table X, the oxygen contents of initial reactants and products of SiC are listed. The oxygen contents of SiC powders fabricated by SHS were reduced by almost one order in comparison with that of mixed reactant. This fact suggests the possibility that the SHS reaction of SiC has a self-purification effect to remove oxide film probably existed on Si particles.

As the results, it has been shown that a stoichiometric β-SiC powder could be synthesized economically in an extremely short time by using a new ignition method which can effectively excite the SHS reaction by direct passing of low electric power current through a reactant.

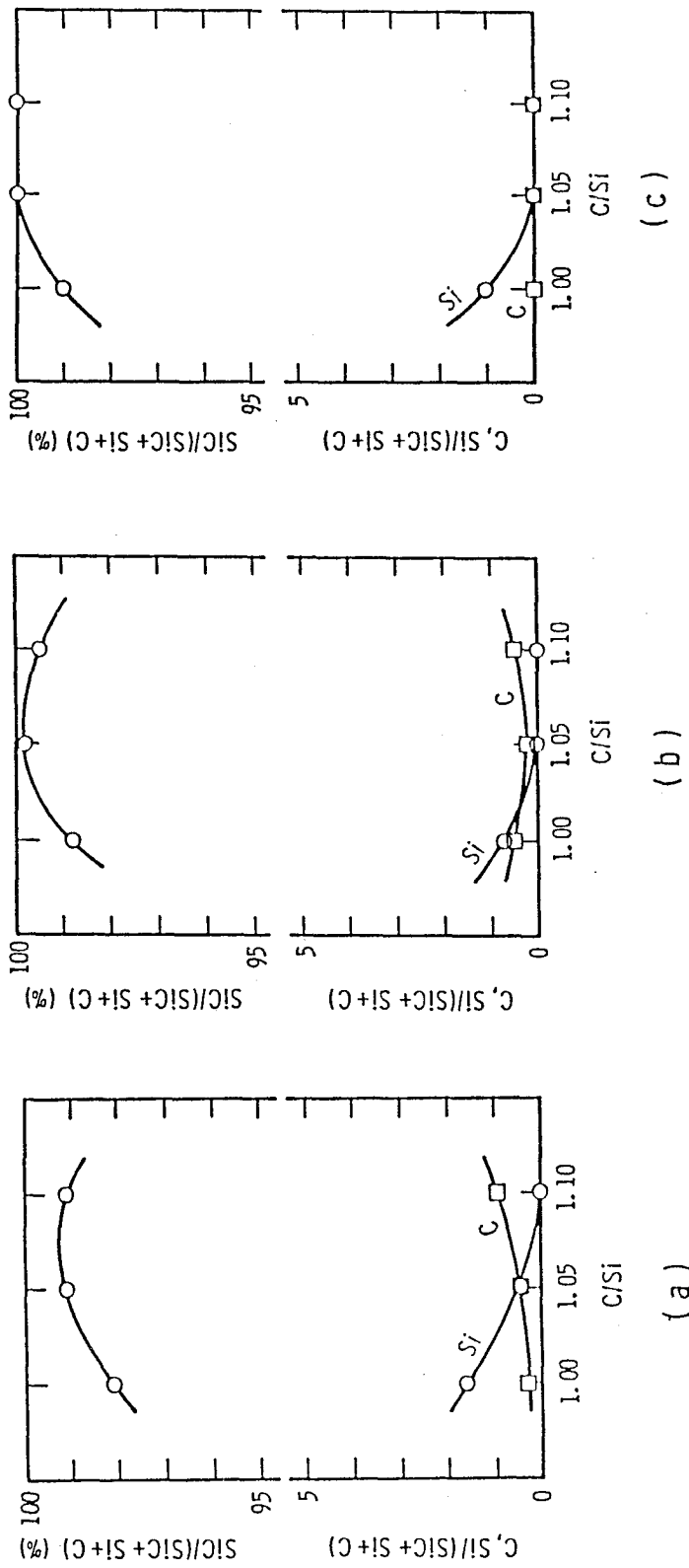
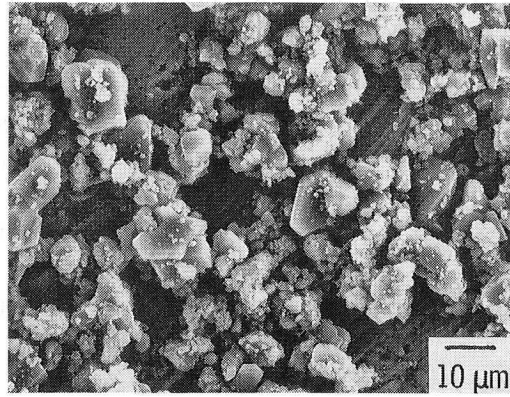


Fig. 11 Conversion efficiencies into β -SiC and contents of residual elements as a function of mixing molar ratio of Si and C powders.

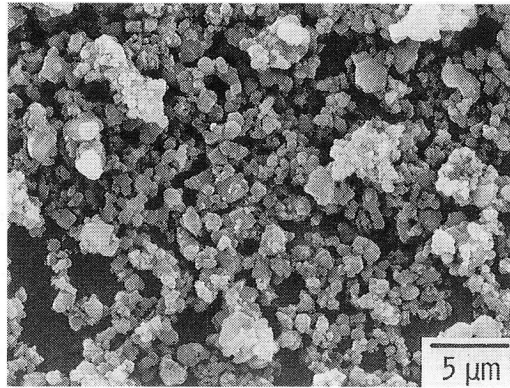
(a) $S_1 + C_2$

(b) $S_3 + C_2$

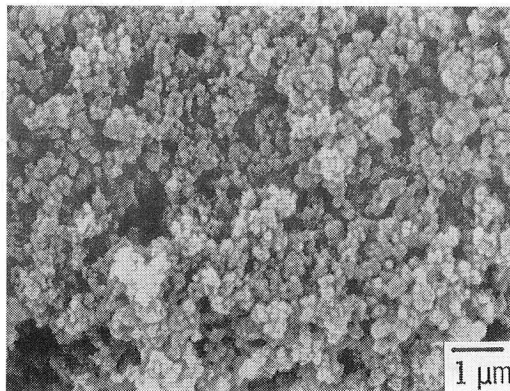
(c) $S_3 + C_3$



$S_1 (<5\mu\text{m}) + C_2 (0.031\mu\text{m})$



$S_3 (0.01\mu\text{m}) + C_2 (0.031\mu\text{m})$



$S_3 (0.01\mu\text{m}) + C_3 (0.021\mu\text{m})$

Fig. 12 Scanning electron micrographs of SiC powders fabricated from the mixed reactants with different particle sizes.

Table X Oxygen content of SiC powders analyzed by thermal decomposition method using "LECO" apparatus.

| | Oxygen content (wt%) |
|-----------------------------|-------------------------|
| Reactant (Si + C) | 0.79 |
| SiC powder after combustion | 0.085 |
| Commercial powder of SiC | |
| A company | 0.55 |
| B company | 0.72 |
| C company | 1.2 |

2-4 Discussion

2-4-1 Selection of Suitable Ignition Method by Adiabatic Temperatures

The possibility of self-sustaining combustion reaction is dependent on the magnitude of the combustion temperature. It is considered that a combustion temperature above 2500K is required to propagate the synthesis reaction at atmospheric pressure. The adiabatic temperature, T_{ad} , which has been proposed to predict the feasibility of combustion [18], is the attainable temperature of the product in ideal adiabatic system and thus T_{ad} gives an upper limit to actual combustion temperature. T_{ad} is calculated under the assumption that all the heat released by the reaction is used ultimately to raise the temperature of the final product up to T_{ad} . The adiabatic temperature is calculated by the following equation,

$$\Delta H_{T_0} = \int_{T_0}^{T_{ad}} C_p(S) dT$$

where ΔH_{T_0} is heat of formation at T_0 and $C_p(S)$ is the heat capacity of the product. When the transformation to molten phase of the product is included, the heat balance can be expressed as follows.

$$\Delta H_{T_0} = \int_{T_0}^{T_m} C_p(S) dT + \Delta H_m + \int_{T_m}^{T_{ad}} C_p(L) dT$$

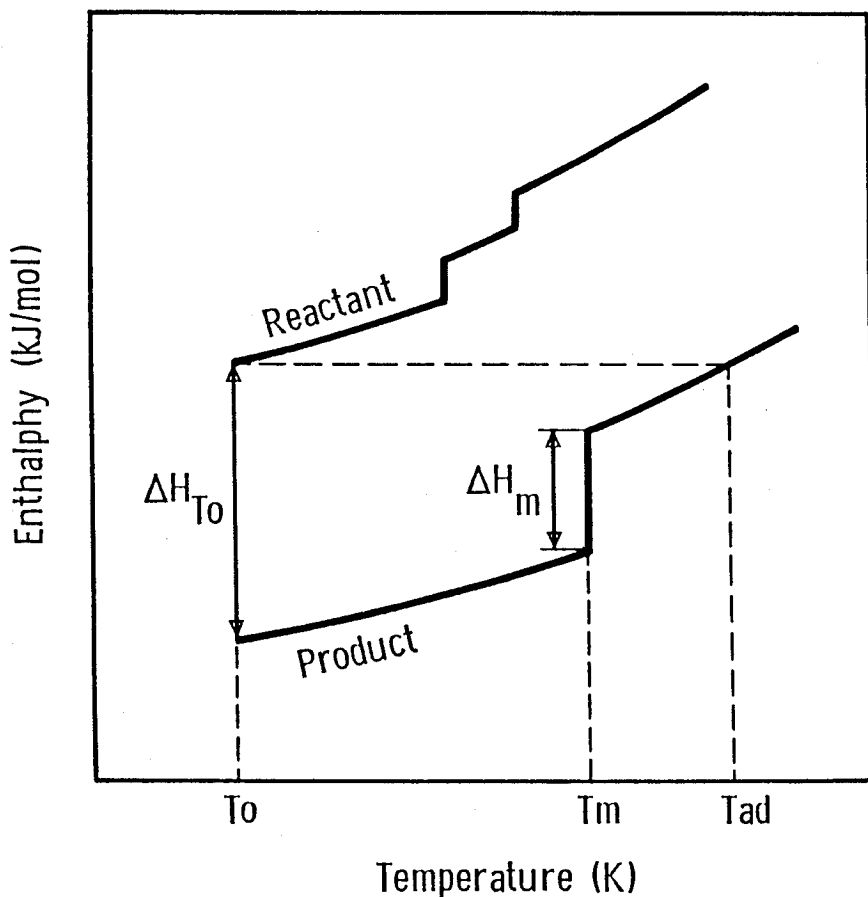


Fig. 13 Schematic representation of enthalpy curves for reactant and product.

This equation is applied to a case in which a product fuses at T_m . C_p (S) and C_p (L) are the heat capacities of solid and liquid phases of the product, respectively. The heat of fusion for the product is represented by ΔH_m at T_m . In practice, T_{ad} can be obtained diagrammatically by drawing the enthalpy curves for the mixed reactant and the product using available enthalpy data as seen in Fig. 13. In Table XI, T_{ad} are listed for some refractory materials.

In case of TiB_2 and TiC , the adiabatic temperature coincide with the melting points of TiB_2 (3193K) and TiC (3210K), which are high enough to produce the combustion reaction, so that the reactants can be ignited easily at one end of the pellets and well burned in an very short time. Since the coalescence of molten grains of TiC (Fig. 6) and TiB_2 (Fig. 14) was observed in the combustion products, the

Table XI Summary of melting points and adiabatic temperatures for some non-oxides.

| Compound | Melting temperature (K) | Adiabatic temperature (K) |
|--------------------------------|-------------------------|---------------------------|
| SiC | 3073 (decomposition) | 1850 |
| TiC | 3210 | 3210 |
| TiB ₂ | 3193 | 3193 |
| TaB ₂ | 3273 | 2729 |
| TiN | 3203 | 4889 |
| Si ₃ N ₄ | 2173 (Sublimation) | 4856 |

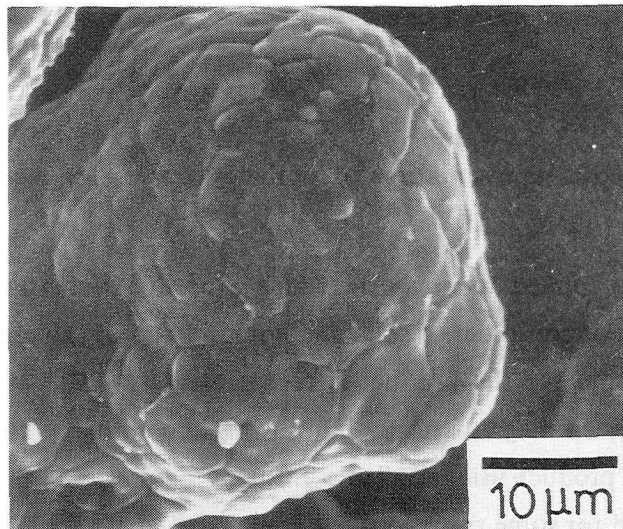


Fig. 14 Scanning electron micrograph of the fracture surface of the TiB₂ compact which was fabricated by SHS.

actual combustion temperature is considered to have reached the adiabatic temperature. Thus, the concept of the adiabatic temperature is useful in making general predictions.

The formation of SiC from the constituent elements has an adiabatic temperature of 1850K which is significantly lower than the minimum temperature of 2700K required to produce the combustion reaction. In fact, a conversion efficiency into SiC was very low ($\sim 64\%$) when the reactant was ignited at one end of the pellet without preheating. An increase of T_{ad} to 2700K is performed by raising the initial temperature from 300K to at least 1300K as shown in Appendix I. In actual, this has been accomplished by preheating the mixed reactant prior to ignition.

Direct passing of electric current developed in the present investigation has the following advantages to initiate combustion reaction.

- 1) Preheating the reactant to 1300K rapidly and uniformly.
- 2) Effective break-down of the oxide layer to activate SHS reaction.

This ignition method can be applied to the fabrication of many other ceramics with low heat of formation if the reactant is electrically conductive.

2-4-2 Effect of SHS Reaction on Self-Purification

The high temperature of combustion provides a "self-purification" effect by evaporating volatile impurities contained in the reactants and by removing oxide films on metal particles. Self-purification effect was recognized for SiC, but not for TiC. This fact suggests that whether self-purification takes place or not is owing to the possibility of oxygen substitution to form an oxycarbide compound. Same results were observed in case of Si_3N_4 synthesized through SHS reaction [22]. Therefore, in case of TiC, the purity of the final product is essentially controlled by the purity of the initial elements.

2-4-3 Effect of Isostatic Pressure on SHS Reaction

When a cold-pressed reactant body mixed with Ti and B fine powders was ignited to produce TiB_2 , the original shape of the body could not be kept after SHS reaction owing to the fragmentation into many small pieces. Same feature was also observed on SiC fabricated by direct passing method of electric current. In these cases, reaction temperatures of each fragment dropped suddenly, followed by the decrease in the total yield of the product. On the other hand, the samples of TiC

after combustion remained the original shape in any conditions under investigation.

It is suggested from these results that the boiling of reactants should blow out the compact, which depends on whether adiabatic temperature exceeds the boiling point of constituent elements, or not. Appendixes I and II indicate that boiling points of boron and silicon are lower than the adiabatic temperatures of TiB_2 and SiC when excited by preheating up to 1300K, respectively. The boiling points of both Ti and C are higher than the adiabatic temperature of TiC , and consequently boiling can not take place in this system. It is well known that the boiling points of elements generally increase by applying pressure. So, SHS reactions of TiB_2 and of SiC under preheating were examined under Ar gas pressure of 20MPa using HIP equipment. The original shape of TiB_2 and SiC compacts was kept by increasing boiling points of elements, and a significant effect of applying pressure was confirmed on the explosive SHS reaction.

Chapter 3 APPLICATION OF HIGH PRESSURE TECHNIQUE TO SINTERING OF REFRACTORY MATERIALS

3-1 Introduction

In general, refractory compounds are difficult to be sintered because of their high melting points and small self-diffusion coefficients of constituent elements which refract high covalency in chemical bond of atoms. It is almost impossible to densify refractory materials without binding agents by a conventional sintering method which is usually conducted at lower pressures below 30MPa. Common methods of densification at present are normal sintering and hot-press sintering in the presence of additives such as oxides or other appropriate elements. Although these additives play an important role to densification, they frequently cause the formation of secondary phases at grain boundaries. These secondary phases give rise to the degradation of mechanical and thermal properties at elevated temperatures.

An useful way to densify refractory materials without additives is to apply higher pressure by means of high pressure hot-pressing at GPa order [24] and hot isostatic pressing at 100-200MPa order [50]. The densification without additives is significant not only in pursuit of high temperature strength, but also in clarifying the characteristics of the ideal refractory ceramic materials composed of self-bonded grains. Advantages of high pressure hot-pressing (HPHP) and hot isostatic pressing (HIP) are indicated as follows in (1) - (5) and (4) - (8), respectively.

- (1) High pressure of GPa order can activate the sintering process by promoting fragmentation, rearrangement and plastic flow of particles, so that porous green compacts of starting materials are densified to nearly theoretical density.
- (2) High pressure hot-pressing is performed in a closed reaction system, which enables to prevent the decomposition of products at high temperatures.
- (3) Metastable compounds at room temperature such as diamond can be sintered in their stable regions at high temperature – pressures.
- (4) Materials can be densified to nearly theoretical density without additives in shorter sintering duration at the same or lower temperature conditions comparing to conventional hot-pressing or normal sintering in the presence of additives.
- (5) These conditions of shorter sintering duration and high pressure control the exaggerated grain growth, and hence ceramics with fine grained microstructures

are obtained.

- (6) Nearly net shape products can be sintered by applying isostatic pressure.
- (7) Decomposition or vaporization of the compound are prevented by applying high pressure of one order higher than conventional hot-pressing.
- (8) Materials can be sintered homogeneously by applying isostatic pressure resulting in the reliability such as mechanical strength.

In the present study, an attempt was made to densify ceramics without additives by applying high pressure and to examine the high performance characteristics of fully dense, pure and self-bonded refractory materials. Silicon carbide, titanium carbide and aluminum nitride are selected for these investigations because of their attractive properties to wide technological applications as shown in Table III. In addition, it is expected that the solid solutions of non-oxide system produce the potentiality of new ceramics by varying the chemical bond. Therefore, another attempt was made to fabricate anion-substituted solid solution ceramics of zirconium carbonitride without additives by high pressure hot-pressing and hot isostatic pressing.

3-2 Experimental Procedure

3-2-1 Starting Materials

It is well known that the characteristics of the starting material affect the densification behavior in the sintering process [23]. Four kinds of SiC powders, one kind of TiC powder and three kinds of AlN powders were used for the HPHP without additives. The mixed powders of ZrC and ZrN were used for fabricating the anion substituted solid solutions of $ZrN_{1-x}C_x$ by both methods of HPHP and HIP without additives. The two compounds were well mixed at a desired molar ratio in acetone and dried in vacuum. Characteristics of these starting materials are listed in Table XII.

3-2-2 High Pressure Sintering

HPHP Starting powders were compressed into disks of 5 mm x 3 mm in diameter and thickness at 30MPa. The powder compact was put into a BN capsule and charged into a high pressure cell. The high pressure cell assembly is illustrated in Fig. 15. High pressure hot-pressing was conducted by means of a cubic-anvil type

Table XII Characteristics of starting powders used in the present study.

| Compound | Designation | Manufacturer | Purity+ (wt%) | Particle size (μm) | Structure |
|----------|-------------|-------------------------------|------------------|---------------------------------------|--------------|
| SiC | SC1 | In house* | 99.9 | < 10 | 3C \geq 6H |
| | SC2 | In house* | 99.7 | < 10 | 3C \geq 6H |
| | SC3 | In house* | 99.7 | < 10 | 3C \geq 6H |
| | SCC | Central Glass, Co., Ltd. | 98.8 | 0.3 | 3C \geq 6H |
| TiC | - | In house* | 99.7 | < 30 | F.C.C. |
| AlN | ANT | Toshiba Ceramics, Co. Ltd. | 92.5 | 0.93 | Hex. |
| | ANR | Rare Metallic, Co., Ltd. | - | < 74 | Hex. |
| | ANS | H. C. Starck, Co., Ltd. | 95.1 | 3.10 | Hex. |
| ZrN | - | H. C. Starck, Co., Ltd. | 91.7 | 9 | F.C.C. |
| ZrC | - | H. C. Starck, Co., Ltd. | 97.1 | 3 - 5 | F.C.C. |

* Powder synthesized by SHS

+ With respect to anion impurities

apparatus [24]. The sample was subjected up to 3GPa and then heated at desired temperature by passing electric current through a carbon sleeve heater. After the sintering experiment, the sample were cooled to room temperature at a rate of 1000 K/min. and pressure was released.

HIP Mixed powders were compressed into pellets with 7 mm x 3 mm in diameter and thickness at 100MPa. The green compact was put into BN capsule, enclosed tightly with Mo foil and tied up by Mo wires, then placed in pyrex glass container as shown in Fig. 16. The glass container was evacuated to 0.1MPa and sealed. Hot isostatic pressing experiments were performed using Ar gas as pressure-

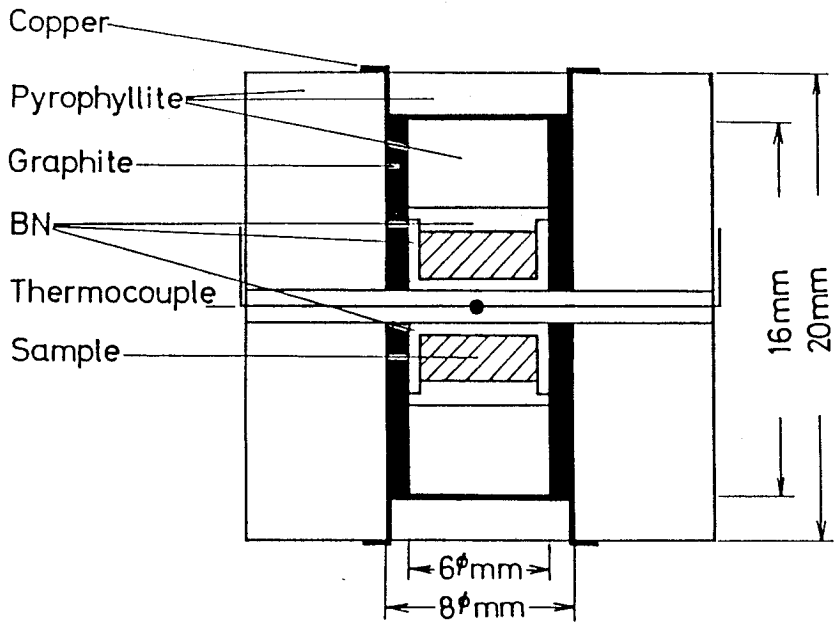


Fig. 15 Cell assemblage used for cubic anvil type high pressure hot-pressing.

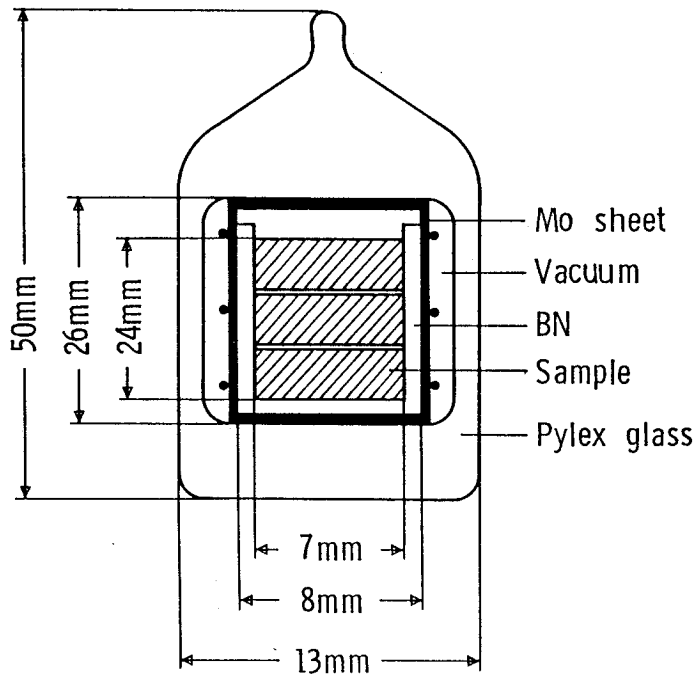


Fig. 16 Cell assemblage for hot isostatic pressing.

transmitting medium. The specimen was heated to glass softening temperature under a pressure of 2MPa and then pressure and temperature were simultaneously raised up to desired conditions. The container was stripped after HIP treatment and the specimen was cleaned by polishing the surface.

3-2-3 Characterization of the Products

The bulk density of the hot-pressed specimens was measured by means of a water displacement method. For porous specimens, the density was measured after coating the surface with nitrocellulose lacquer. The phases of the products were identified by X-ray powder diffractometry using Ni-filtered $\text{Cu}\alpha$ radiation. The microstructure of the fracture surface was observed by scanning electron microscope.

Microhardness, H_v , was measured by a diamond Vickers indenter from room temperature to 1473K in a vacuum of 4Pa. The load and loading time were 200g and 5 seconds, respectively. The fracture toughness K_{IC} , was measured by the indentation microfracture method reported by Eaves et al. [25] and Niihara [49]. This method is very useful for the rapid evaluation of K_{IC} on small specimens. An indenter load of 1 kg was applied to the specimen for 5 seconds.

Thermal conductivity, λ , was measured by means of laser flash technique (ruby laser) using a thermal constants analyzer. It can be calculated from thermal diffusivity, α , specific heat, C_p , and the bulk density, ρ , by the following relation : $\lambda = \alpha \times C_p \times \rho$ (W/mK). Thermal diffusivity was determined by irradiating a energy pulse on the front surface of a disk specimen and monitoring the temperature response of Pt/PtRh thermocouple attached on the back surface. The specific heat was determined by evaluating the absorbed energy which was calibrated using a standard sample of sapphire single crystal. The accuracy of specific heat was within $\pm 10\%$.

3-3 Results and Discussion

3-3-1 Preparation and Properties of Dense SiC Ceramics

It is expected that the densification can be enhanced not only by the fragmentation and rearrangement of SiC particles under high pressure of 3GPa, but also by the plastic deformation and volume diffusion at high temperature over 2300K.

These high pressure and temperature conditions enable to decrease sintering duration which needs for fully densification of SiC pellet. Three kinds of β -SiC powders prepared by SHS and commercial β -SiC powder were sintered at the temperature of 2800K for 10 seconds by HPHP without additives. The temperature was estimated by extrapolating the relation between applied electric power and temperature of the sample.

Highly densified SiC compacts without additives could be obtained by a sintering process at extremely high pressure – temperature conditions. The relative densities of the obtained compacts are listed in Table XIII. A typical X-ray diffraction pattern of SiC compact is shown in Fig. 17. Generally, it has been reported that $\beta \rightarrow \alpha$ irreversible phase transition was accelerated by the formation of liquid phase above 2300K [29] [30]. Nevertheless, the product was mainly considered of stoichiometric β -SiC phase. This fact suggests that the irreversible transformation of β to α phase is retarded not only by applying high pressure, but also by no presence of liquid phase which is usually formed by adding the sintering aids. Figure 18 shows the fracture surface of SiC compact fabricated with fine powders prepared by SHS. The fracture pattern exhibits the transgranular type which indicates that grains are well self-bonded with each other. The specimen did not produce exaggerated grain growth even though the sintering temperature was relatively high.

It is important from the view point of basic research on ceramics to clarify the intrinsic mechanical properties of pure and dense SiC ceramics composed of self-bonded grains. Vickers microhardness of the specimens A1 and A3 fabricated by

Table XIII Relative density of SiC compact fabricated by high pressure hot-pressing.

| Specimen | Starting powder | Relative density (%) | Phase of sintered compact |
|----------|-----------------|----------------------|---------------------------|
| A1 | SC1 | 98.6 | $\beta \gg \alpha$ |
| A2 | SC2 | 98.2 | $\beta \gg \alpha$ |
| A3 | SC3 | 98.0 | $\beta \gg \alpha$ |
| B1 | SCC | 97.2 | - |

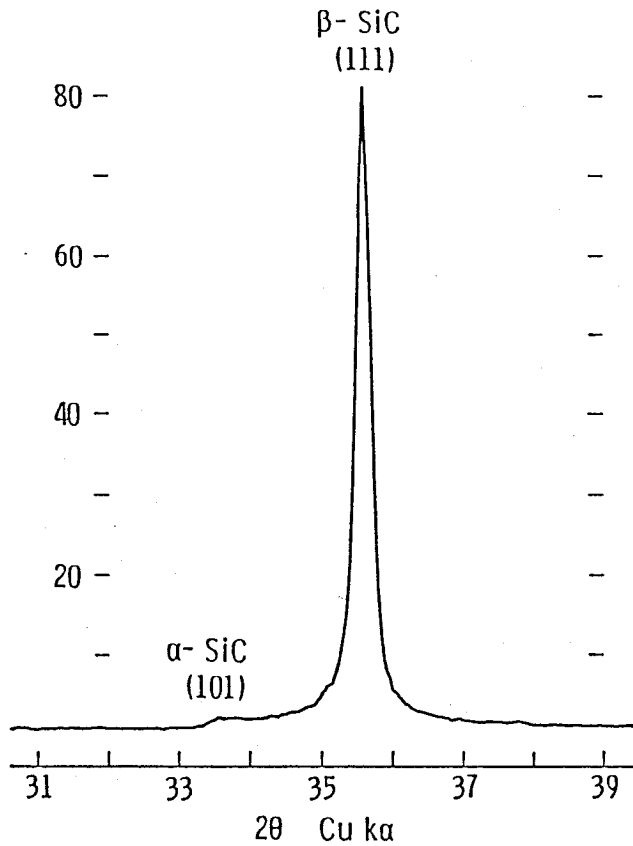


Fig. 17 Representative X-ray powder diffraction pattern of SiC compact fabricated by HPHP without additives.

HPHP indicated high value of 36 and 35GPa at room temperature, respectively, which are higher than that of hot-pressed compact with B and C additives in the temperature region from 300K to 1500K, as shown in Fig. 19. These specimens, A1 and A3, maintained high values of hardness at elevated temperature without any drastic degradation which occurred by grain boundary sliding due to the softening of secondary phase. As seen in Fig. 20 illustrating the temperature dependence of the fracture toughness of specimen A1, the K_{IC} value was $5.6\text{MN}/\text{m}^{3/2}$ at room temperature, which was higher than that of HEXOLOY prepared by pressureless sintering with B and C additives. The K_{IC} of dense SiC ceramics without additive decreased gradually with increasing temperature.

SiC is known as an excellent thermal conductor. In general, the principal carriers of heat transportation in solids are conduction electrons and phonons, leading to

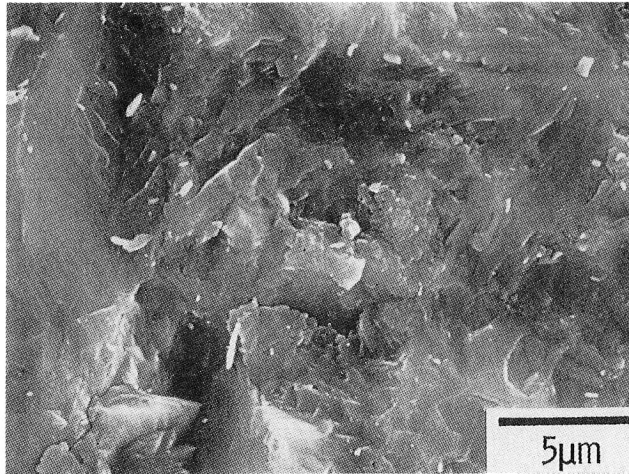
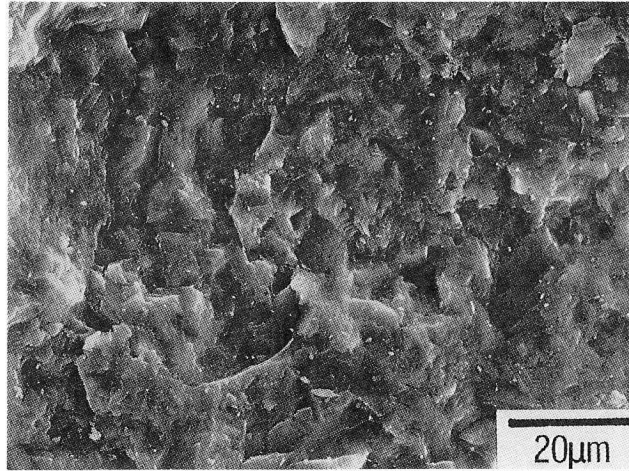


Fig. 18 Scanning electron micrographs of the fracture surface of SiC compact, Specimen A1, fabricated by HPHP without additives.

an overall thermal conductivity : $\lambda = \lambda_e + \lambda_l$, where λ_e is the electronic component and λ_l the lattice component. In semiconducting material such as SiC, λ_e and λ_l are frequently comparable except at low temperatures where λ_e is small. In most cases of semiconductors the electronic thermal conductivity is considered only at higher temperatures. The relative importance of λ_e and λ_l thus depends on the magnitude of λ_l at low temperatures. It is predicted that thermal conductivity decreases with increasing temperature because λ_l decreases with increasing thermal

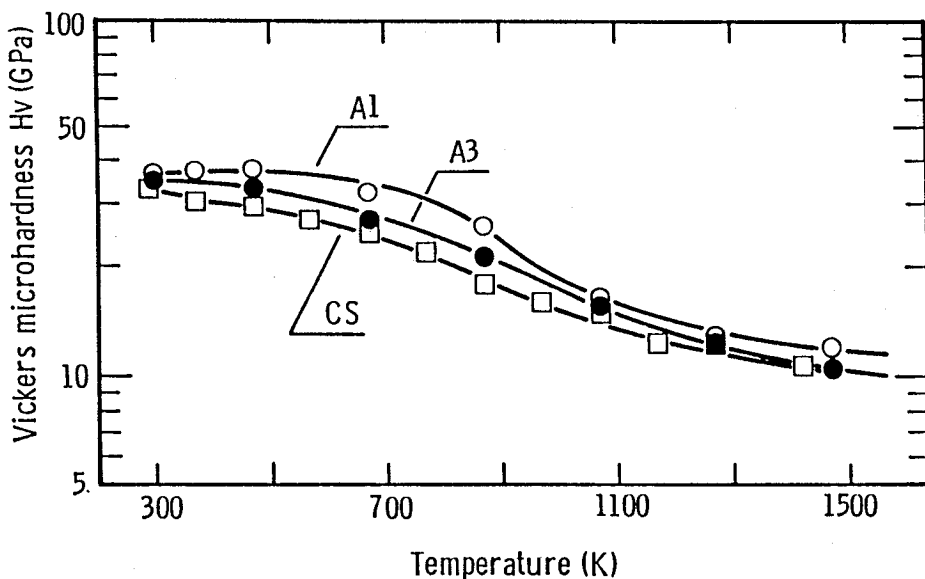


Fig. 19 Temperature dependence of Vickers microhardness of SiC compacts with and without additives.

- A1; HPHP of SC1 powder at 3GPa
- A3; HPHP of SC3 powder at 3GPa
- CS; Hot-pressing of commercial power with additives of B and C at 30 MPa

resistance caused from phonon-phonon interaction at elevated temperatures. Certainly, thermal conductivity of specimen A3 dropped to $159 \pm 14 \text{ W/mK}$ at 400K in comparison with $220 \pm 15 \text{ W/mK}$ at 326K, which are higher than reported in reference [31].

3-3-2 Preparation and Properties of Dense TiC Ceramics

Since there are few reports in terms of fundamental studies on sintering process of single phase titanium carbide, the sinterability of the TiC powder synthesized from SHS process was examined by HPHP without additives. Sintering conditions were fixed at the temperature of 2800K for 10 seconds under 3GPa. Relative density of the compact reached to 98.2% of theoretical. The observation of fracture surfaces showed that each particle was well bonded with themselves and fracture pattern was almost transgranular type, as seen in Fig. 21. Furthermore, the exaggerated grain growth was not observed so that good mechanical properties

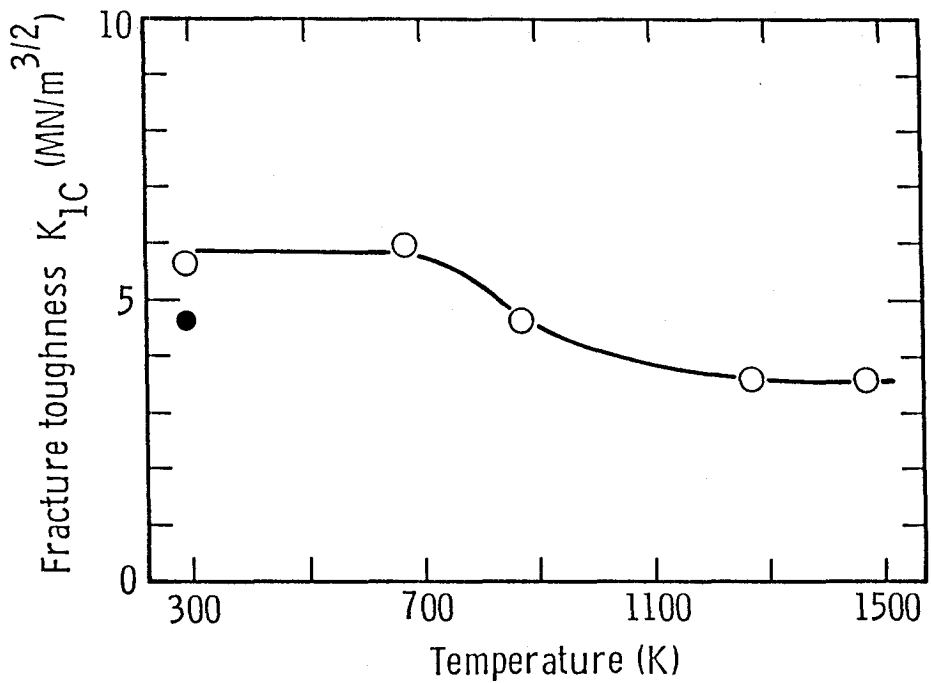


Fig. 20 Temperature dependence of fracture toughness of SiC compact, specimen A1, with a relative density of 98.6%. The full circle indicates a reported value of HEXOLOY.

were anticipated. The relation between the Vickers microhardness and temperature is shown in Fig. 22. Microhardness of the obtained TiC body was 35GPa at room temperature which is considerably higher than the reported value of 28GPa in reference [3].

The fracture of brittle materials occurs by the catastrophic propagation of crack when the stress concentration at the top of flaw exceeds the critical value for rupture. In the evaluation of mechanical property of brittle materials, an inherent parameter is not the fracture stress but the fracture toughness, K_{IC} . K_{IC} is a resistance to fracture and an important parameter to design structural components. The temperature dependence of K_{IC} for TiC ceramics without additives is shown in Fig. 23. It is well known that K_{IC} of ceramics with additives increased at elevated temperatures due to the softening of the secondary phase at grain boundary [32]. While, K_{IC} of this sample was almost independent of temperature up to 400K and decreased gradually with increasing temperature, which reflect the inherent properties of pure TiC compact without secondary phases.

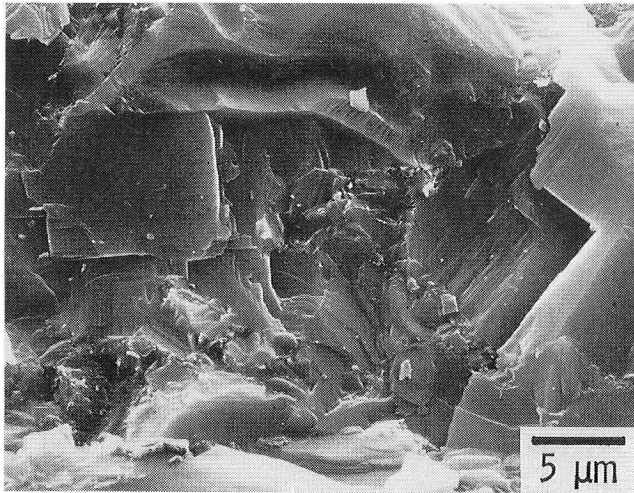
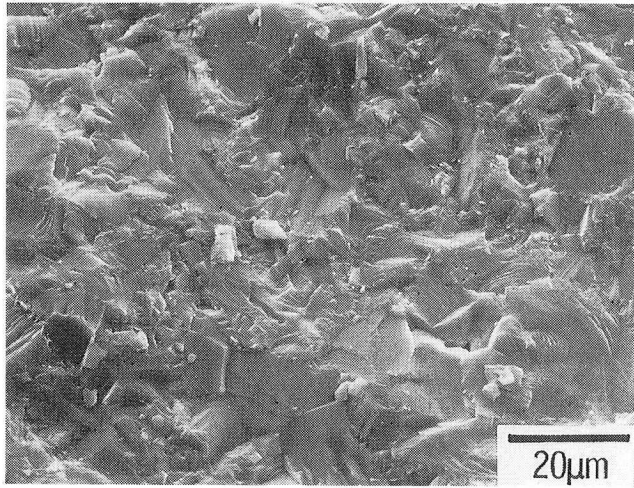


Fig. 21 Scanning electron micrographs of the fracture surface of dense TiC compact fabricated by HPHP using powders synthesized by SHS.

3-3-3 Preparation and Properties of Dense AlN Ceramics

AlN ceramics have excellent thermal conductivity, high electrical resistance and low thermal expansion coefficient. However, AlN is one of the typical unsinterable materials. Long and Foster tried to fabricate AlN rods without additives, however it was not sufficient for practical use [33]. A current fabrication method is pressurless and hot-pressing sinterings in the presence of additives such as CaO, Al₂O₃,

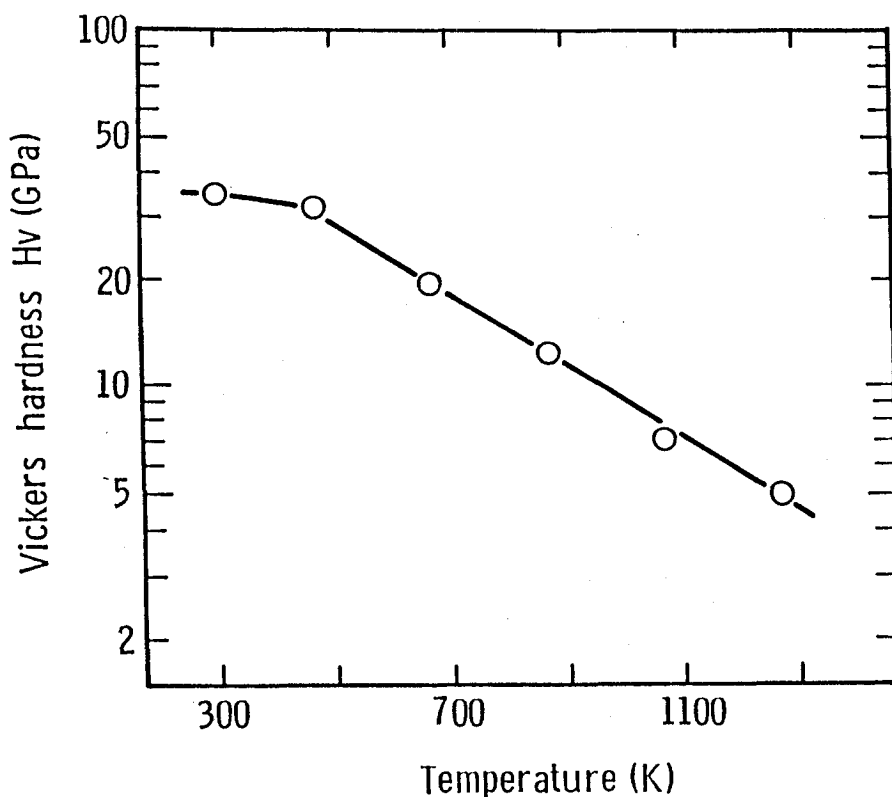


Fig. 22 Temperature dependence of Vickers microhardness of dense TiC compact fabricated by HPHP at 2800K and 3GPa for 10s.

Y_2O_3 and SiO_2 [34] [35]. Three kinds of AlN powders listed in Table XII were sintered without additives by high pressure hot-pressing. The effect of sintering temperature on final densities is shown in Fig. 24. When ANT powder was sintered at 3GPa for 60 minutes, a fully dense and self-bonded AlN body was obtained at the low sintering temperature of 1773K, but the relative densities of the specimens sintered with ANR and ANS powders were slightly lower than the theoretical density. A slight difference in final density was considered to be caused from the difference in size distribution of starting particles. The dependence of sintering duration on relative density is shown in Fig. 25. The rapid increases in relative density occurred within 5 minutes at 1973K and fully densified AlN were obtained after holding over 15 minutes. In this case, a remarkable effect of high pressure on the densification was recognized as advantages of low sintering temperature and short heating duration. The hot-pressing conditions and density of specimens

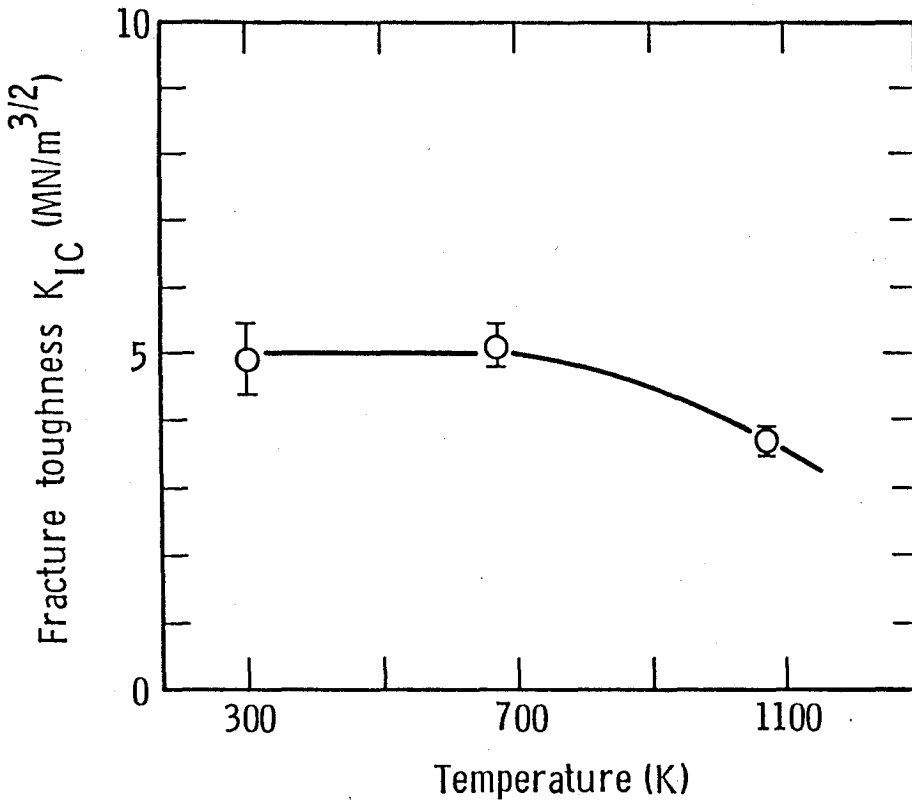


Fig. 23 Temperature dependence of fracture toughness of dense TiC compact fabricated by HPHP.

are listed in Table XIV, which includes the results for the specimens with additives.

Temperature dependence of Vickers microhardness for AlN ceramics with and without additives is shown in Fig. 26. The microhardness of fully dense AlN ceramics without additives was 13GPa at room temperature except for sample T1, and it degraded gradually with increasing temperature. The microhardness at 1473K was about 7GPa. The remarkable degradation was observed above 1173K for the sample T9 with CaO 2.5 wt% additives, which is probably due to the softening of secondary phase at grain boundary. The temperature dependence of microhardness for AlN ceramics fabricated in various sintering duration showed no drastic decrease in all pure specimens as seen in Fig. 27.

The change of K_{IC} as a function of temperature for fully dense AlN ceramics without and with oxide additives is shown in Fig. 28. K_{IC} of pure AlN ceramics slightly decreased with increasing temperature showing the same tendency as the

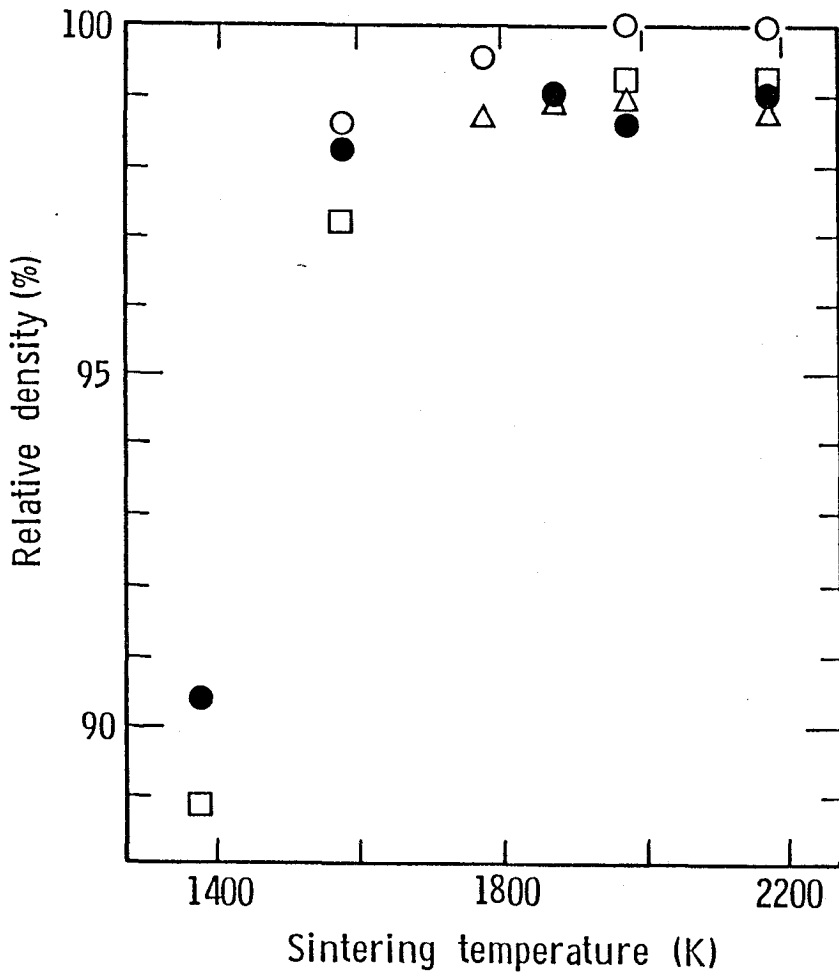


Fig. 24 Effect of sintering temperature on relative density of the samples fabricated by HPHP without additives.

- HPHP at 3GPa for 60 min. using ANT powder
- △ HPHP at 3GPa for 60 min. using ANR powder
- HPHP at 3GPa for 15 min. using ANR powder
- HPHP at 3GPa for 15 min. using ANS powder

results of SiC compacts. The K_{IC} values at room temperature was 3.1-3.8MN/m^{3/2}, which were higher than those reported in reference [36] [37]. It was found that the correlation existed between hardness and fracture toughness at room temperature as seen in Fig. 29.

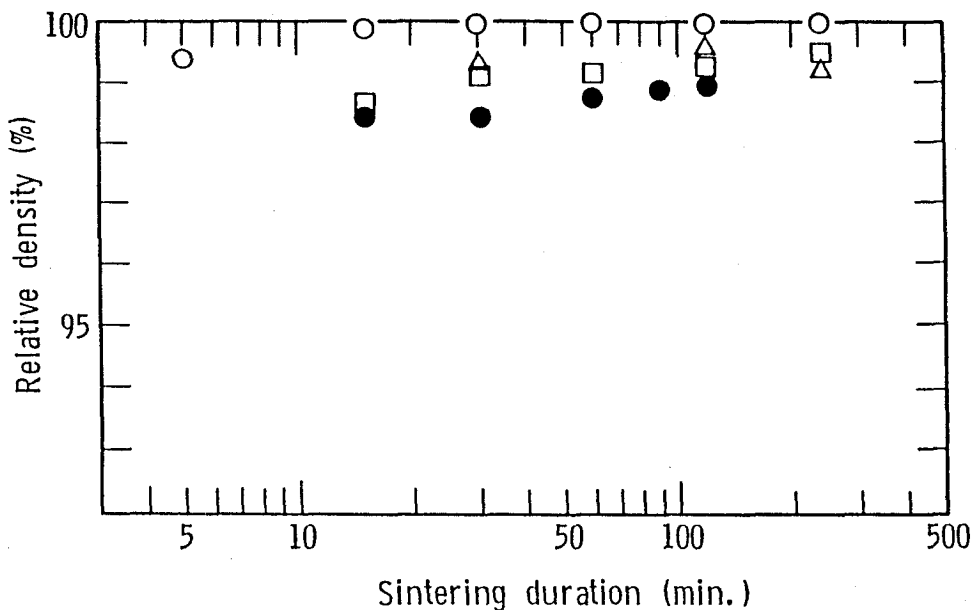


Fig. 25 Effect of sintering duration on relative density of the samples fabricated by HPHP without additives.

- HPHP at 1973K and 3GPa using ANT powder
- △ HPHP at 1973K and 3GPa using ANR powder
- HPHP at 1773K and 3GPa using ANR powder
- HPHP at 1773K and 3GPa using ANS powder

The thermal conductivity of AlN ceramics without additives decreased with increasing temperature except sample T4 as seen in Fig. 30. The thermal conductivity value of each specimen became smaller in the following order, $T_2 > T_1 > T_3 > T_4$. T. Sakai et al. [38] reported that rapid decrease of thermal conductivity is considered to be caused from the heterogeneous oxygen distribution within grains, which acted as phonon scattering center. This trespass of oxygen atom into grains depends on the sintering temperature. The considerable degradation for specimen T4 compared with other pure specimens should result from its higher sintering temperature. Thermal conductivity of the insulative ceramics above the Debye temperature is expressed as the following equation; $\lambda = 1/W = 1/(mT + n)$, where W is the thermal resistivity, m and n is the constant determined by phonon-phonon and phonon-imperfection interaction, respectively. The temperature dependences of thermal resistivity of the specimens fabricated with ANT, ANS

Table XIV The hot-pressing conditions and relative density of AlN specimens

| Specimen | Powder | Additives (wt%) | Hot-pressing conditions | | | Relative density (%) |
|----------|--------|-------------------------------------|-------------------------|-------------------|--------------------|----------------------------|
| | | | Temp. (K) | Pressure (GPa) | Duration (min.) | |
| T1 | ANT | None | 1573 | 3 | 60 | 98.7 |
| T2 | ANT | None | 1773 | 3 | 60 | 99.5 |
| T3 | ANT | None | 1973 | 3 | 60 | 100.0 |
| T4 | ANT | None | 2173 | 3 | 60 | 99.8 |
| T5 | ANT | None | 1973 | 3 | 15 | 99.9 |
| T6 | ANT | None | 1973 | 3 | 30 | 100.0 |
| T7 | ANT | None | 1973 | 3 | 120 | 100.0 |
| T8 | ANT | None | 1973 | 3 | 240 | 100.0 |
| T9 | ANT | CaO (2.5) | 1973 | 3 | 60 | 95.8 |
| T10 | ANT | CaO (2.5) | 1973 | 3 | 15 | 95.6 |
| T13 | ANT | Al ₂ O ₃ (10) | 1973 | 3 | 60 | 98.9 |
| S1 | ANS | None | 1973 | 3 | 60 | 98.6 |
| R1 | ANR | None | 1973 | 3 | 60 | 99.0 |

and ANR powders are illustrated in Fig. 31. They were proportional to temperature with the same gradient in the lower temperature range. The results indicate that the thermal resistivity of these specimens was controlled by phonon-imperfection interaction. The thermal resistivities at 300K are plotted as a function of impurity content in Fig. 32. The value of thermal conductivity of highly pure AlN ceramic is estimated to be about 300W/mK at room temperature by extrapolating the thermal resistivity curve. This value is nearly the same as theoretical value of 320 W/mK [39]. From the present results, it is concluded that purity of AlN ceramics is one of important factors governing the thermal conductivity.

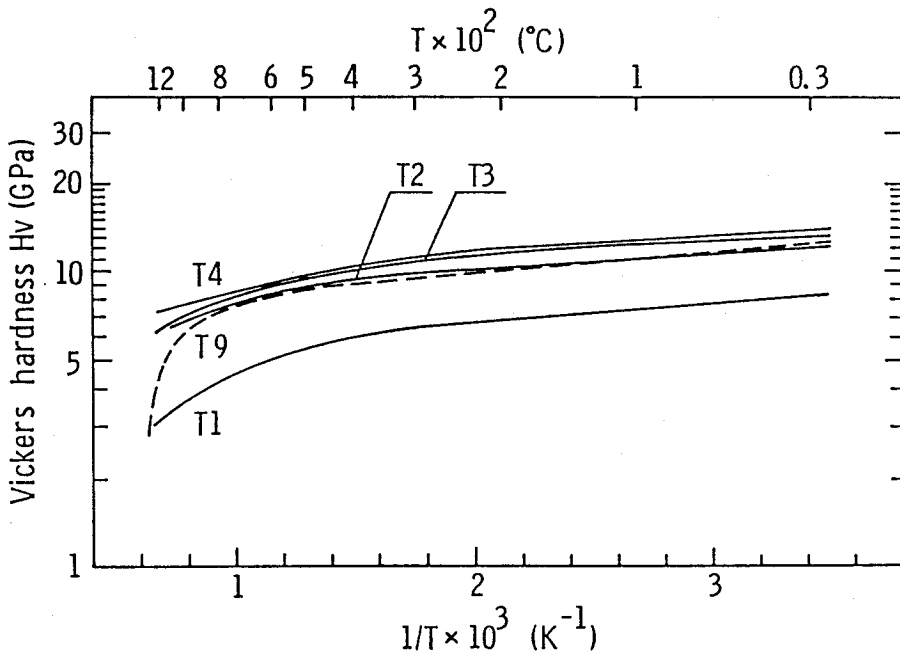


Fig. 26 Temperature dependence of Vickers microhardness of AlN ceramics fabricated by HPHP at various sintering temperatures with and without additives.

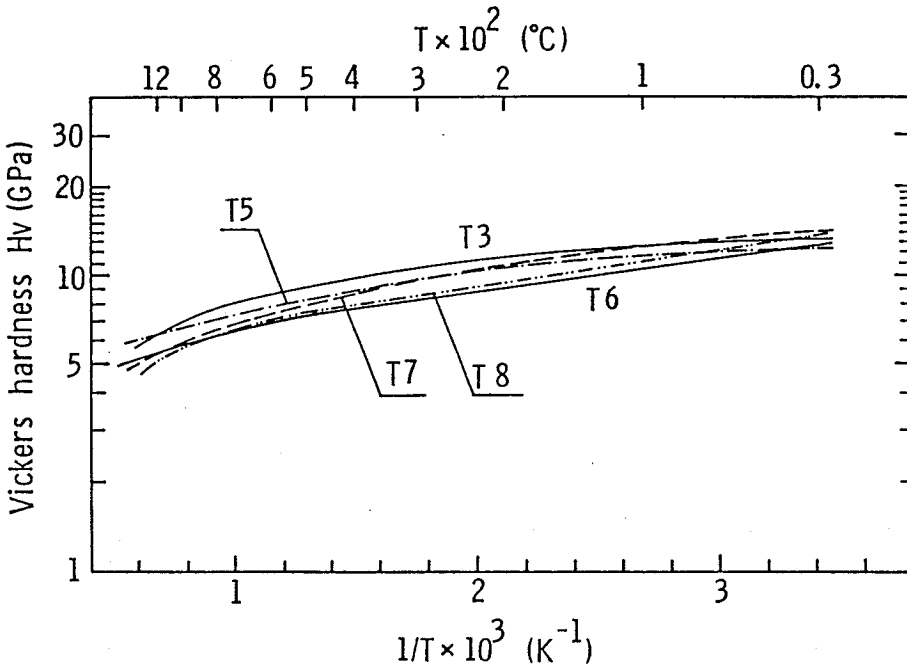


Fig. 27 Temperature dependence of Vickers microhardness of AlN ceramics fabricated by HPHP at 1973K for various sintering durations between 15 - 240 min.

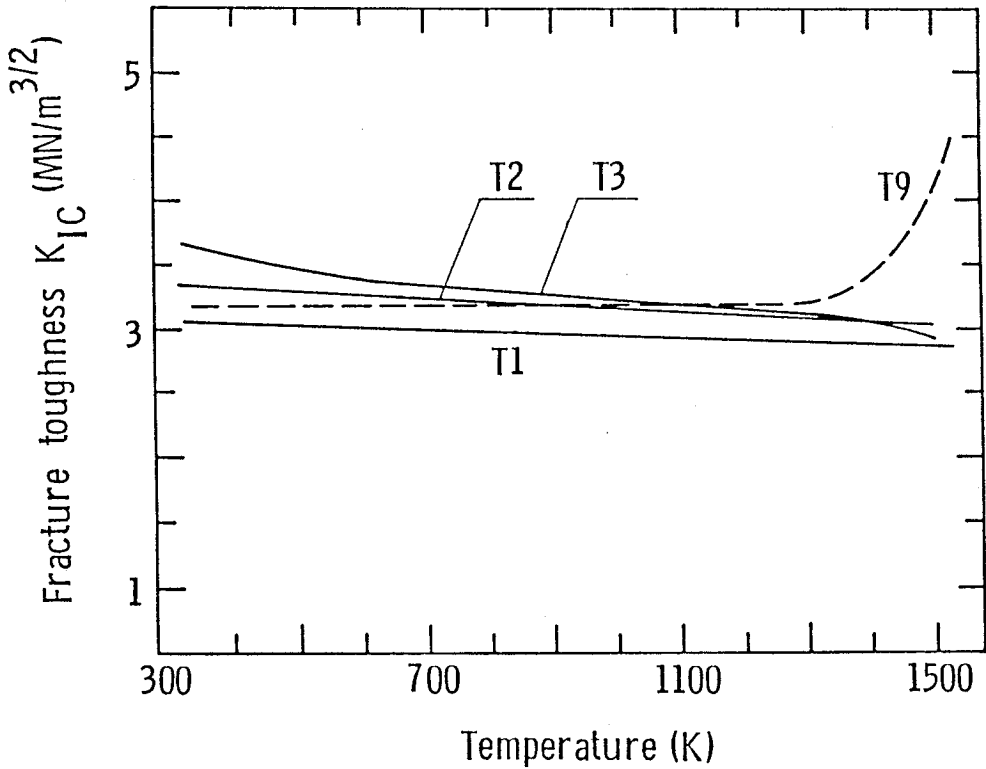


Fig. 28 Temperature dependence of fracture toughness of dense AlN ceramics with and without additives.

3-3-4 Preparation and Properties of $ZrN_{1-x}C_x$ Ceramics

Many of transition-metal carbides and nitrides have the same crystal structure and their solid solutions can be easily formed. Since the properties of ceramics materials strongly depends on their chemical bonds, the solid solutions of non-oxide system produce the potentiality of new ceramics with superior mechanical and thermal properties by varying the chemical bond. A full system of anion substituted solid solution of $ZrN_{1-x}C_x$ ($0 \leq x \leq 1.0$) were fabricated by high pressure reaction hot-pressing at 2073K and 3GPa for 1h and by hot isostatic pressing at 1973K and 100MPa for 2h.

Solid solutions of zirconium carbonitride were identified as cubic NaCl type structure by X-ray powder diffractometry. Figure 33 shows compositional dependence of the density and lattice constant, which were calculated from the results of

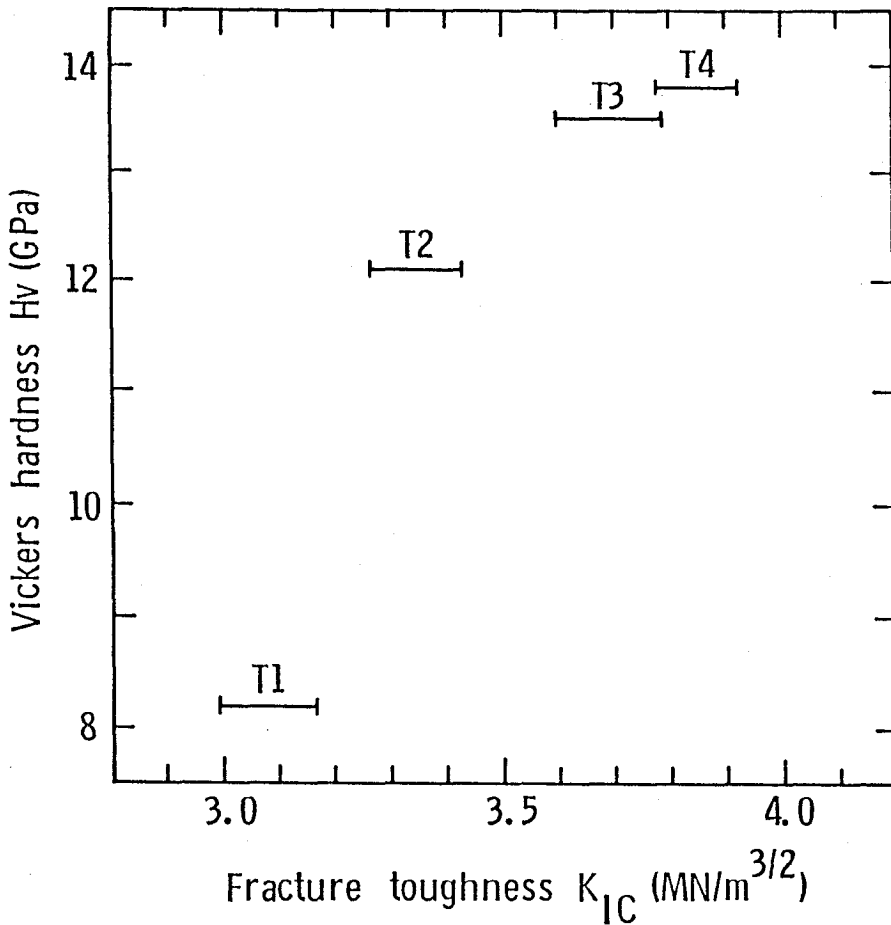


Fig. 29 Relation between Vickers microhardness and fracture toughness at room temperature of pure and highly dense AlN ceramics.

X-ray powder diffraction pattern using Si compact as an external standard. The unit-cell dimensions varied linearly with composition in accordance with Vegard's law. The lattice constant of end members (ZrN : 4.579Å, ZrC : 4.691Å) coincided with the reported value [40] [41]. The relative density of sintered $ZrN_{1-x}C_x$ is shown in Fig. 34. Increase of relative density were observed in comparison with the mean values between end members.

Temperature dependence of Vickers microhardness of solid solutions and end members was measured, of which results are shown in Fig.35(a) and (b). Microhardness at room temperature was smaller in the following order, $ZrC \cong ZrN_{0.5}C_{0.5} > ZrN$ in HPHP treatment and $ZrC > ZrN_{0.5}C_{0.5} > ZrN$ in HIP treatment. It is

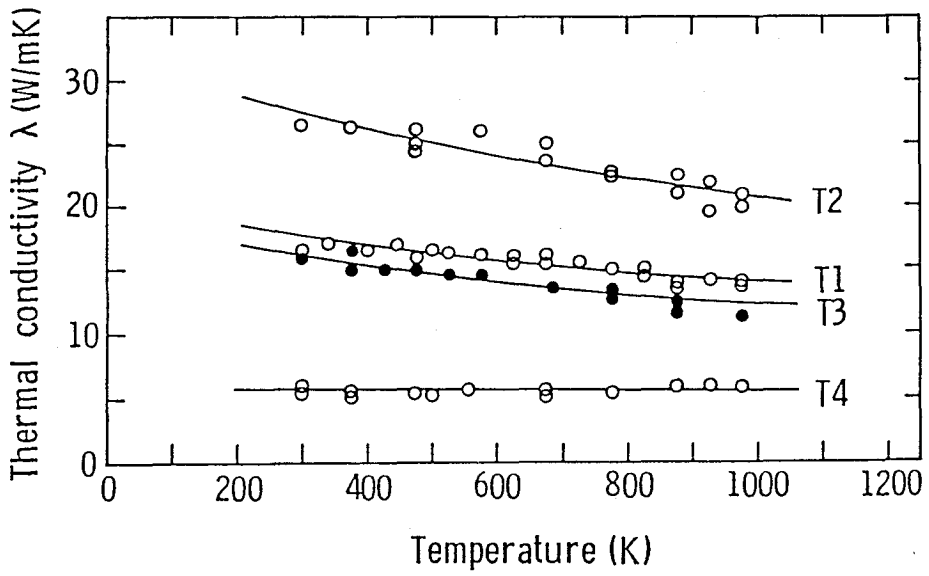


Fig. 30 Temperature dependence of thermal conductivity of AlN ceramics without additives.

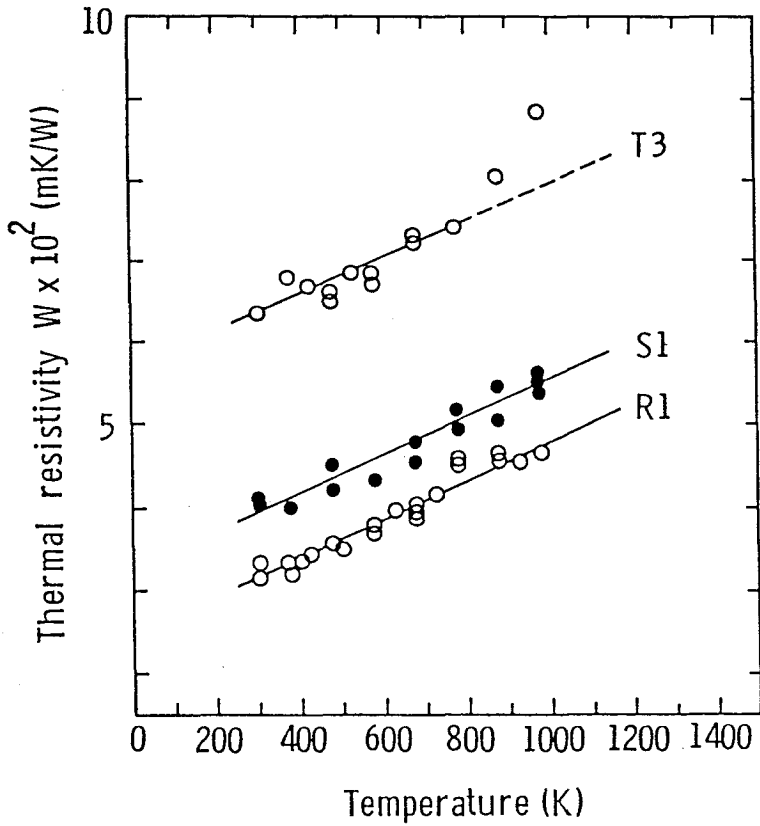


Fig. 31 Temperature dependence of thermal resistivity of AlN ceramics.

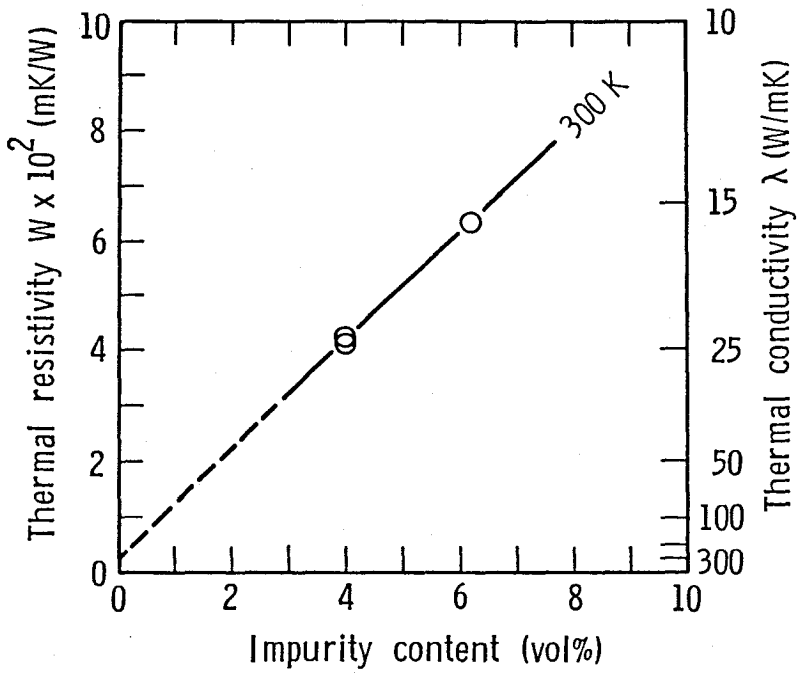


Fig. 32 Relation between thermal resistivity and impurity content in AlN ceramics.

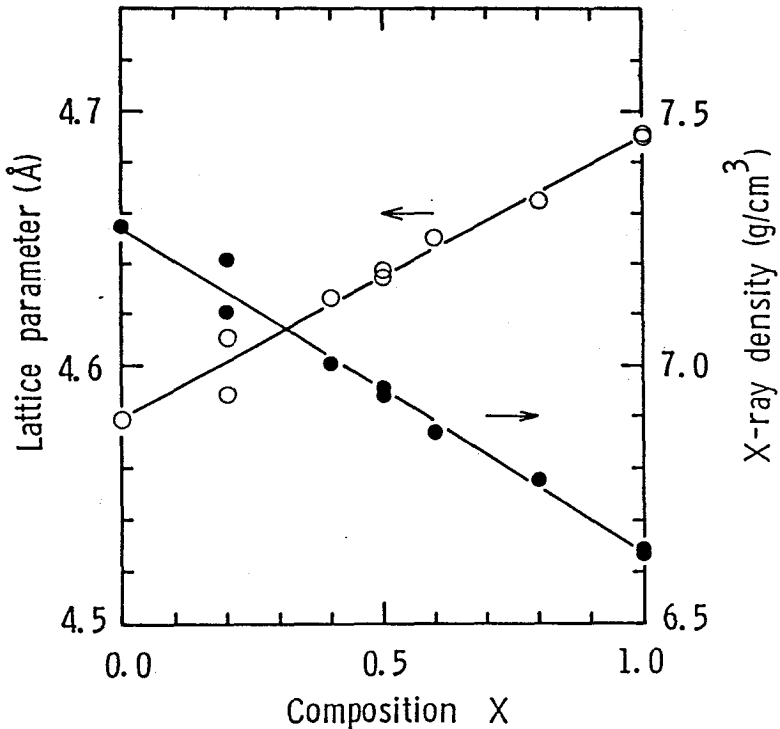


Fig. 33 Compositional dependence of lattice constant and X-ray density of $ZrN_{1-x}C_x$ ($0 \leq x \leq 1.0$) fabricated by high pressure hot-pressing at 2073K and 3GPa for 2h.

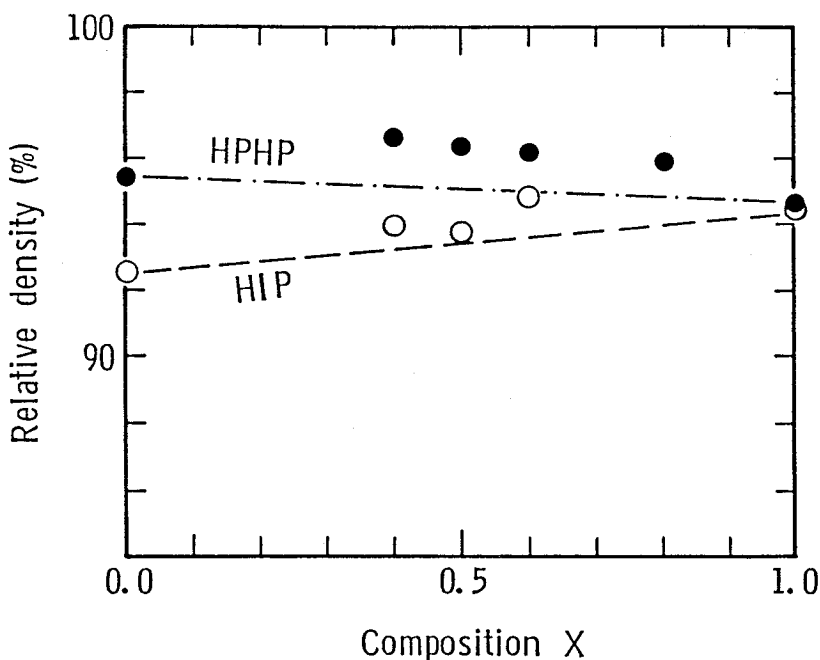


Fig. 34 Compositional dependence of relative density of $ZrN_{1-X}C_X$ compacts fabricated by HPHP and HIP.

- HPHP at 2073K and 3GPa for 2h
- HIP at 1973K and 100MPa for 2h

considered that the low microhardness of ZrN compact was due to the low purity of starting powders, as seen in Table XII. Microhardness of the solid solutions decreased gradually up to 1500K, but reversed against that of ZrC compact above 873K which dropped suddenly. The remarkable degradation of microhardness is frequently observed when the secondary phase exists in grain boundary at elevated temperatures. The refractory monocarbide such as ZrC can not dissolve so much oxygen as ZrN and is liable to form oxide layer on surface of ZrC particles [42]. The oxide phases are considered to cause the remarkable degradation of microhardness. The compositional dependence of fracture toughness is plotted in Fig. 36. The fracture toughness decreased linearly from $4.6MN/m^{3/2}$ at ZrN to $3.3MN/m^{3/2}$ at ZrC with increasing carbon contents in the solid solutions.

Figure 37 shows the temperature dependence of thermal conductivity of the zirconium carbonitride and the end members. Since ZrC and ZrN are electrically conductive, the principal carriers of heat are electron and phonon. The overall thermal conductivity is expressed as $\lambda = \lambda_e + \lambda_1$, where λ_e is the electronic compo-

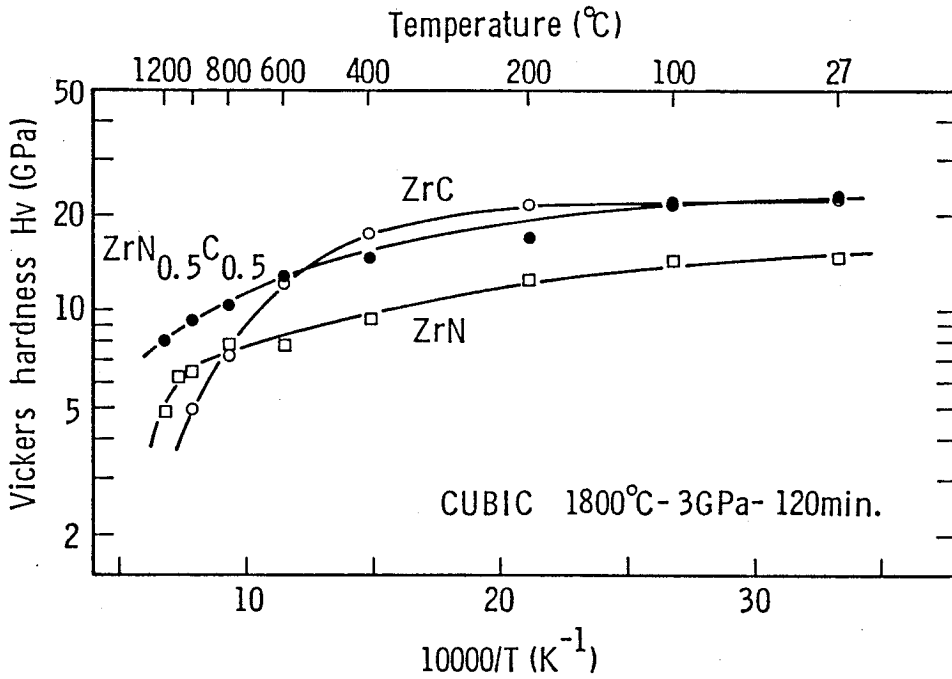


Fig. 35(a) Temperature dependence of Vickers microhardness of dense ZrC, $ZrN_{0.5}C_{0.5}$ and ZrN compacts fabricated by HPHP at 2073K and 3GPa for 2h.

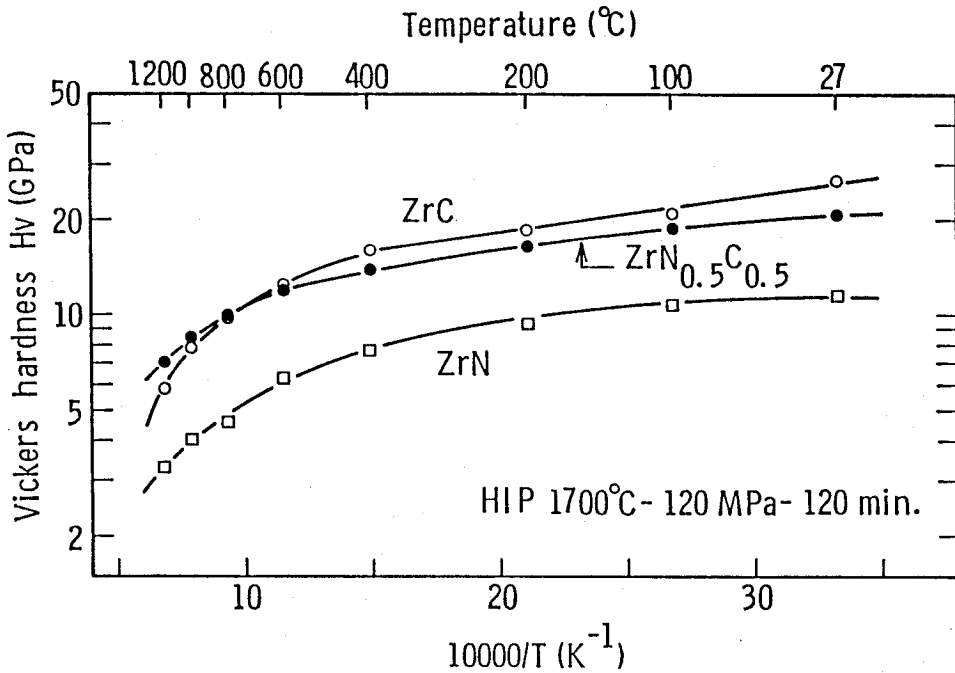


Fig. 35(b) Temperature dependence of Vickers microhardness of dense ZrC, $ZrN_{0.5}C_{0.5}$ and ZrN compacts fabricated by HIP at 1973K and 100MPa for 2h.

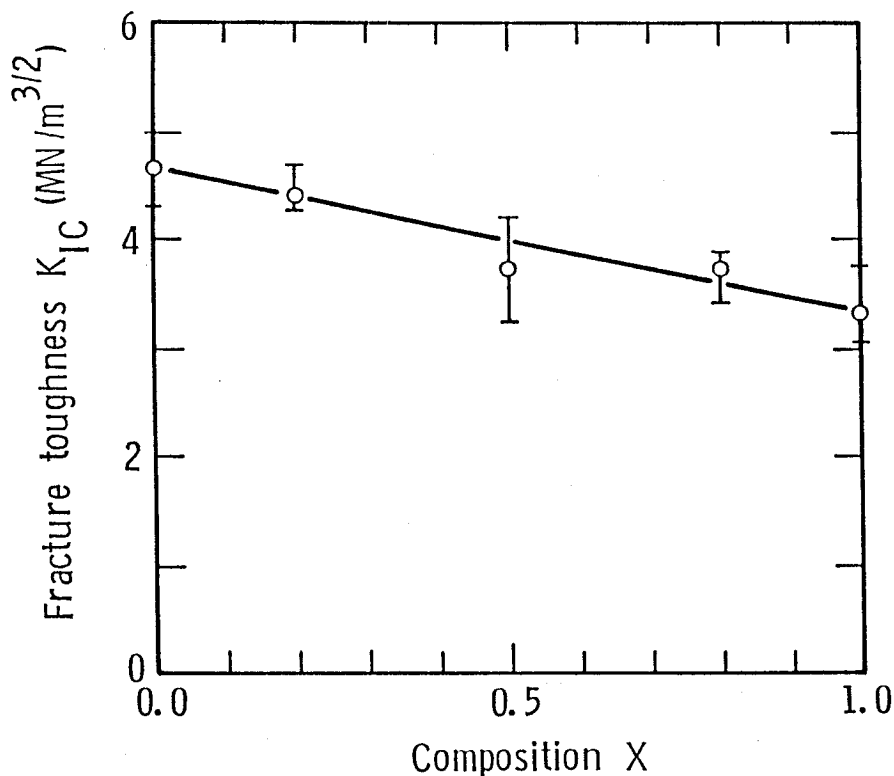


Fig. 36 Compositional dependence of fracture toughness at room temperature of $ZrN_{1-X}C_X$ fabricated by HIP at 1973K and 100MPa for 2h.

ment and λ_1 the lattice component. T. Williams [43] and Radosevich and Williams [44] have shown that λ_1 at high temperature is nearly independent of temperature due to strong phonon-point defect interactions. λ_e is estimated by the following equation of Wideman-Franz law : $\lambda_e = L_0 T / \rho$, where L_0 is Lorenz number and ρ is electrical resistivity. This equation is expressed using the relationship of $\rho = aT + b$ for metallic materials as follows, where a is the temperature coefficient and b is the residual resistance : $\lambda_e = L_0 T / (aT + b)$. If the value of b term, which is the residual resistance due to grain boundaries, lattice defect and impurities, is larger than that of aT term, the thermal conductivity increases with increasing temperature. The thermal conductivity in this system, which is shown in Fig. 37, seems to be controlled by such imperfections. Measured values of 38W/mK for ZrN and 19W/mK for ZrC at room temperature showed a good agreement with 18.4W/mK of ZrC and 36.8W/mK of ZrN, which were calculated using the parameters : $L_0 = 2.45 \times 10^{-8} \Omega W / K^2$ and $\rho = 20 \mu\Omega \text{ cm}$ and $40 \mu\Omega \text{ cm}$ for ZrN and ZrC, respectively.

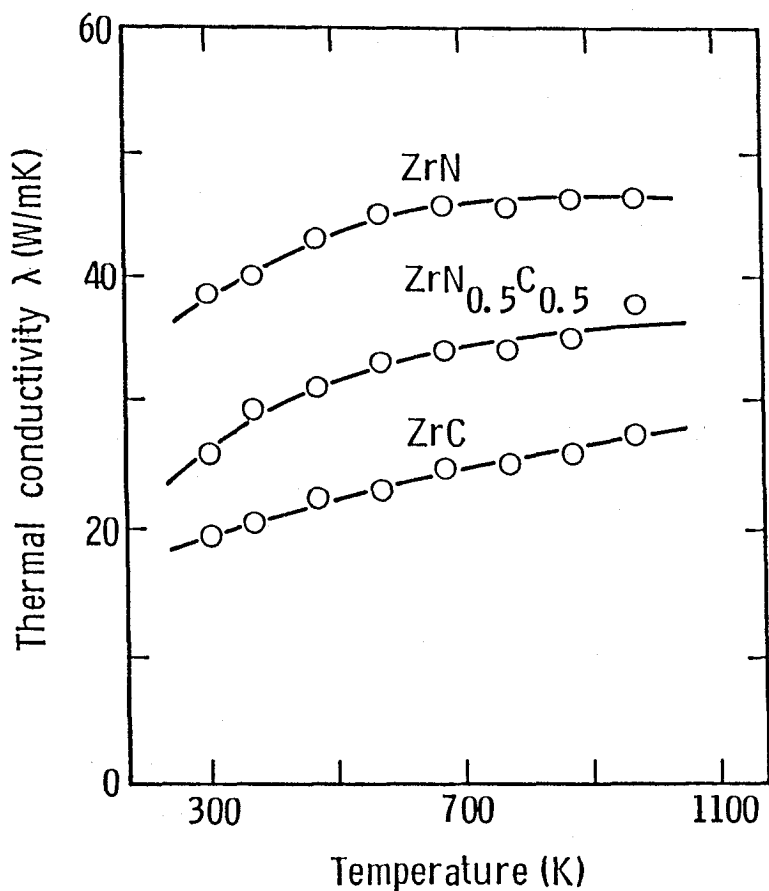


Fig. 37 Temperature dependence of thermal conductivity of ZrN, $ZrN_{0.5}C_{0.5}$ and ZrC compacts fabricated by HIP at 1973K and 100MPa for 2h.

Chapter 4 DEVELOPMENT OF NEW SYNTHESIS AND SIMULTANEOUS SINTERING PROCESS

4-1 Introduction

A newly developed processing for fabrication of dense ceramics, which is characterized as a simple and effective sintering method, is described in this chapter.

Ceramics are fabricated usually through powder preparation and subsequent sintering processes. This complex processing takes several days and consumes a lot of energy for long time firings. By contrast, the high pressure self-combustion sintering process (HPCS), which was newly developed by combining the SHS process and high pressure techniques, enables to synthesize and simultaneously sinter ceramics from constituent elements and to finish in a very short time. A comparison of the HPCS process and the conventional process is exemplified in Fig.38. Thus, the complex process of ordinary method is greatly simplified. Figure 39 shows the schematic of the HPCS process.

4-2 Experimental Procedure

4-2-1 Starting Materials

Each two element powders, Ti powder (T_1 and T_2) and B powder (B_1) for TiB_2 , Ti powders (T_1 and T_2) and C powder (C_2) for TiC and Si powders (S_1 and S_2) and C powder (C_2) for SiC, were well mixed in n-hexane and dried in vacuum. The characteristics of these powders are summarized in Table V. The mixing molar ratio of B/Ti was fixed at 2.0, but those of C/Ti and C/Si were changed from 0.70 to 1.10 and from 1.00 to 1.20, respectively.

4-2-2 Cell Assemblage and Ignition Procedure

Two types of high pressure cell assemblage (type A and type B) were used for the HPCS experiments. Cross sections of the cell assemblage were shown in Fig. 40. The pellets were 6 mm in diameter and 9 mm in length for type A cell, and 6 mm in diameter and 6 mm in length for type B cell. In the type A cell, a graphite rod was embedded in the top of a pelleted reactant and used for the ignition by an electric heating. A BN sleeve was set to prevent contamination from the pyrophyllite cell. In the type B cell, a carbon sleeve was arranged so as to preheat the reactant prior

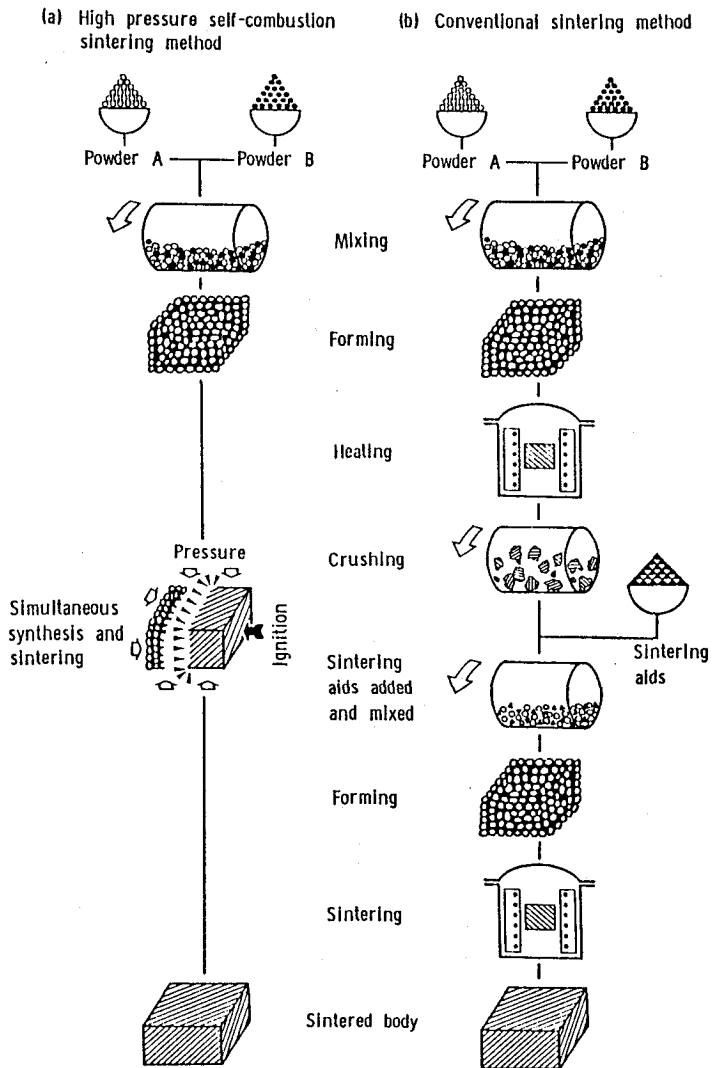


Fig. 38 A comparison of the high pressure self-combustion sintering (HPCS) method and the conventional sintering method.

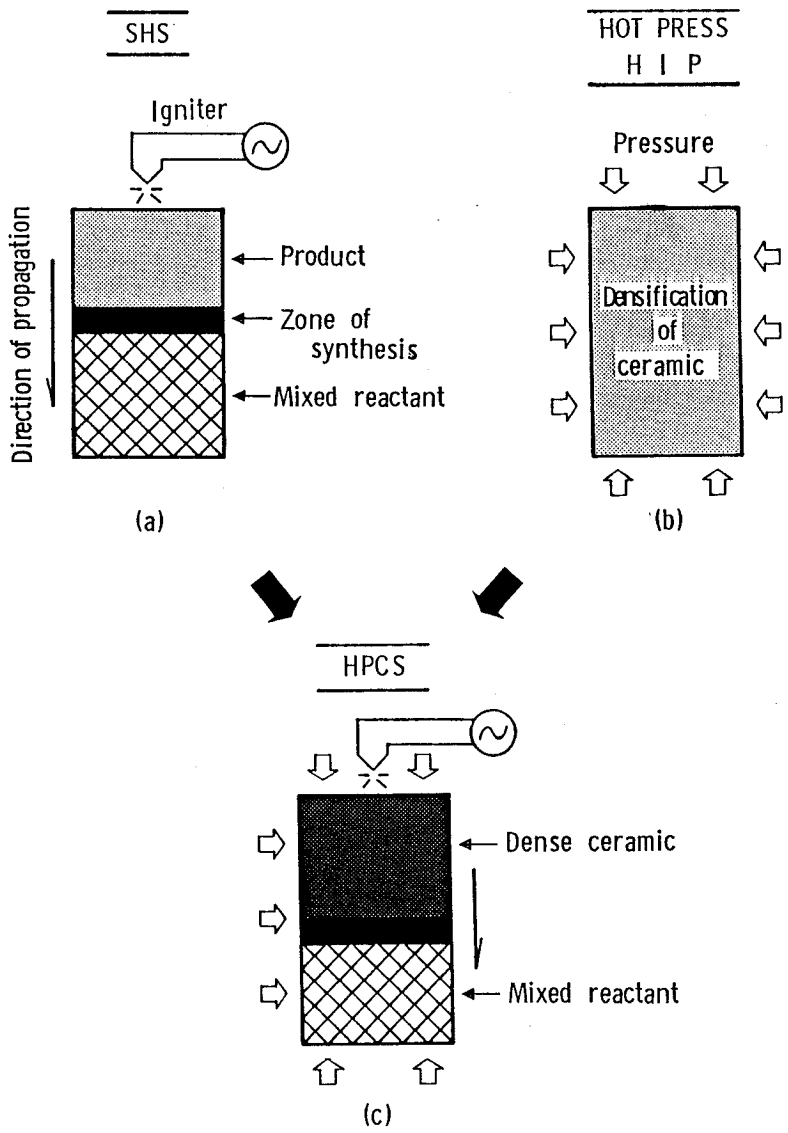


Fig. 39 Schematic diagram of high pressure self-combustion sintering as a combination of self-propagating high temperature synthesis and a high pressure technique.

to ignition and serves as a ignitor with large ignition area. The reactant was inserted into central part of the carbon sleeve so as to contact directly. The reactant was subjected up to 3GPa by means of a cubic anvil type high pressure apparatus and then ignited by passing electric current of 400A for 2 seconds through a carbon rod in the type A cell, and of 600A for 2 seconds through a carbon sleeve in the type B cell. The temperature of the carbon heater should reach over 2300K almost instantaneously in order to supply the sufficient energy for ignition effectively. After the combustion treatment, the pressure was released to ambient pressure, and the sample was removed.

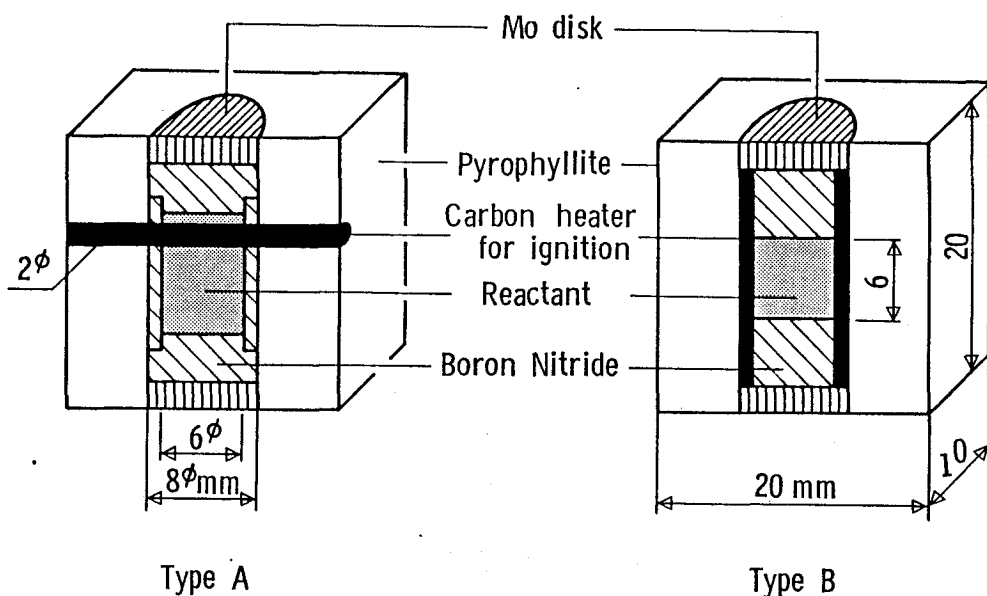


Fig. 40 Cross sections of cell assemblages for high pressure self-combustion sintering.

4-2-3 Characterization of the Products

The products were examined by optical microscopy, scanning electron microscopy and X-ray powder diffractometry with $\text{CuK}\alpha$ radiation. The conversion efficiency and lattice constant were calculated from the results of X-ray powder diffraction pattern. The density, hardness and fracture toughness of the product

were measured by the Archimedes method, the Vickers microindentation method and the indentation microfracture method reported by Niihara [49], respectively. Oxygen contents were analyzed by thermal decomposition method. The details of characterization are explained in chapters 2 and 3.

4-3 Results of HPCS Processing and Characteristics of the Products

4-3-1 Preparation and Properties of TiB_2 Dense Ceramics

HPCS Processing of TiB_2

Figure 41 shows a photograph of the cross section of the sample cell (type A) after HPCS experiment. The product lying on center of the cell was a dense compact of stoichiometric TiB_2 with a relative density of 95%, which was the same density when TiB_2 powder was sintered at 2200K for 1h under 3GPa. It was thus proved that the heat release from the strong exothermic reaction was sufficient to synthesize and simultaneously densify TiB_2 under high pressures in a few seconds without other external heat supply.

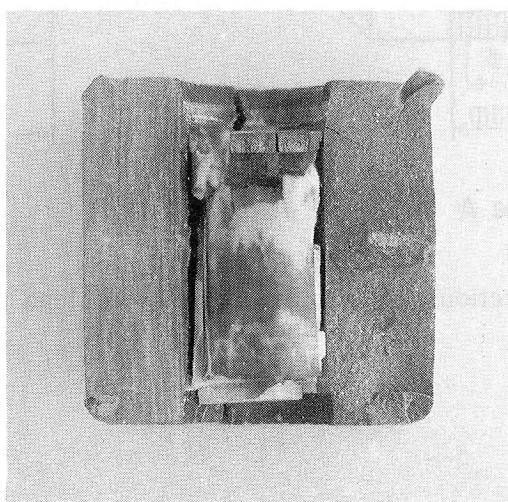


Fig. 41 Cross section of high pressure cell assemblage after HPCS experiment. TiB_2 compact lies on center axis of cell. Top of compact is partly cut away to show graphite rod (black) used for ignition.

Characteristics of TiB₂ compacts

The X-ray powder diffraction pattern of the product showed only the hexagonal TiB₂ phase and thus the initial reactant converted entirely into stoichiometric compound, independently of the particle size of Ti powder. A small amount of TiN was detected in the compact by X-ray microanalysis. Nitrogen seems to be introduced from BN sleeve or air contained in the cell. The relative density of TiB₂ was 93-96% and did not almost vary with the particle size of the starting Ti powders. These results are summarized in Table XV. Figure 42 shows a typical microstructure of fracture and polished surfaces. Fine particles with uniform grain size of about 5 μ m are self-bonded tightly. As well as the same results of TiB₂ in SHS, the grain size of the sintered body became smaller than the particle size of Ti powder. The grain size was not so sensitive to the particle size of starting Ti.

The microhardness of the TiB₂ compact was 26GPa at room temperature, which was higher than the value, 18GPa, of the sintered body fabricated by HPHP using TiB₂ commercial powder at the condition of 2200K for 1h under 3GPa. The hardness decreased with increasing temperature as shown in Fig. 43, but kept to be about 5GPa at 1273K, which is two times higher than the reported value of the other TiB₂ ceramics at high temperatures[17].

4-3-2 Preparation and Properties of TiC Dense Ceramics

HPCS processing of TiC

The HPCS experiments were conducted by using two types of ignition method, types A and B, at 3GPa. When stoichiometric mixtures of Ti and C powders were ignited for 2 seconds in type A cell, the conversion efficiency was 72% although

Table XV Collective results of TiB₂ in HPCS experiments.

| Cell type | Starting composition | Results | Product | Relative density (%) |
|-----------|------------------------|--------------------------|----------------------------|----------------------|
| A | Ti (< 40 μ m) + 2B | Ignitable, Sintered body | TiB ₂ \gg TiN | 94-96 |
| A | Ti (< 10 μ m) + 2B | Ignitable, Sintered body | TiB ₂ | 93 |

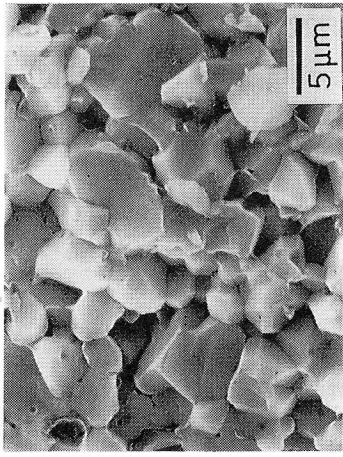
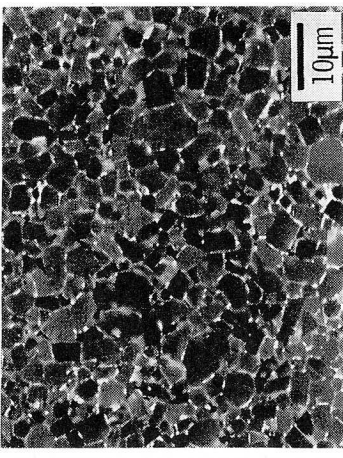
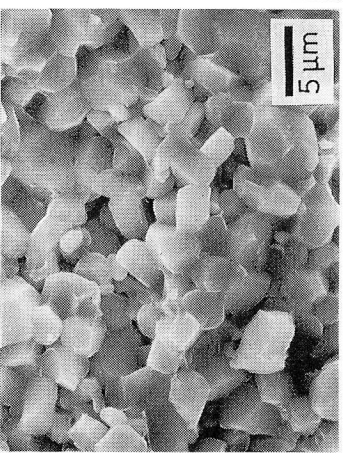
| | Fracture surface | Polished surface |
|-----------------------|------------------------------------------------------------------------------------|-----------------------------------------------------------------------------------|
| Ti (<40 μ m) + 2B |  |  |
| Ti (<10 μ m) + 2B |  | |

Fig. 42 Scanning electron micrographs of representative microstructure of TiB₂ compact.

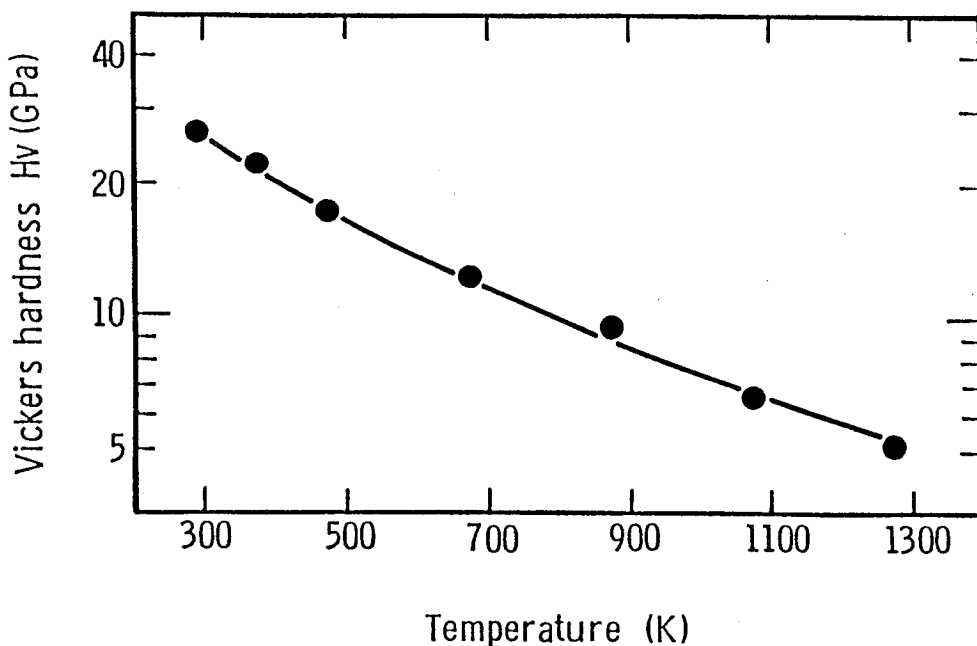


Fig. 43 Temperature dependence of Vickers microhardness of TiB_2 compact fabricated by HPCS using type A cell. Ti ($<40 \mu\text{m}$) and B were mixed for reactant.

the combustion reaction proceeded throughout the reactant. This fact suggests that the heat loss in type A cell results in the reduction of conversion efficiency. It is expected that the reactivity of combustion should be improved by preheating the mixed reactant. Experimentally, a carbon sleeve heater in type B cell was effective in fabricating dense TiC ceramics with high conversion efficiency. The conversion efficiency and density for different ignition methods of HPCS are summarized in Table XVI.

Characteristics of TiC compacts

As shown in Fig. 44, conversion efficiency was related not to the particle size of Ti powders, but to the mixing molar ratio of constituent elements in HPCS. The reactants with various mixed molar ratios in the range of $0.70 \leq \text{C/Ti} \leq 0.95$ converted entirely to the single but nonstoichiometric phases of TiC_x . When the mixing ratio exceeded 0.95, the starting elements remained slightly. This critical

Table XVI Conversion efficiency into TiC and density for different ignition methods of HPCS at 3GPa. The stoichiometric mixtures of T₁ and C₂ powders were used as a reactant.

| | | Type A Cell | Type B cell |
|------------|--------------------|------------------------|------------------------|
| Conversion | TiC/(TiC + Ti + C) | 72 % | > 99 % |
| Density | | 3.93 g/cm ³ | 4.61 g/cm ³ |

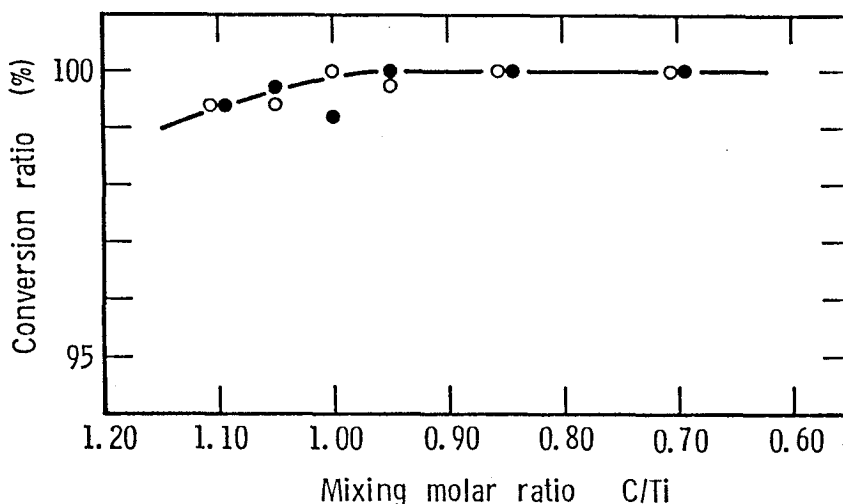


Fig. 44 Conversion efficiency into TiC_x as a function of mixed molar ratio of Ti and C powders.

● T₁ + C₂ ○ T₂ + C₂

value corresponded with the maximum solubility of carbon to titanium, which was seen in Fig. 45 on the phase diagram of Ti-C system [19]. The relative density of the sintered TiC_x was plotted as a function of mixed molar ratio of constituent elements in Fig. 46, where the reported density for TiC_{0.97}, 4.90 g/cm³, was adopted as the theoretical density. The maximum density was over 96% of theoretical which was independent on the particle size of Ti powders.

Figure 47 shows the lattice constant as a function of mixed molar ratio of C/Ti. Variations of the lattice constant showed the same tendency as reported in the

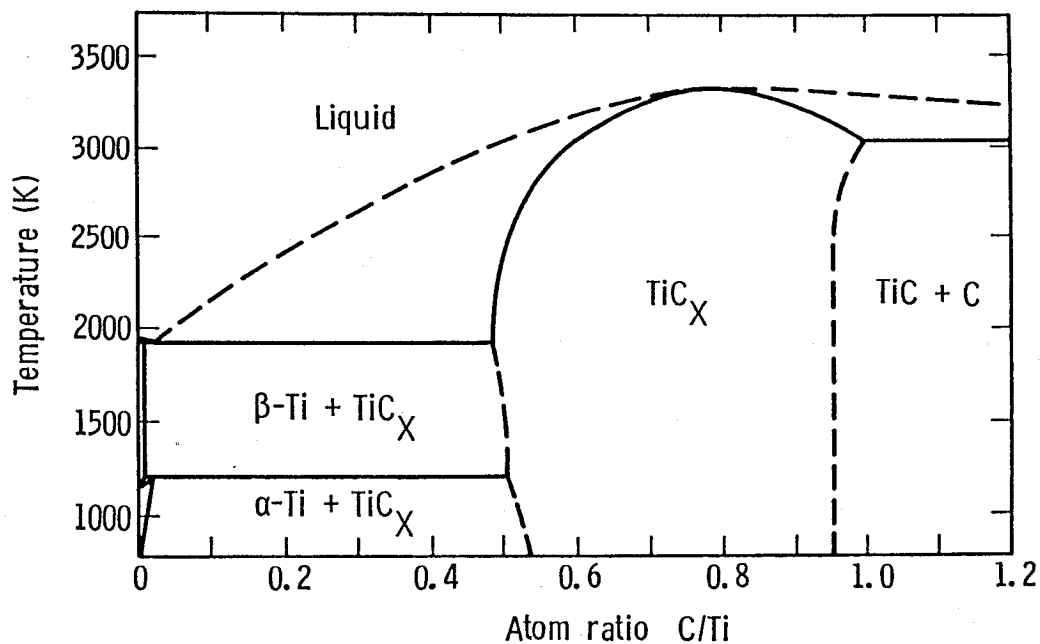


Fig. 45 Phase diagram of Ti-C system.

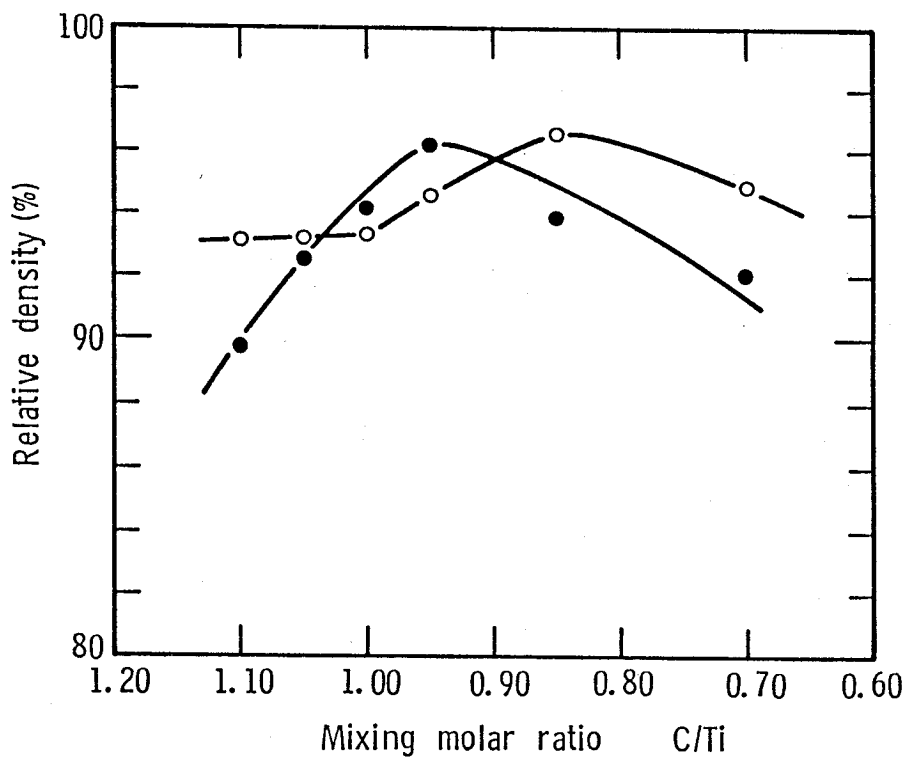


Fig. 46 Relative density of TiC_X as a function of mixed molar ratio of constituent elements.

● T₁ + C₂ ○ T₂ + C₂

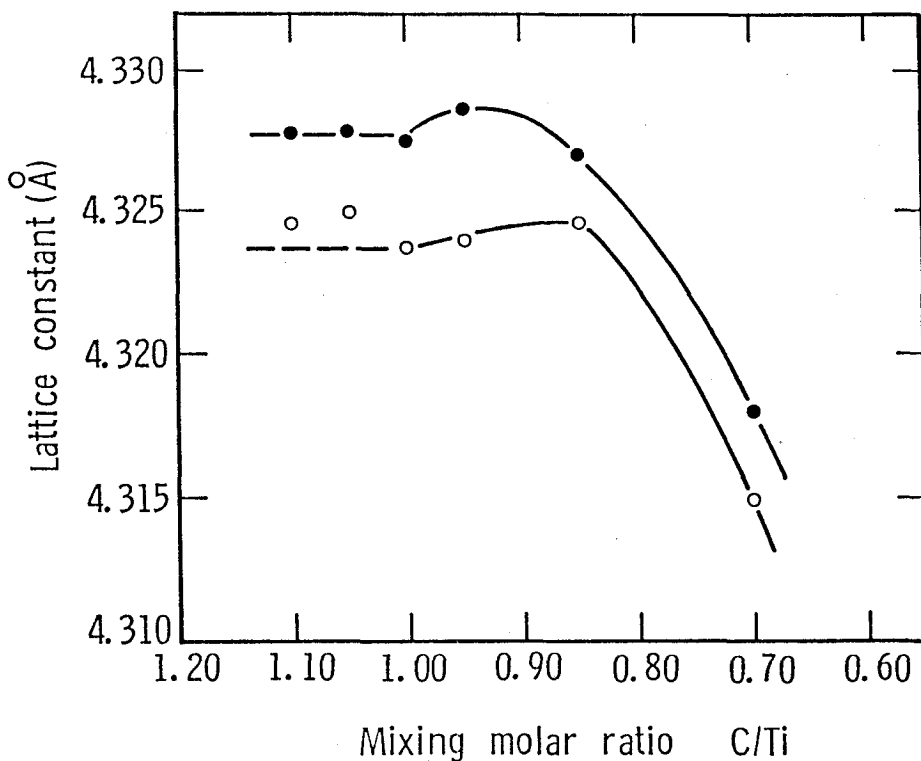


Fig. 47 Lattice constant as a function of mixed molar ratio of constituent elements.
 ● T₁ + C₂ ○ T₂ + C₂

reference [20]. But the absolute values were much lower especially in case of the starting powder of T₂, which contained more oxygen than T₁ powders. It was considered that the reduction of lattice constant related to the amount of oxygen contents in the product. In fact, lattice constant of TiC reduced with increasing oxygen contents as shown in Fig. 48. Lattice constant of free from oxygen TiC is estimated to be 0.4330 nm by extrapolation in the figure. This value is strictly coincident with the reported value of stoichiometric TiC single crystals [45].

Figure 49 shows microstructures of TiC compacts fabricated from the mixed reactants at fixed molar ratio of C/Ti = 1.00 using Ti powders with different particle sizes. It was observed that the mean diameter of TiC grains decreased with the decrease of particle size of Ti powders. However, the formation of finer particles of TiC compared to the starting Ti particle like TiB₂ did not occur. Figure 50 shows the microstructure of fracture surfaces of TiC_x compacts fabricated by HPCS. The distinctive feature was that the mean diameter of the grains increased

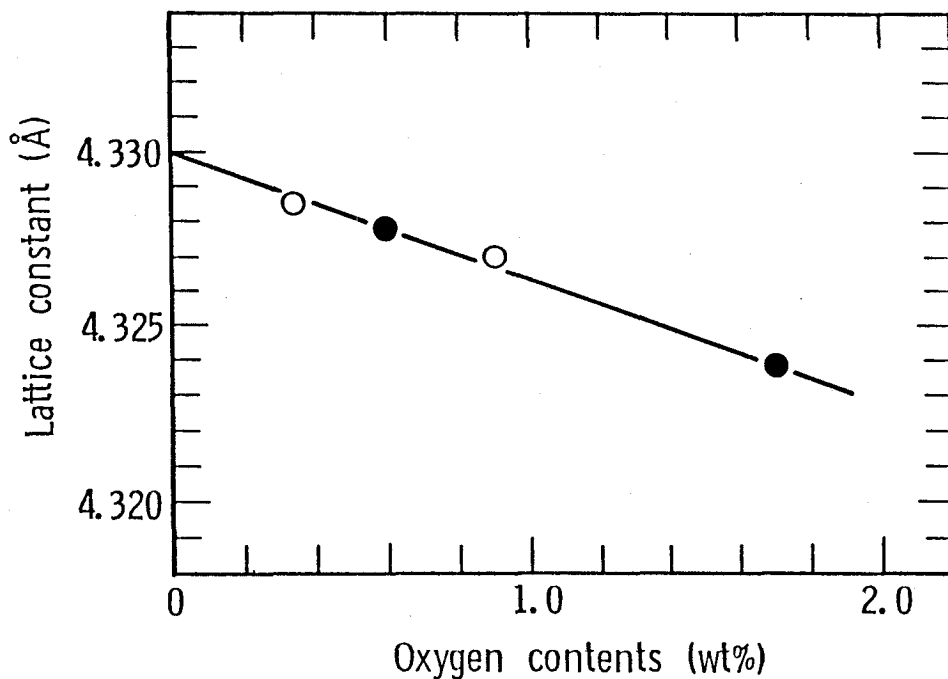
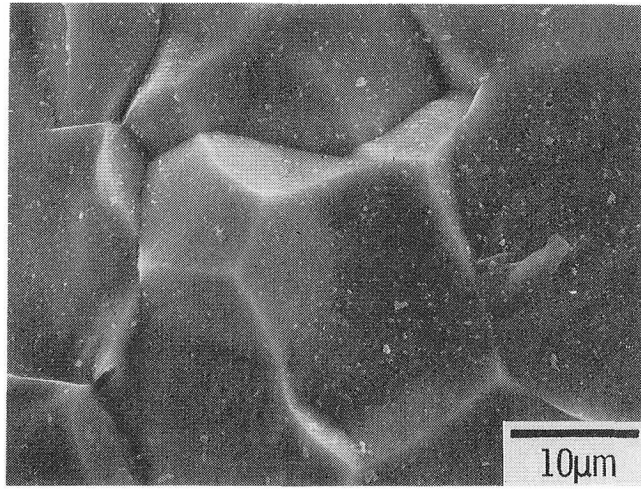


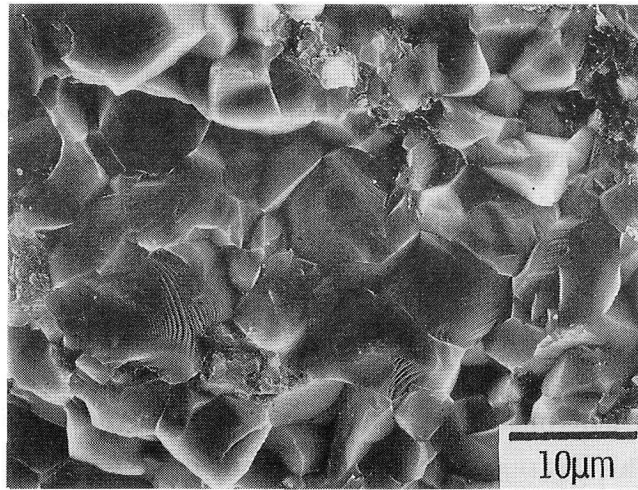
Fig. 48 Lattice constants of stoichiometric TiC compounds as a function of oxygen contents.

- sample fabricated by SHS
- sample fabricated by HPCS

and the fracture pattern became rich in transgranular type with increasing carbon deficiency, X. This fact suggests that the grain growth was promoted by the increase of atom mobility due to carbon vacancy. The Vickers microhardness was proportional to the relative density as seen in Fig. 51. The microhardness of TiC having theoretical density without additives was estimated to be about 35GPa at room temperature, which was larger than the value, 29GPa, for single crystal as reported in reference [46]. The temperature dependence of Vickers microhardness for TiC and $\text{TiC}_{0.85}$ were illustrated in Fig. 52. The microhardness at room temperature was about 31 GN/m² and 29 GN/m², respectively. With increasing temperature, the hardnesses of both specimens decreased gradually in the same way regardless of the carbon contents.



(a)

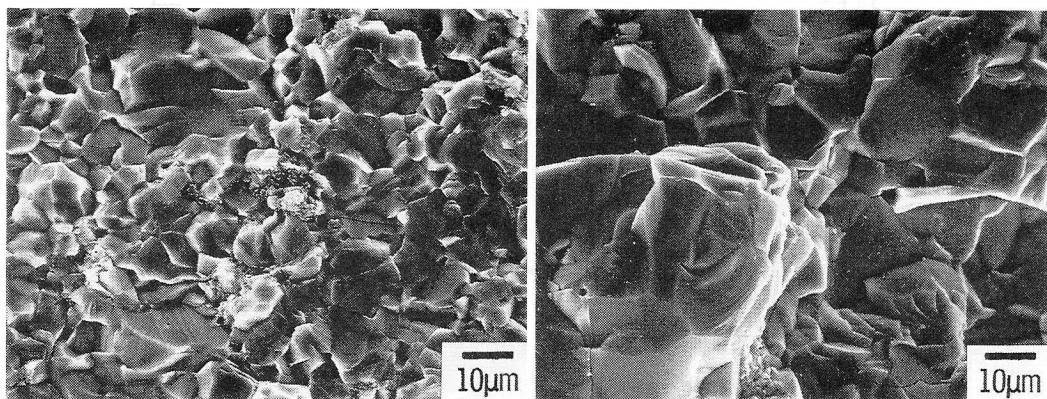


(b)

Fig. 49 Scanning electron micrographs of the fracture surfaces of TiC compacts fabricated using Ti powders with different particle sizes as a element in the reactant which was mixed at fixed molar ratio of C/Ti = 1.00.

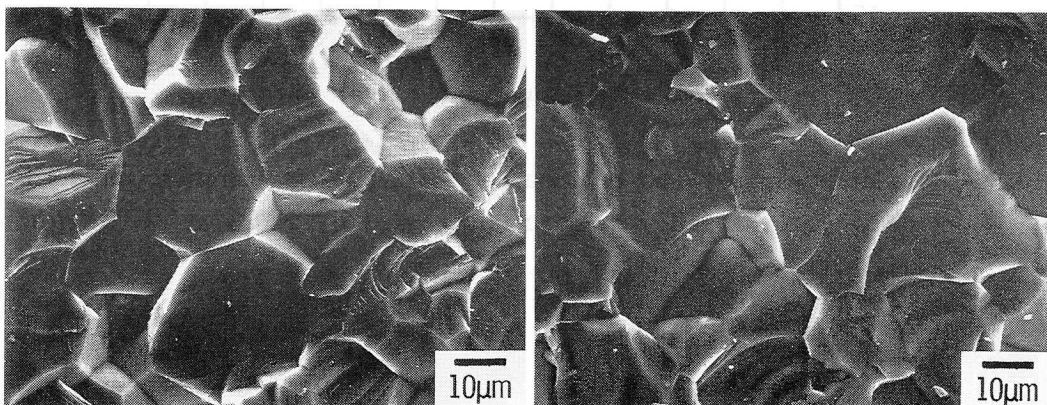
(a) $T_1 + C_2$ as reactant

(b) $T_2 + C_2$ as reactant



(a)

(b)



(c)

(d)

Fig. 50 Scanning electron micrographs of the fracture surfaces of TiC_x compacts fabricated by HPCS. The mixed molar ratio of constituent elements (T_2 and C_2) was ranged from 0.70 to 1.00.

(a) $C/Ti = 1.00$

(b) $C/Ti = 0.95$

(c) $C/Ti = 0.85$

(d) $C/Ti = 0.70$

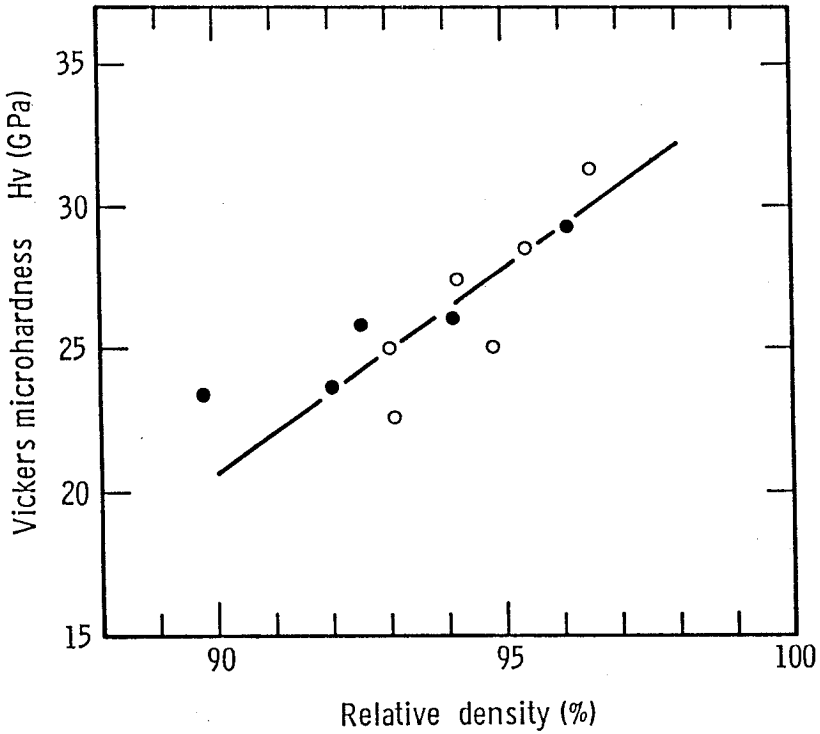


Fig. 51 Relationship between microhardness at room temperature and relative density of the TiC_X compacts fabricated by HPCS at 3GPa without additives.

● $T_1 + C_2$ ○ $T_2 + C_2$

4-3-3 Preparation and Properties of SiC Dense Ceramics

HPCS processing of SiC

The quantity of heat released on formation of SiC from the constituent elements is reported as 69 kJ/mol at room temperature, which is relatively low in comparison with the heat released on TiB_2 formation (293 kJ/mol). The formation of SiC gives an adiabatic temperature of 1850K which is significantly lower than the minimum temperature required to proceed the combustion reaction. The yield of conversion into SiC by HPCS seemed to be less than that by SHS because high pressure increase the activation energy of atom diffusion. In fact, conversion efficiency into SiC decreased to about 36% when the reactant was ignited at one end of the pellet in type A cell at 3GPa. An increase of adiabatic temperature to 2500K

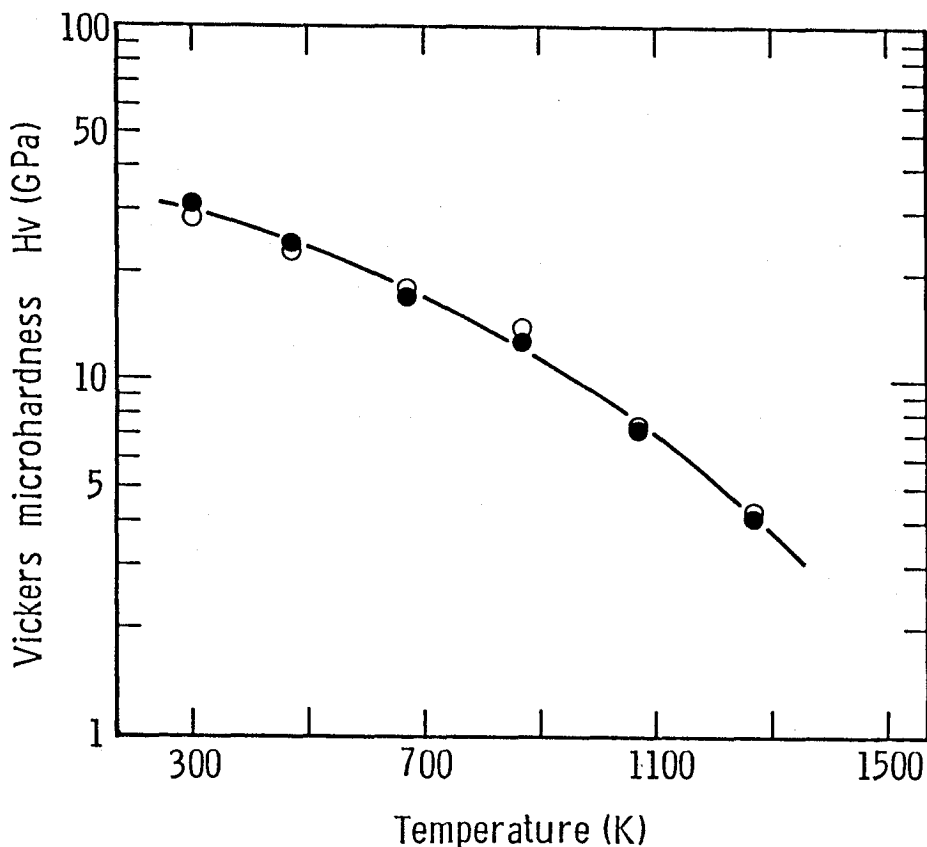


Fig. 52 Temperature dependence of Vickers microhardness for TiC and TiC_{0.85} compacts fabricated by HPCS using T₂ + C₁ powders as a reactant.

○ TiC

● TiC_{0.85}

would be performed by increasing the initial temperature from 300K to at least 1100K as mentioned already in SHS of SiC. Experimentally, it could be accomplished by using the carbon sleeve heater which is available for preheating the mixed reactant rapidly and uniformly as well as for a ignitor.

Characteristics of SiC compacts

It was revealed from the representative X-ray powder diffraction pattern as shown in Fig. 53 that the product consisted of stoichiometric β-SiC containing a small amount of α-SiC. The sharp β-SiC peaks indicated that the grains were well crystallized. It is generally said that β-SiC is a low temperature form being stable at

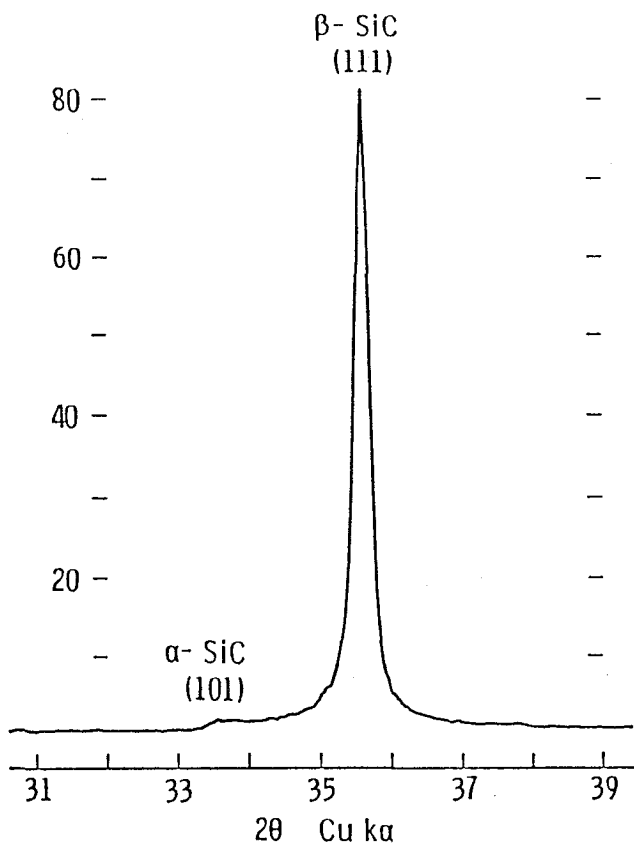


Fig. 53 Representative X-ray powder diffraction pattern of SiC compact fabricated by HPCS at 3GPa.

equilibrium state below 2300K. However, it is known that the crystallization of β -SiC can take place even at temperatures above 2300K by the sublimation-recrystallization of SiC and the precipitation from a solvent of molten Si [47]. In case of combustion synthesis, β -SiC might be formed as a meta-stable phase because of the rapid crystallization in the reaction of molten Si and carbon even if the actual combustion temperature exceeded 2300K. In Table XVII the relation between particle size of starting powders, conversion efficiency into SiC and relative density of SiC compacts is listed. Conversion efficiency increased with decreasing particle size of starting Si and reached 99.6% when 0.1 μm size Si powder (S_2) was used. Finer particles of the reactants should increase the contact areas between particles and reduce the diffusion path of elements. While the relative density was constant

Table XVII Effect of particle size of starting powders on conversion efficiency into SiC and relative density of SiC compacts fabricated by HPCS at 3GPa.

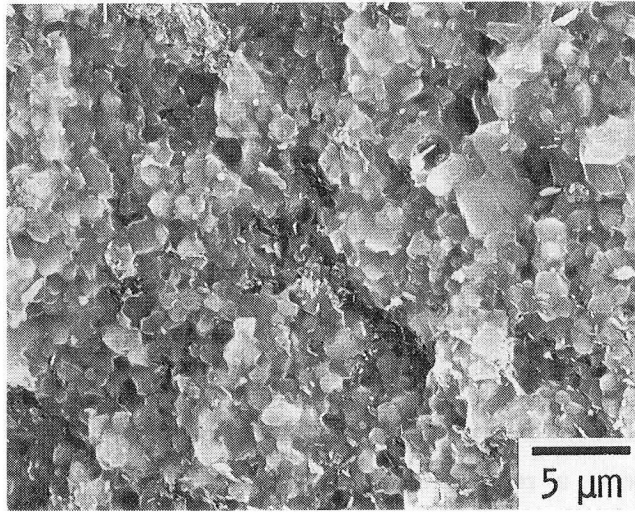
| Starting powder | Conversion efficiency (%) | Relative density (%) |
|---------------------------------|---------------------------|----------------------|
| S ₁ + C ₂ | 95.2 | 91.3 |
| S ₂ + C ₂ | 99.6 | 92.6 |

at 91-93% and independent on the particle size of Si.

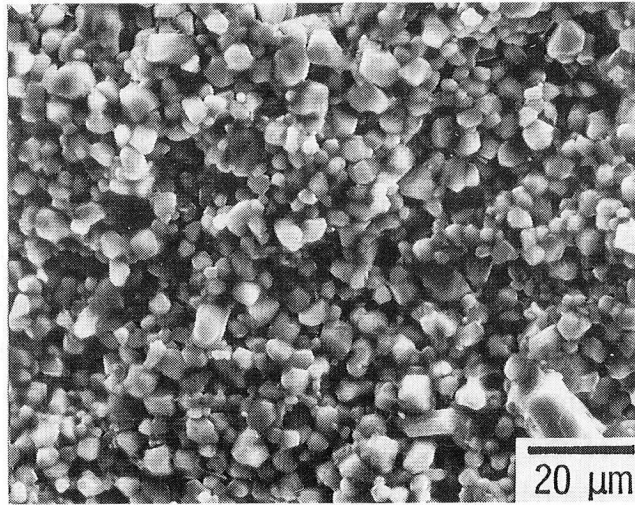
Figure 54 shows a representative microstructure of fracture surfaces, which indicate that the grain size of SiC compact decreased from 5 μm to 1 μm with the decrease of that of starting Si from 5 μm to 0.1 μm . This fact shows that the grain size of the product can be controlled to a certain degree by changing the particle size of reactant. The size distribution of SiC grains was narrow and the exaggerated grain growth was scarcely observed.

However, the self-bonding between grains was considered not to be sufficient since the intergranular type fracture was dominant as seen in the pictures of Fig. 54. If the heating duration in HPCS is slightly extended, it was expected that the sintering between grains would be promoted by the supplemental heating. In fact, when the heating duration was extended from 2s to 10s, the fracture pattern changed from an intergranular type to a transgranular type as shown in Fig. 55; moreover, the grain growth was not observed.

Characteristics of the compacts fabricated by heating for 10s are summarized in Table XVIII. The relative density of the compacts was nearly the same, which was almost independent on the particle size of Si as a starting powder and on the heating time. Vickers microhardness and fracture toughness of the compacts were compared to those of SiC ceramics with boron and carbon additives sintered by the conventional methods. Besides, characteristics of Hv and K_{IC} were slightly improved with using finer Si powder. Temperature dependence of Vickers microhardness of the compact fabricated by heating for 10s in HPCS is shown in Fig. 56. Microhardness of the compact without additives decreased gradually with increasing temperature, but maintained 8GPa at 1500K.



(a)



(b)

Fig. 54 Scanning electron micrographs of the fracture surfaces of SiC compacts fabricated by varying the particle size of Si powder in HPCS at heating time for 2s for ignition at 3GPa.

(a) $S_2 + C_2$, particle size of $Si \cong 0.1 \mu m$

(b) $S_1 + C_2$, particle size of $Si \cong 5 \mu m$

Table XVIII Characteristics of SiC compacts fabricated by heating for 10s in HPCS at 3GPa.

| | S ₂ + C ₂ | S ₁ + C ₂ |
|-------------------------------------------|---------------------------------|---------------------------------|
| Relative density (%) | 92.8 | 92.0 |
| Vickers microhardness (GPa) | 27 | 23 |
| Fracture toughness (MN/m ^{3/2}) | 4.5 | 4.3 |

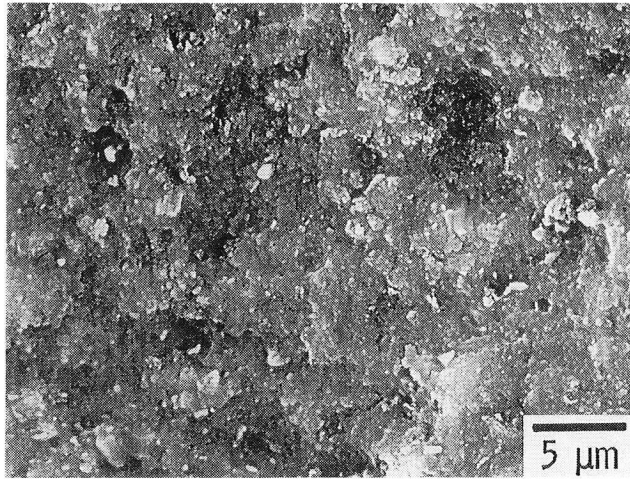
4-4. Discussion

4-4-1 Intrinsic Volume Change of Product before and after Combustion

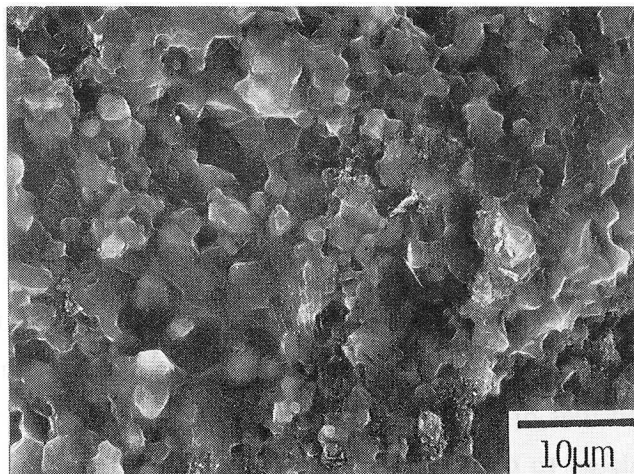
The conversion from reactant to compound by the combustion reaction gives rise to the volume change of the system. The intrinsic volume change, which are quite substantial, is described by the following equation when the conversion is completed.

$$X = \frac{V_P - V_R}{V_R} = \left(\frac{M}{\rho_{thP}} - \frac{M}{\rho_{thR}} \right) \bigg/ \frac{M}{\rho_{thR}}$$

where X is the fraction of intrinsic volume change between product and reactant, M is the mass of the system which is assumed to be unchanged, and ρ_{thP} and ρ_{thR} are theoretical densities of product and reactant, respectively. The intrinsic volume changes are calculated to be over -20% for TiB₂, TiC and SiC as shown in Fig. 57. If there is no change in shape of sample pellet after combustion, porosity of over 20% will be appeared in the product. In actual cases, the porosity increases further because the compact density of the reactant is lower than that of theoretical, extrinsically. Therefore, pressure is required to reduce the porosity and to bond the grains during the combustion reaction. On the other hand, it is expected that the HPCS reactions of TiB₂ and TiC, of which adiabatic temperatures coincide with their melting points, would reduce or eliminate porosity as a result of molten phase appearance. In fact, the relative densities of TiB₂ and TiC were higher than that of SiC which had no molten phase of SiC.



(a)



(b)

Fig. 55 Scanning electron micrographs of the fracture surfaces of SiC compacts fabricated by HPCS at heating time for 10s.

(a) $S_2 + C_2$ used as a reactant

(b) $S_1 + C_2$ used as a reactant

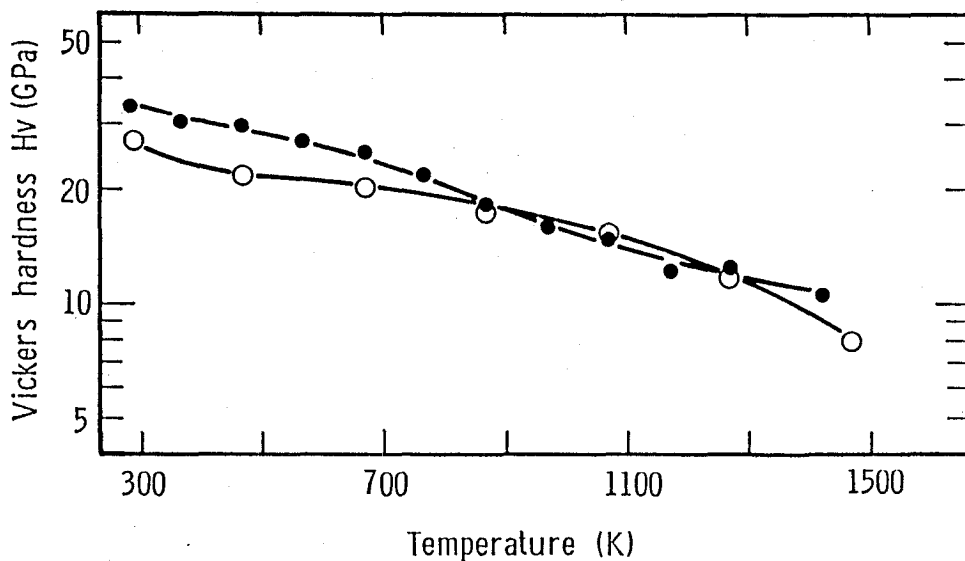


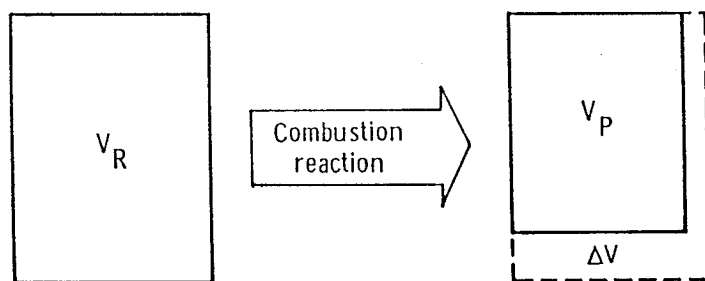
Fig. 56 Temperature dependence of Vickers microhardness of SiC compact fabricated by heating for 10s in HPCS at 3GPa.

- Fabrication by HPCS
Mixed powders of $S_2 + C_2$ used for the reactant
- Fabrication by hot-pressing using commercial SiC powder with B and C additives

These HPCS reactions are the rapid reactions accompanied large volume contraction of the products. Therefore, flexibility and responsibility of media for transmission of pressure is one of the important factors for densification of the product. It is considered that the solid media of pyrophyllite for transmitting pressure used in the present studies acted on densification of product effectively. Further improvement on mechanism for transmission of pressure should enable to attain full densification even at lower pressures.

4-4-2 Mechanism of Combustion Sintering under High Pressure

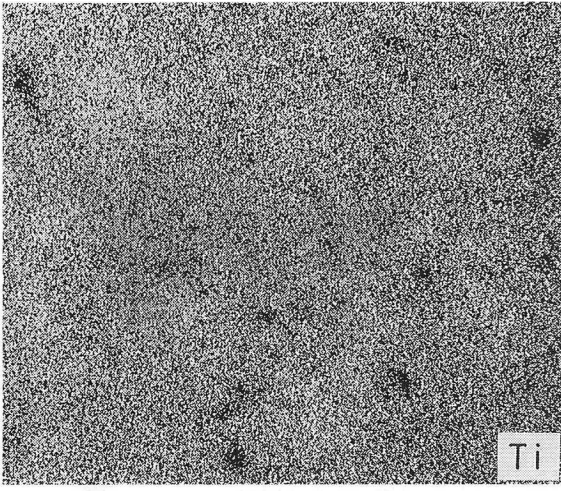
Reaction mechanism of synthesis and simultaneous sintering of TiB_2 under high pressure was investigated from the results of SEM and EPMA observations. Figure 58 shows the microstructure and distributions of Ti and B elements at the unreacted region in TiB_2 compact which was probably caused from heterogeneous distribution of element powders and existence of large particles in a reactant. It was



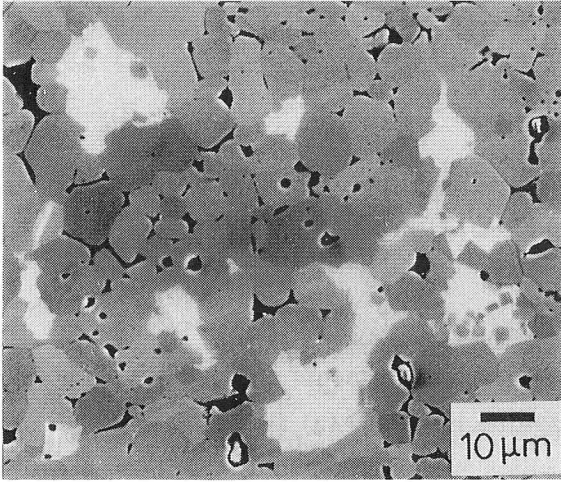
| | ρ_{thR} (g/cm ³) | ρ_{thP} (g/cm ³) | X (%) |
|----------------------------|--------------------------------------|--------------------------------------|----------|
| Ti + 2B → TiB ₂ | 3.5 | 4.5 | -22 |
| Ti + C → TiC | 3.8 | 4.9 | -22 |
| Si + C → SiC | 2.3 | 3.2 | -28 |

Fig. 57 Intrinsic volume changes of some ceramics before and after combustion.

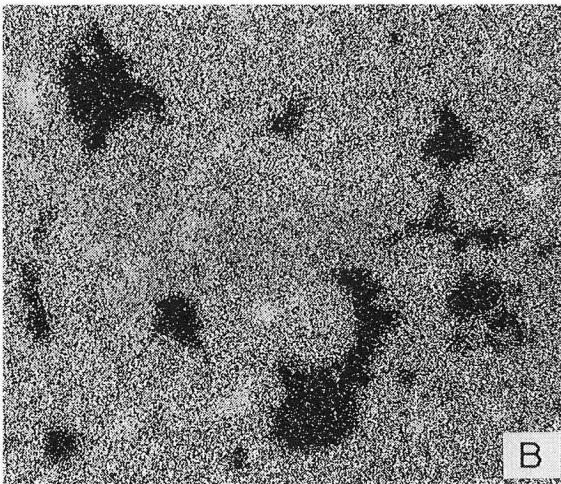
observed that a number of small TiB₂ crystals with particle size below 2 μm precipitated in Ti islands (whitish region in SEM photo). This result led to a simple model to account for the reaction mechanism on HPCS of TiB₂, which is schematically illustrated in Fig. 59. When the combustion zone proceeds along the axis of the cylindrical reactant, the neighboring region in front of combustion zone would be preheated by thermal conduction of reaction heat and begin to fuse Ti particles prior to the reaction. Subsequently, a number of nucleations of TiB₂ originate in molten Ti particles as a result of rapid diffusion of B atoms into them at the combustion reaction. The TiB₂ nuclei grow rapidly up to 5 μm in average size and coalesce each other under pressures until the system cools down. This model based on the nucleation-growth mechanism of crystal can also explain that the grains in TiB₂ compact became smaller after HPCS treatment than the initial Ti particles. On the contrary, such crystallizations with finer grains were not observed in HPCS of SiC and TiC, which consisted of grains same or large in dimension than the starting Si or Ti particles. These differences in crystallization are summarized in Fig. 60.



(a)



(b)



(c)

Fig. 58 Scanning electron micrographs of the partly unreacted regions in TiB_2 compact fabricated by HPCS (a), and X-ray images of element distributions for titanium (b) and boron (c).

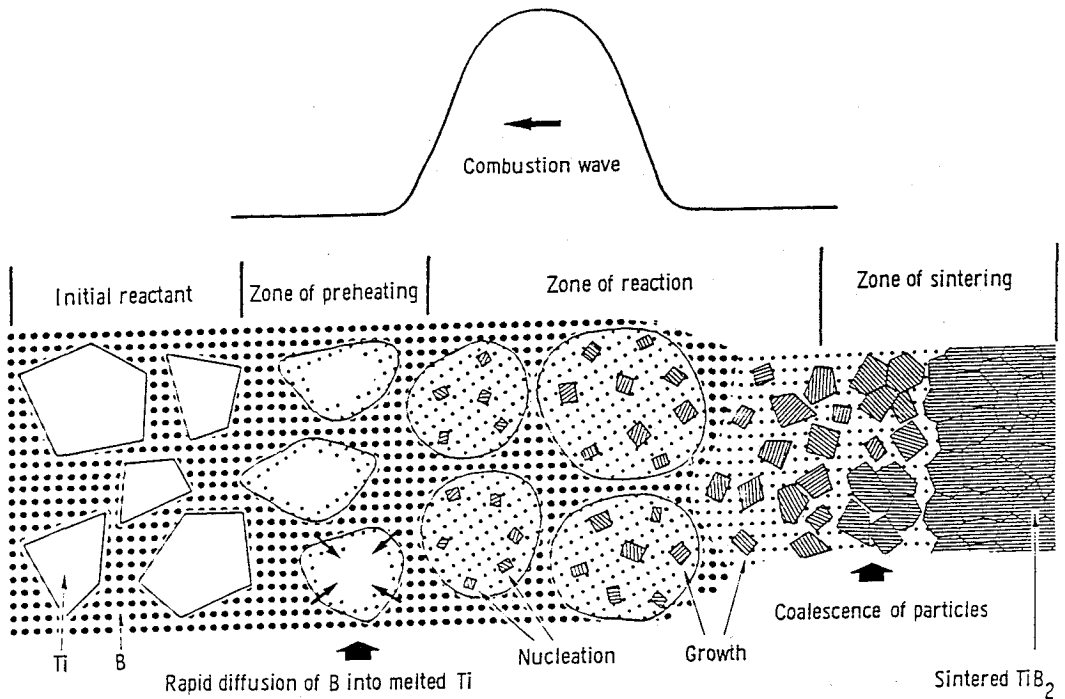
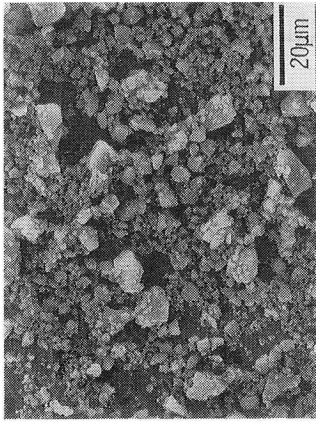
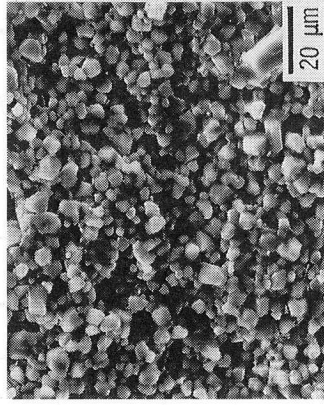


Fig. 59 Schematic of reaction mechanism of synthesis and simultaneous sintering of TiB_2 under high pressures.

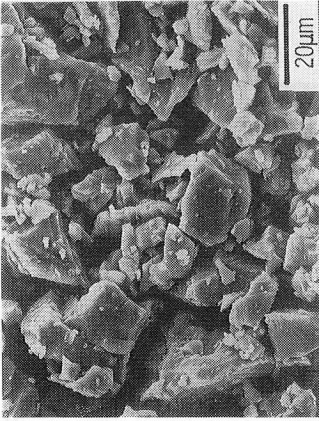
Phase relationships between constituent elements and products are shown with reference to the adiabatic temperatures in Fig. 61 (a), (b) and (c). If the combustion temperature is close to the adiabatic temperature in HPCS, both elements of Ti and B for TiB_2 might have melted prior to reaction, but in case of TiC and SiC , C remains in solid phase. The atom diffusion between liquid-liquid phases, such as in the combustion reaction of Ti-B system, should be faster than that between liquid-solid phase such as in that of Ti-C and vapour-solid phase such as in that of Si-C system. These differences concerning with atom mobility should result in the possibility whether finer crystallization of the compound in comparison with starting powder particles can take place or not.



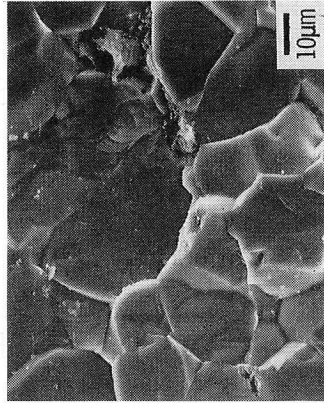
Si (<math>< 5 \mu\text{m}</math>)



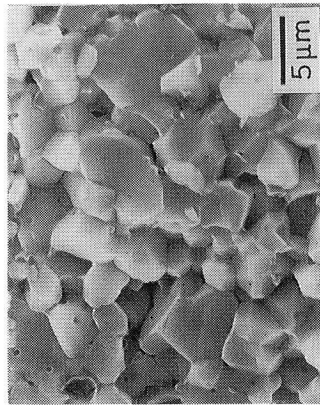
SiC



Ti (<math>< 40 \mu\text{m}</math>)



TiC



TiB₂

Element

Product

Fig. 60 Relationship between powder particle size of reactants and grain size of products.

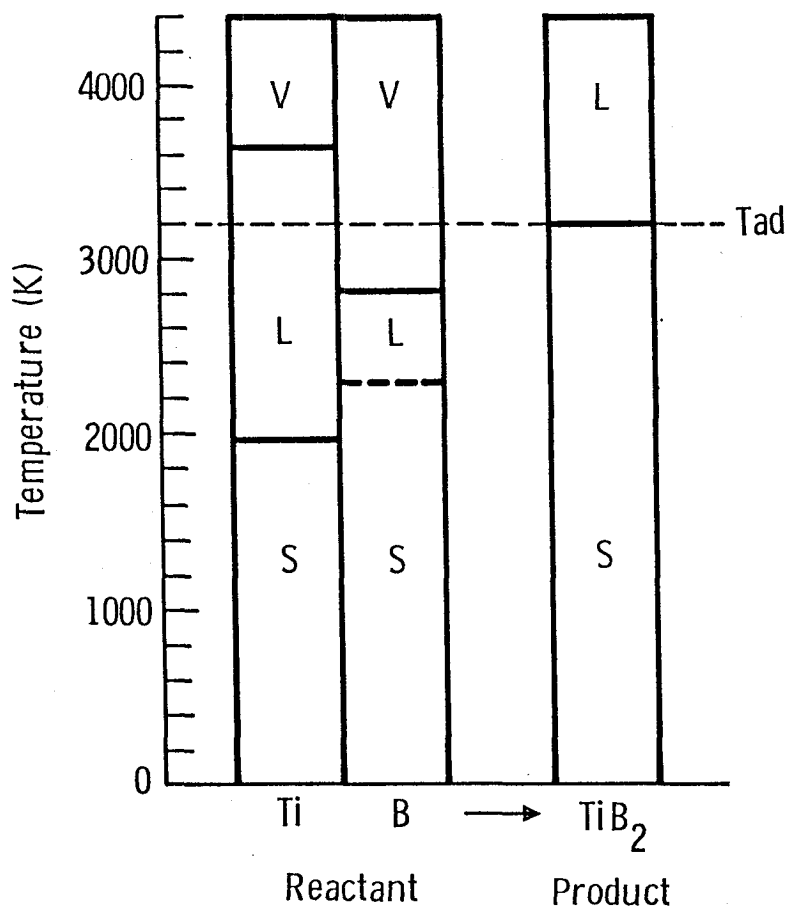


Fig. 61(a) Phase data for TiB₂ system in HPCS without preheating.

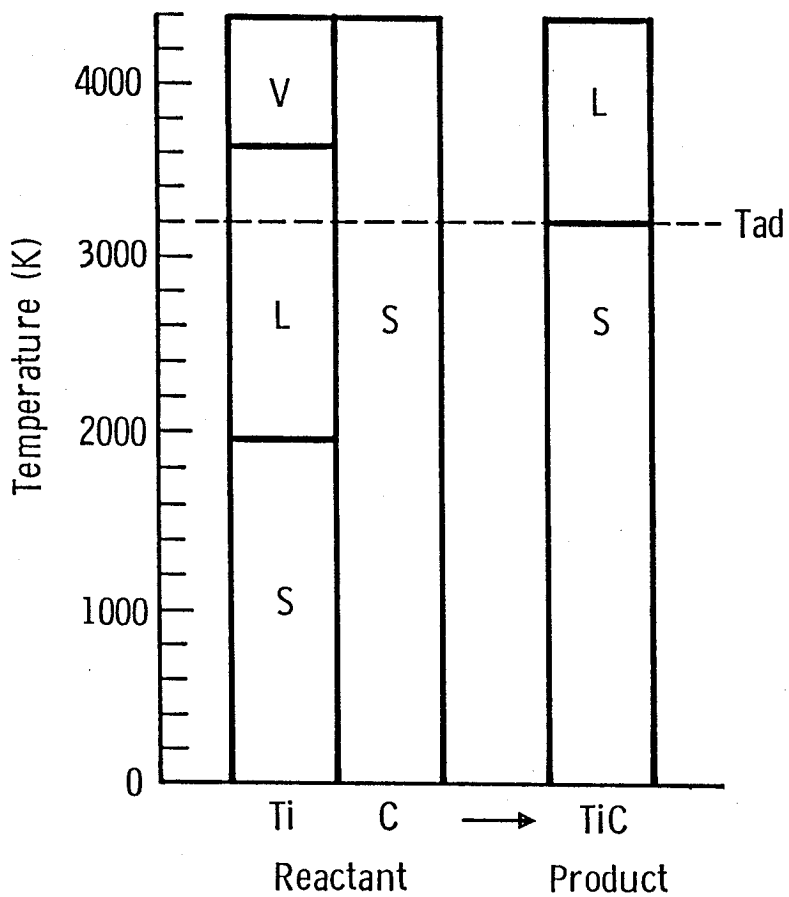


Fig. 61(b) Phase data for TiC system in HPCS without preheating.

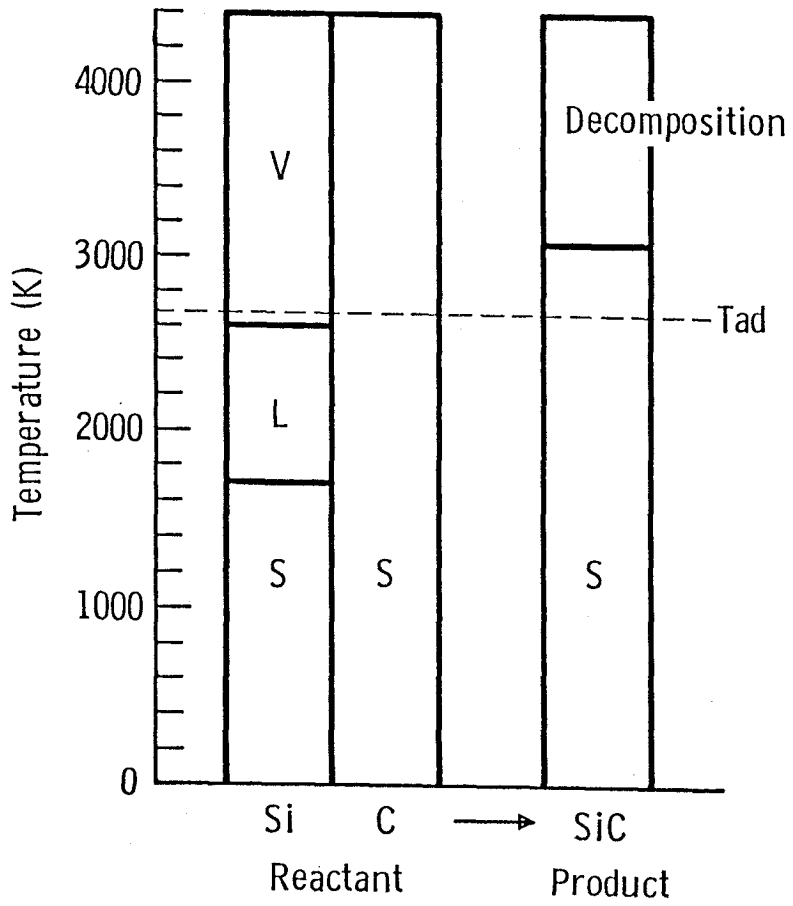


Fig. 61(c) Phase data for SiC system in HPCS with preheating at 1300K.

Chapter 5 APPLICATION OF HPCS PROCESS

5-1 Introduction

Applications of this newly developed method, high pressure self-combustion sintering, can be expected not only to the production of sintered fine ceramics, but also to the other wide range of fields listed below by utilizing exothermic high heat under high pressures.

- (1) Synthesis of new materials under high pressures and at high temperatures of 3000K.
- (2) Synthesis of new solid solutions and intermetallic compounds.
- (3) Production of super conductive materials.
- (4) Production of composite materials and cermet.
- (5) Ceramic coating and welding of ceramic-metal and ceramic-ceramic systems.

In these wide applications of the HPCS, the welding of ceramics to metals or to ceramics is of importance in order to construct ceramic components to actual devices especially for engineering use. The new welding process, which we call pressurized combustion welding, is illustrated in Fig. 62. It is expected by this process that the dense compacts are fabricated and simultaneously welded to metal by chemical reaction between metal and ceramic due to the released high heat of combustion. A similar process is known as thermite welding utilizing the exothermic reaction of powdered Al and Fe_2O_3 [7].

5-2 Experimental Procedure

5-2-1 Starting Materials

The refractory metal Mo was used as a metal component, whereas TiB_2 and TiC were chosen for ceramic components. It has been already mentioned that these ceramics could be fabricated by HPCS in a very short time. The calculated adiabatic temperatures were about 3200K for both ceramics, which enable Mo to melt. The both differences of thermal expansion coefficients between TiB_2 or TiC and Mo are below $2 \times 10^{-6}/\text{K}$ from room temperature to 2200K [48]. The fine powders of titanium (T_1) and amorphous boron (B_1) for TiB_2 , or titanium (T_1) and amorphous carbon (C_2) for TiC , were well mixed in their stoichiometric ratios respectively.

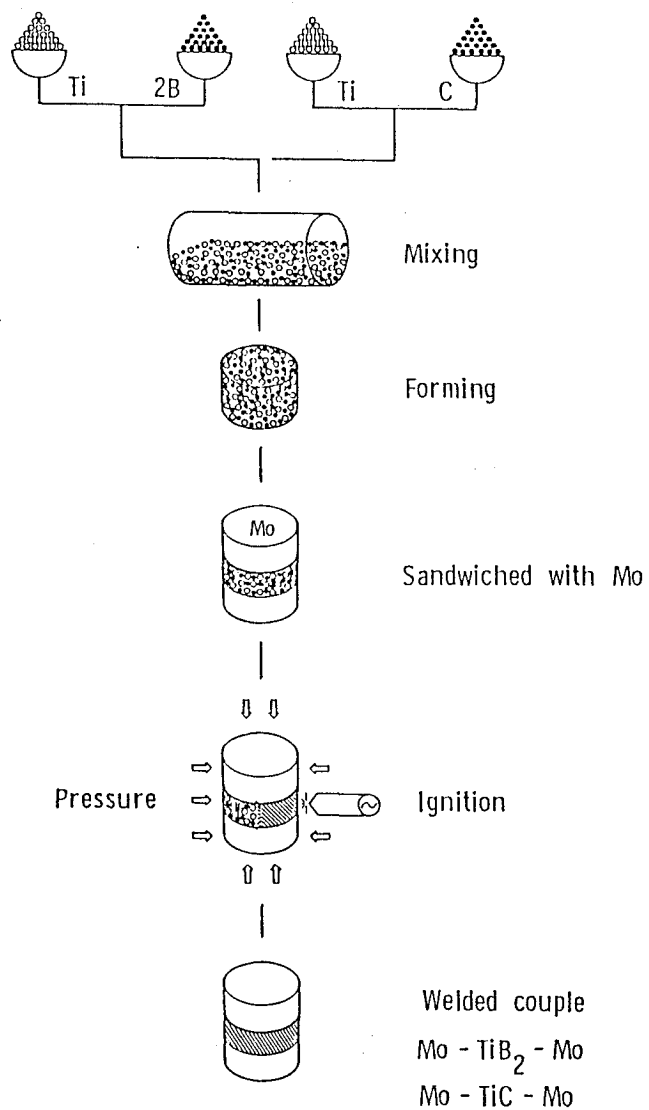


Fig. 62 Schematic of a new welding process utilizing the combustion reaction under high pressure.

5-2-2 Cell Assemblage for Welding by HPCS

Each mixed powder was press-formed to a thin disk with 5.8 x 2 mm in diameter and thickness, and then sandwiched directly between two Mo disks with 5 x 2.5 mm. This sandwiched assembly with Mo is useful to evaluate the welding strength by tensile test. The pieces for welding were placed into a reaction cell as shown in Fig. 63. An insulative BN sleeve was inserted between Mo disks and a cylindrical carbon heater for ignition so that only the mixed reactant might contact with the heater. The sample was subjected up to 3GPa by means of a cubic anvil device. Then the reactant was ignited at the periphery by passing electric current through a carbon heater at 1.5 kVA for 1 or 2 seconds.

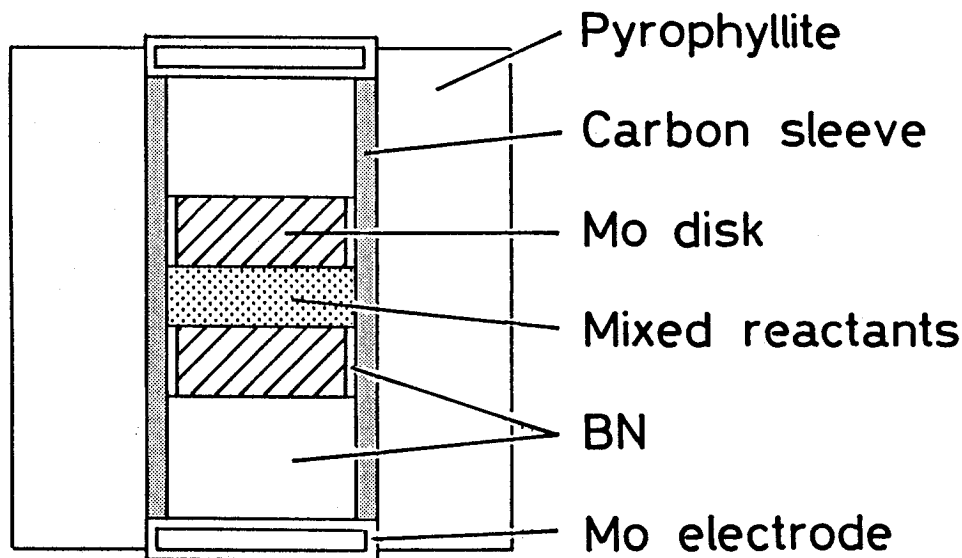


Fig. 63 High-pressure cell assemblage used for the pressurized combustion welding.

5-2-3 Characterization of the Products

The welded couples were examined by scanning electron microscopy and X-ray diffractometry. X-ray images of element distributions were observed by electron probe micro-analyzer (EPMA). The welding strength evaluated by tensile test.

5-3 Results and Discussion

Figure 64 shows a scanning electron micrograph of the cross section of Mo-TiB₂-Mo welded couple. X-ray diffraction showed that the mixture of Ti and B converted to the stoichiometric TiB₂. The TiB₂ ceramic was a dense body having fine grains with mean size of 5 μm, and almost free from pores and cracks. The reaction regions were formed at the upper and lower interfaces between TiB₂ and two Mo disks, where extended for about 80 and 170 μm respectively. A major product was identified as Mo₂B phase by XRD. A feature of reaction region and the element distributions in that region are shown in Fig. 65. The welding strength of several Mo-TiB₂-Mo couples evaluated by tensile test was in the range of 20-40 MPa. The couples were fractured at the boundary between Mo and the reaction region or in the reaction region near Mo.

In case of Mo-TiC-Mo couple, the mixture of Ti and C was converted to sintered TiC and welded with Mo. Figure 66 shows a photograph of the appearance of Mo-TiC-Mo welded couple. The sintered TiC was a porous body having large grains with 15 μm in average, but the cracks were not observed. The reaction regions extended for 70 and 160 μm at the upper and lower interfaces between TiC and Mo respectively. The XRD and electron probe microanalysis indicated that a

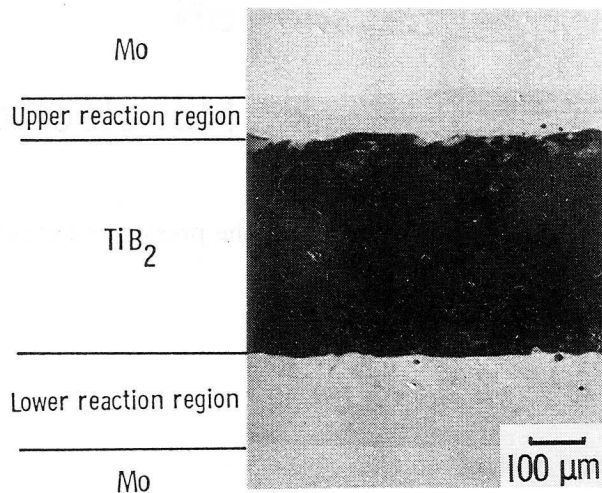


Fig. 64 Scanning electron micrograph of the cross section of Mo-TiB₂-Mo welded couple.

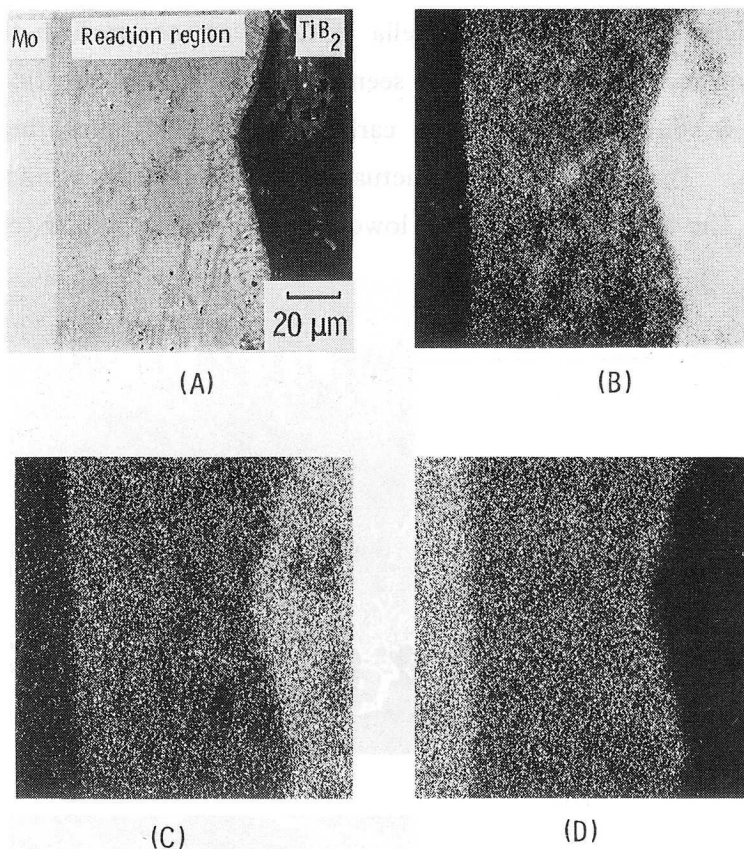


Fig. 65 Scanning electron micrograph of the reaction region between TiB₂ and Mo (A), and X-ray images of element distributions for boron (B), titanium (C) and molybdenum (D).

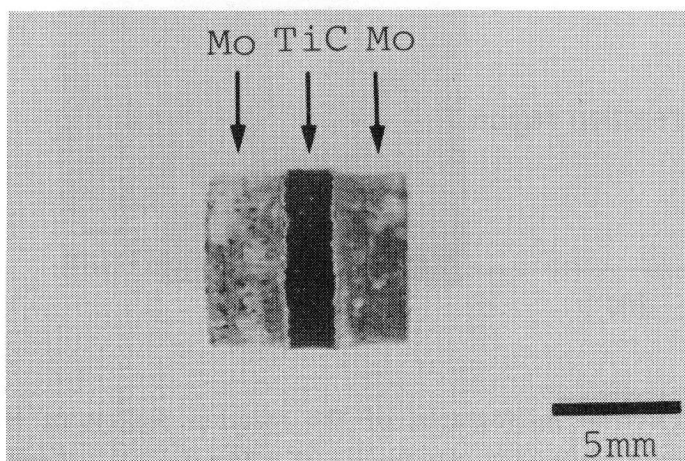


Fig. 66 Appearance of Mo-TiC-Mo welded couple fabricated by pressurized combustion welding.

main reaction phase would be Mo_2C slightly dissolving Ti. The precipitation of dendritic micro crystals and the lamella texture were observed in the lower and upper reaction regions, respectively as seen in Fig. 67. The dendritic crystals were not identified, but inferred to be a carbide, $(\text{Mo}, \text{Ti})\text{-C}$, including Mo and Ti from EPMA. The compositional fractuation in the lamella structure is obscure at present. The thicker width of the lower reaction region similar to $\text{Mo-TiB}_2\text{-Mo}$

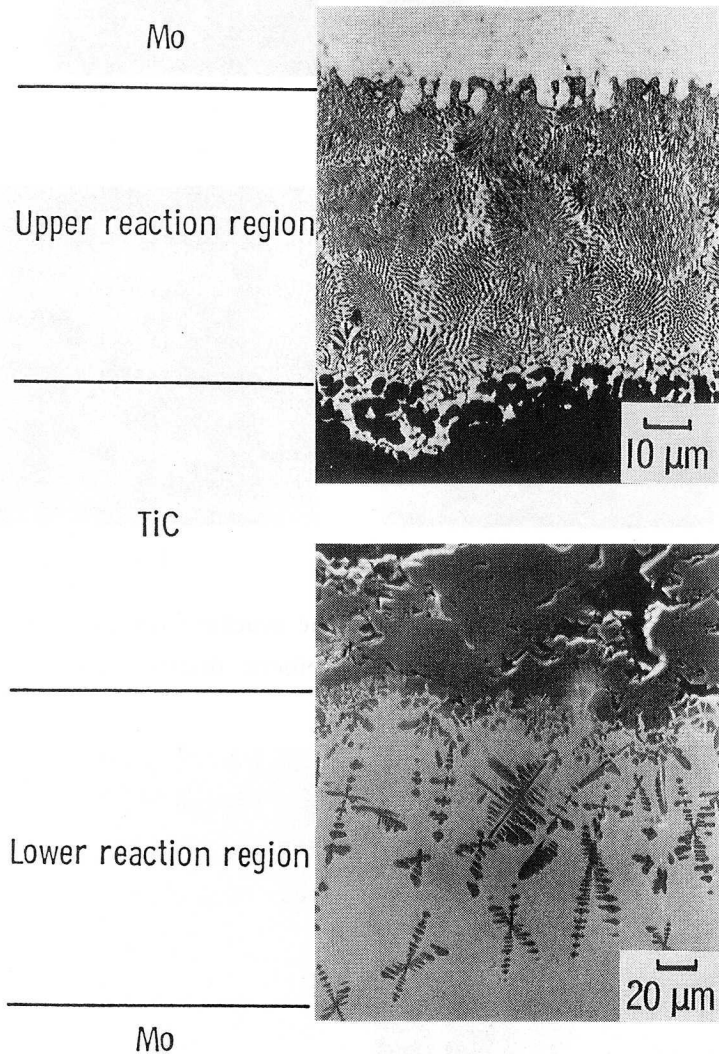


Fig. 67 Scanning electron micrographs of the reaction regions of Mo-TiC-Mo welded couple. Different structures with a lamella texture and dendritic micro crystals appeared in the upper and lower reaction regions respectively.

couple and the precipitation of crystals suggest that the reaction heat tends to be accumulated at the bottom of welding part in the present sample assembly. The tensile strength of Mo-TiC-Mo couple was 10MPa in average. The fracture occurred in porous TiC body.

It is noted that the bonding of ceramic to metal by pressurized combustion welding is performed rapidly and only by local heating for ignition. Further developments in the welding at lower pressures and in finding effective reactants as a strong bonding agent are needed for wide applications in actual use. Nevertheless, the present method is believed to have a new potential for joining in ceramic-metal and ceramic-ceramic, and also ceramic coating. The thick coatings of TiC and TiB₂ on Mo are significant for the construction of first wall of fusion reactor.

Chapter 6 SUMMARY AND CONCLUSION

By promoting research on refractory materials of which importance should increase hereafter, a simple and economical method to fabricate dense refractory materials could be developed by utilizing highly exothermic chain reaction under high pressure. In order to develop this HPCS method, the combustion reactions and synthesis of TiB_2 , TiC and SiC in SHS, role of pressure on densification of ceramics were extensively investigated. The obtained results are summarized as follows.

The combustion feasibility in SHS reaction depended on the adiabatic temperature which is an attainable temperature of product in ideal adiabatic system. The adiabatic temperatures of TiB_2 and TiC , which coincide with the melting points of TiB_2 (3193K) and TiC (3210K), are higher enough to produce the combustion reaction, so that the reactants could be ignited easily at one end of the pellet and well burned in a few seconds accompanying with the formation of final products. The constituent elements of Ti and B or C were entirely converted to their single phase compounds. On the contrary, SHS reaction of SiC is liable to be incomplete, since the formation energy of SiC from constituent elements gives an low adiabatic temperature of 1850K. This disadvantage could be overcome by direct passing method of electric current through reactant for ignition, which enables to increase the adiabatic temperature by preheating the mixed reactant rapidly and uniformly prior to ignition. As the results, the conversion efficiency into SiC reached to 100% when the reactant consisting of small particles was preheated at 1300K and then ignited. This direct passing method of low electric power current for ignition can be applied to fabrication of many other ceramics with low adiabatic temperatures if the reactants are electrically conductive.

A remarkable effect of applying high pressures was recognized on densification of refractory materials without additives. Almost fully densified β - SiC and TiC compacts could be obtained by high pressure hot-pressing at 2800K and 3GPa for 10s. The Vickers microhardness and fracture toughness at room temperature were 35-36GPa and $5.6MN/m^{3/2}$ for SiC , and 35GPa and $5.0MN/m^{3/2}$ for TiC , which are higher than reported values because of their own intrinsic characteristics based on the pure compacts composed of tightly self-bonded grains. SiC and AlN are known as excellent thermal conductors, of which thermal conductivities were 220W/mK and 27W/mK respectively. It was revealed for AlN that the purity of

the sintered compacts affected significantly thermal conductivity. For the application of high pressure, anion substituted solid solution ceramics of $ZrN_{1-x}Cx$ could be fabricated by both HPHP and HIP densification techniques.

By combining the efficient SHS and the effective high pressure technique for sintering, a new process of high pressure self-combustion sintering was produced, which enables direct fabrication of dense ceramics from constituent elements in seconds. The dense compact of TiB_2 with a relative density of 95% could be fabricated by electric ignition at one end of the reactant without additives. Initial reactant converted entirely into stoichiometric TiB_2 . The heat release from the strong exothermic reaction was sufficient to synthesize and simultaneously sinter TiB_2 under 3GPa without external heat supply. Reaction mechanism on HPCS of TiB_2 was understood by a proposed model based on the nucleation-growth mechanism of crystal. The HPCS of TiC could be performed by electric ignition on lateral surface of the reactant and the compacts were densified to 96.5% of theoretical with high conversion efficiency. The Vickers microhardness of TiB_2 and TiC compacts were 26GPa and 31GPa at room temperature respectively, which were higher than the reported values. Dense compacts of SiC with fine grains of 1 μm in average size could be fabricated directly from constituent elements of fine silicon and carbon powders without additives by HPCS. The reactants were converted into β - SiC with high efficiency by increasing the ignition area in order to enhance the weak exothermic reaction. It was revealed that the powder particle size of the reactant was one of the important factors affecting the conversion efficiency and the grain size of SiC .

The combustion reaction under high pressure was applied to ceramic-metal welding utilizing the exothermic heat released at the combustion reaction like thermite welding. Two couples of $Mo-TiB_2-Mo$ and $Mo-TiC-Mo$ could be welded by electric ignition on powdered mixture of Ti and B or C placed between Mo disks under 3GPa. The mixed reactants converted to sintered TiB_2 and TiC respectively by the combustion reaction under high pressure, and the chemical reaction between ceramic and metal due to the released high heat of combustion welded them simultaneously.

These results indicate that the high pressure self-combustion reaction has large potentialities for sintering, synthesis of high temperature materials and even for construction of their components.

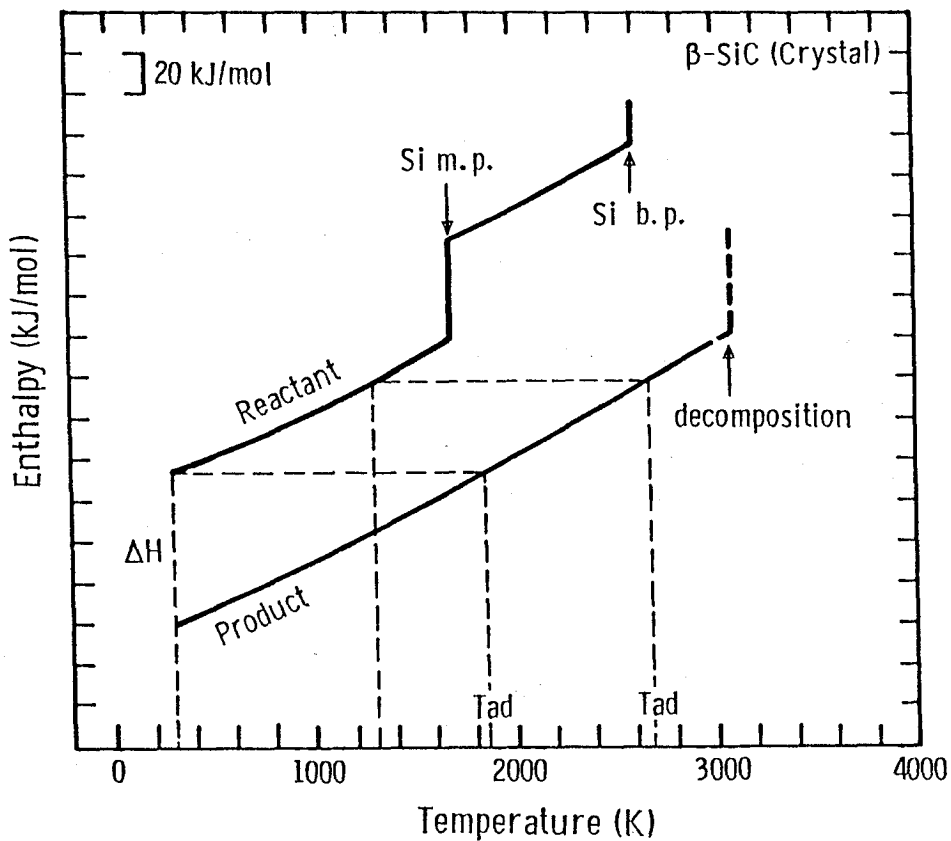
Acknowledgement

The author is greatly indebted to Professor M. Koizumi at Osaka University for his continuing help throughout this work and to Professors F. Kanamaru, T. Shono and T. Yamane at Osaka University for their valuable discussions.

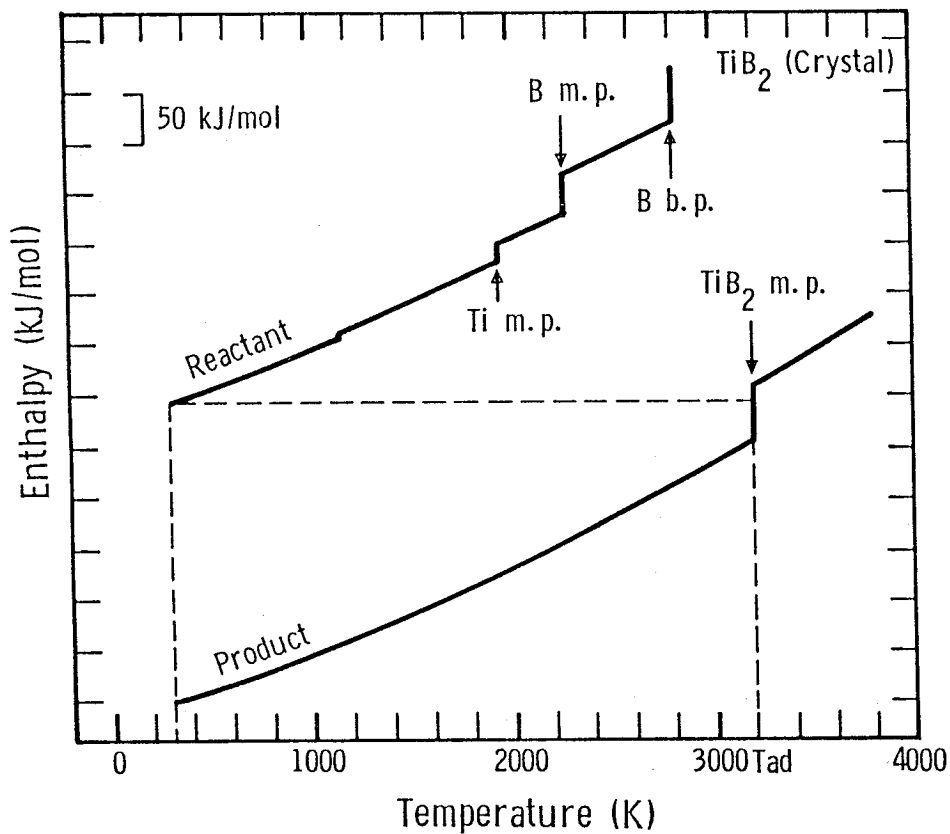
The author would like to acknowledge Associate professor Y. Miyamoto at Osaka University for the continuing guidance and helpful discussions and encouragement throughout this work.

The author would like to thank Professor M. Shimada at Touhoku University for his significant suggestions.

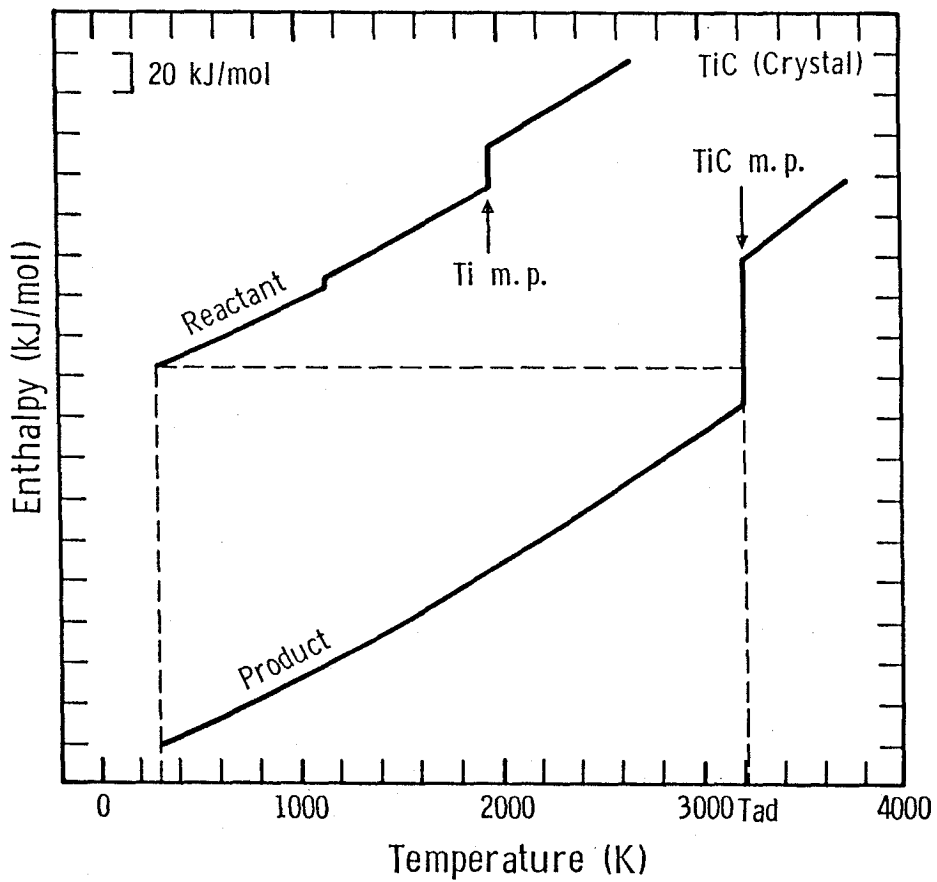
The author wishes to thank all members of the laboratories under the direction of Professors M. Koizumi and S. Kume at Osaka University.



Appendix II Enthalpy curves of Ti-B system.



Appendix III Enthalpy curves of Ti-C system



References

- [1] V. I. Matkovich, "Boron and Refractory Borides", Springer-Verlag, Berlin (1977).
- [2] G. V. Samsonov and I. M. Vinitiskii, "Handbook of Refractory Compounds", IFI/Plenum (1980).
- [3] M. C. I. C. Report, "Engineering Property Data on Selected Ceramics, Vol. II", Battelle Columbus Laboratories (1979).
- [4] J. D. Latva, *Metal Prog.*, **82**, 139 (1962).
- [5] H. E. Helms and P. W. Heitman, *Proc. 1st Int. Symp. Ceramic Components for Engines*, p. 33(1983).
- [6] A. G. Merzhanov and I. P. Borovinskaya, *Dokl. Chem. (Engl. Transl.)*, **204**, 429 (1972).
- [7] Am. Welding Soc., "Welding Handbook", 5th Ed. (1963).
- [8] J. W. McCauley, N. D. Corbin, T. Resetar and P. Wong, *Ceram. Eng. Sci. Proc.* **3**, 538(1982).
- [9] P. D. Zavitsanos and J. R. Morris, Jr., *Ceram. Eng. Sci. Proc.*, **4**, 624 (1983).
- [10] Y. Miyamoto, M. Koizumi and O. Yamada, *Comm. Am. Ceram. Soc.*, **67**, C-224 (1984).
- [11] L. E. Toth, "Transition Metal Carbides and Nitrides", Academic Press (1971).
- [12] G. Schwier, *Industrial Rare Metal (in Japanese)*, **73**, 98 (1980).
- [13] H. Tanaka, Report of the National Institute of Research for Inorganic Materials (in Japanese) (1967).
- [14] A. Kato, *Jap. J. Chem.*, **2**, 188 (1980).
- [15] JANAF, "Thermochemical Tables", p.88 (1965).
- [16] W. F. Henshaw, A. Niiler and T. Leete, *Ceram. Eng. Sci. Proc.*, **4.**, 634 (1983).
- [17] R. B. Kotelnikov, S. N. Bushli'kov, Z. G. Galiakbarov and A. I. Kashtanov, "Handbook of Highly Refractory Elements and Compounds", Table 4, *Metallurgiya, Moscow* (1969).
- [18] J. B. Holt and Z. A. Munir, *Proc. 1st Int. Symp. Ceram. Components for Engines*, p. 721 (1983).

- [19] E. K. Storms, "The Refractory Carbides", p. 3, Academic Press, New York (1967).
- [20] *ibid.*, p. 8.
- [21] J. F. Crider, *Ceram. Eng. Sci. Proc.*, **3**, 519 (1982).
- [22] K. Hirao, private communication.
- [23] S. Kato, *Bull. Ceram. Soc. Japan*, **11**, 1101 (1976).
- [24] J. Osugi, K. Shimizu, K. Inoue and K. Yasunami, *Rev. Phys. Chem. Japan*, **34**, 1 (1964).
- [25] A. G. Evans and E. A. Charles, *J. Am. Ceram. Soc.*, **59**, 371 (1976).
- [26] W. J. Parker, R. J. Jenkins, C. P. Butler and G. L. Abbott, *J. Appl. Phys.*, **32**, 1979 (1961).
- [27] R. E. Taylor and J. Morreale, *J. Am. Ceram. Soc.*, **47**, 69 (1964).
- [28] R. A. Dinovi, *J. Sci. Instrum (J. Phys., E)*, Ser. 2, **1**, 379 (1968).
- [29] D. H. Stutz, S. Prochazka and J. Lorenz, *J. Am. Ceram. Soc.*, **68**, 470 (1985).
- [30] Y. Inomata, H. Tanaka, Z. Inoue and H. Kawabata, *Yogyo Kyokaishi (in Japanese)*, **88**, 49 (1980).
- [31] T. Kurata and M. Asahi, *Fine Ceramics (in Japanese)*, **4**, 152 (1983).
- [32] R. K. Govila, *J. Am. Ceram. Soc.*, **63**, 3191 (1980).
- [33] G. Long and L. M. Foster, *J. Am. Ceram. Soc.*, **42**, 53 (1959).
- [34] K. Komeya and A. Tsuge, *Yogyo Kyokaishi (in Japanese)*, **89**, 615 (1981).
- [35] K. Komeya and F. Noda, *Toshiba Rev.*, **92**, 13 (1974).
- [36] P. Boch, J. C. Glandus, J. Jarrige, J. P. Lecompte and J. Mexmain, *Ceram. Inter.*, **8**, 34 (1982).
- [37] G. Dewith and N. Hattu, *J. Mater. Sci.*, **18**, 503 (1983).
- [38] T. Sakai, M. Kuriyama, T. Inukai and T. Kizima, *Yogyo Kyokaishi (in Japanese)*, **86**, 174 (1978).
- [39] M. P. Borom, G. A. Slack and J. W. Szymaszek, *Ceram. Bull.*, **51**, 852 (1972).
- [40] A. Christensen, X-ray Powder Data File 31-1493 (ASTM).
- [41] Chase and Juenke, X-ray Powder Data File 19-1487 (ASTM).
- [42] H. J. Goldschmidt, "Interstitial Alloys", p.564, Butterworths, London (1967).
- [43] W. S. Williams, *J. Am. Ceram. Soc.*, **49**, 156 (1966).

- [44] L. G. Radosevich and W. S. Williams, *J. Am. Ceram. Soc.*, **53**, 30 (1970).
- [45] A. Christensen, X-ray Powder Data File 31-1400 (ATSM).
- [46] M. C. I. C. Report, "Engineering Property Data on Selected Ceramics", **2**, 5.2.4-11, Battelle Columbus Laboratories (1979).
- [47] Report of the National Institute of Research for Inorganic Materials (in Japanese), No.1 (1972).
- [48] Thermophysical Properties of Matter, **12**, 208 (1975) for No. **13**, 778 (1977) for TiB_2 , **13**, 891 (1977) for TiC , IFI/Plenum, New York.
- [49] K. Niihara, *Bull. Ceram. Soc. Japan* (in Japanese), **20**, 12 (1985).
- [50] C. B. Boyer, F. D. Orcutt and J. E. Hatfield, *Industrial Heating*, 1 (1970).